Characterizing Memory Trace Reactivation and Biosynthetic Changes During Post-learning Sleep in the Hippocampus

by

Lijing Wang

A dissertation submitted in partial fulfillment
of the requirements for the degree of
Doctor of Philosophy
(Molecular, Cellular, and Developmental Biology)
in the University of Michigan
2023

Doctoral Committee:

Associate Professor Sara Jo Aton, Chair
Associate Professor Dawen Cai
Assistant Professor Eleanor Josephine Clowney
Professor Cunming Duan
Professor Jun Li

Sans la liberté de blâmer, il n'est point d'eloge flatteur. (Without the freedom to criticize, there is no point in flattering eulogies.)

—Pierre Beaumarchais, “The Marriage of Figaro”

Lijing Wang

lijingw@umich.edu

ORCID iD: 0000-0001-9292-841X

Acknowledgements

I would like to first thank my PI, Dr. Sara J. Aton, for being such a genuine, brilliant, and supportive mentor. I learned so much from Sara: from how to perform difficult experiments, to integrating multiple methodologies in the pursuit of a single question, to thinking as a scientist and communicating with colleagues. I could not thank her enough for her mentorship and guidance during the past five years.

I would also like to thank my dissertation committee members, Dr. Josie Clowney, Dr. Samuel Kwon, Dr. Dawen Cai, Dr. Jun Li, and Dr. Cunming Duan. I appreciate all the insight they've provided and all the support they continue to give. I also appreciate all members of the Aton Lab, past and present, as well as our collaborators. I am grateful that I had the opportunity to work with you.

I would like to acknowledge my friends. We not only had fun throughout graduate school, but also supported each other through stressful times, and I truly cherish our friendship. I also want to thank my parents; they have been so supportive, caring, and encouraging this entire time. Lastly, I want to thank my husband, Carlos, whose love has encouraged me at every step of my journey towards my dissertation and our future.

Table of Contents

Acknowledgements ii

List of Tables v

List of Figures vi

Abstract viii

Chapter 1 Introduction 1

1.1 Sleep and memory consolidation 1

1.2 Hippocampal place cells and engram cells 3

1.3 Place cell replay during sleep 7

1.4 Hippocampal engram ensemble reactivation during sleep 8

1.5 Cortex engram ensemble reactivation during sleep 9

1.6 Comparing engram vs. place cell reactivation during sleep 11

1.7 Effects of sleep and sleep loss on engram populations' transcriptomes 11

1.8 Conclusions 13

1.9 Dissertation Outline 13

1.10 References 15

Chapter 2 Ultrastructural Analyses Reflect the Effects of Sleep and Sleep Loss on Neuronal Cell Biology 18

2.1 Introduction 18

2.2 Effects of sleep loss on neuronal nuclear function 19

2.3 Sleep deprivation, cellular energetics, and mitochondrial function 22

2.4 Neuronal proteostasis, and intraneuronal transport - effects of sleep loss on Golgi, endoplasmic reticulum (ER), endosomes, and lysosomes 24

2.5 Future directions 25

2.6 References 27

Chapter 3 Reactivation of Memory-encoding Dentate Gyrus Neurons During Memory Consolidation is Associated with Subregion-specific, Learning- and Sleep-mediated Biosynthetic Changes 32

3.1 Abstract 32

3.2 Introduction 33

3.3 Results 35

3.3.1 Hippocampal engram neuron reactivation during post-learning sleep is subregion-specific. 35

3.3.2 Post-learning SD selectively suppresses activity of DG inferior blade granule cells. . 43

3.3.3 SD causes diverse and subregion-specific alterations in hippocampal gene expression, and drives distinctive responses in the DG blades. 46

3.3.4 DG transcriptional responses to SD can oppose those in CA1 and CA3, and suggest selective disruption of DG inferior blade activity. 58

3.3.5 Transcriptomic differences between superior and inferior DG blades are altered by SD vs. sleep. 63

3.3.6 CFC-induced transcriptomic effects in the hours following learning are restricted to the hippocampal DG. 69

3.3.7 SD and learning differentially affect protein and phosphoprotein abundance between hippocampal subregions 74

3.4 Discussion 81

3.5 Materials and Methods 89

3.6 References 98

Chapter 4 Conclusion and Future Directions 103

4.1 Conclusion 103

4.2 Future directions 106

4.3 References 109

List of Tables

Table 3.1 SD vs Sleep Upstream Regulator - Genes 79

Table 3.2 SD vs Sleep Upstream Regulator - miRNAs 79

Table 3.3 inf vs sup Upstream Regulator..... 80

List of Figures

Figure 1.1 Illustration of two hypotheses for sleep-dependent memory consolidation 2

Figure 1.2 Strategies for activity-dependent labeling in mice 4

Figure 1.3 cFos+ place cells' ensemble firing-rate correlations discriminated between familiar and novel contexts, but cFos- place cells' ensemble did not 6

Figure 2.1 Summary of both morphological and biochemical alterations to neuronal organelles following SD 20

Figure 3.1 Contextual fear conditioning (CFC) reactivates context-labeled neurons 37

Figure 3.2 Post-learning SD disrupts reactivation of dentate gyrus engram neurons in a subregion-specific manner 41

Figure 3.3 Post-learning SD selectively suppresses activity of DG inferior blade granule cells . 45

Figure 3.4 SD causes subregion-specific alterations in hippocampal gene expression 47

Figure 3.5 Select SD-altered transcripts' levels were altered in opposite directions across hippocampal subregions 59

Figure 3.6 Transcriptomic differences between superior and inferior DG blades 64

Figure 3.7 Learning (CFC)-induced transcriptomic effects are restricted to the hippocampal DG. 70

Figure 3.8 Learning and subsequent sleep or SD differentially affect protein expression in hippocampal subregions 76

Supplemental Figure S 3.1 Numbers of tdTomato+ and cFos+ neurons in the DG granule cell layer 38

Supplemental Figure S 3.2 Hippocampal hilus cFos+ tdTomato+ overlap showed no significant difference between any of the paradigms 40

Supplemental Figure S 3.3 Post-learning SD increased cFos+ tdTomato+ overlap in the hippocampal CA1 but not CA3 44

Supplemental Figure S 3.4 Principal component analysis and nuclei count for all regions of interest. 49

Supplemental Figure S 3.5 Overlap of SD-altered DEGs in the superior and inferior blade of DG, CA1, and CA3 51

Supplemental Figure S 3.6 SD-impacted gene ontology term ER chaperone complex 52

Supplemental Figure S 3.7 Differentially expressed pathway genes for SD-impacted pathways in hippocampal subregions 55

Supplemental Figure S 3.8 Diagrams of SD-impacted Circadian entrainment KEGG pathway (KEGG: 04713) in the superior blade, inferior blade, and CA1 56

Supplemental Figure S 3.9 SD vs. Sleep DEG overlap between hippocampal subregions. 62

Supplemental Figure S 3.10 Inferior vs. Superior blade differentially expressed genes annotated to the Regulation of actin cytoskeleton KEGG pathway 67

Supplemental Figure S 3.11 CFC-altered DEGs annotated to gene ontology term synaptic membrane 71

Supplemental Figure S 3.12 Venn diagrams show the overlap for transcripts altered by SD in each hippocampal subregion and those previously reported 85

Supplemental Figure S 3.13 Overlap of SD vs Sleep DEGs with previously-characterized SD-altered translating ribosome affinity purification-seq transcripts 86

Abstract

Over a century of research in both animal models and human subjects shows that sleep may improve, while sleep loss may disrupt, memory task performance. One prevailing hypothesis, active systems consolidation (ASC), posits that during sleep, neurons encoding newly acquired memories are reactivated, and the connections within the network get strengthened, resulting in the formation of a more persistent long-term memory. My thesis tests this hypothesis by quantifying the reactivation of memory traces in the mouse hippocampus during post-learning sleep. I also characterize learning- and sleep-induced biosynthetic changes in different subregions of the hippocampus to clarify the molecular mechanisms associated with this reactivation, in the context of sleep-dependent contextual fear memory consolidation.

Using the targeted recombination in active populations (TRAP) mouse line, I quantified reactivation of hippocampal context-activated engram neurons following contextual fear conditioning (CFC) and subsequent sleep or sleep deprivation (SD). I find that compared with SD, post-CFC sleep promoted reactivation of more engram cells in the hippocampal dentate gyrus (DG). Interestingly, this reactivation had a subregion-specific pattern, with significantly higher proportion of sleep-dependent reactivation in the inferior blade of DG compared with the superior blade.

To characterize learning- and sleep-induced biosynthetic changes in the hippocampus, I used spatial transcriptomics and protein profiling to measure expression changes in the hippocampal DG superior blade, inferior blade, hilus, CA1, and CA3 areas. I found that SD differentially altered the expression of genes in each hippocampal subregion, and hence,

differentially impacted various biological pathways in these subregions. I also found that several hours after learning, CFC-induced transcriptomic changes are restricted to the hippocampal DG granule cell layers, and are particularly affecting the synaptic components of neurons. Together, the results identify spatially divergent effects of learning and sleep in hippocampal subregions, which clarify the cellular- and network-level processes altered by sleep disruption.

Chapter 1 Introduction

1.1 Sleep and memory consolidation

Over a century of research suggests that sleep plays an important role in both learning new information and the storage of long-term memories – i.e., memory consolidation. In both animal models and human subjects, post-learning sleep was shown to have beneficial effects on memory consolidation in different tasks, with sleep deprivation (SD) following learning negatively impacting memory recall at later time points (1, 2). For example, in mice, 5 to 6 hours of SD immediately following single-trial contextual fear conditioning (CFC; pairing placement in a novel context with an aversive food shock) may disrupt hippocampus-mediated contextual fear memory (CFM) consolidation (3, 4).

Various hypotheses have been proposed to explain how sleep improves long-term memory storage. The synaptic homeostasis hypothesis (SHY), for example, posits that experience during wakefulness causes a net increase in synaptic strength throughout the brain, which leads to higher neuronal energy consumption and a reduction in signal-to-noise that subsequently interferes with the brain's ability to acquire and process new information. SHY proposes that sleep can globally downscale synaptic strength, saving energy and space in the brain, and increasing signal-to-noise ratio, resulting in enhanced memory task performance (Figure 1.1) (5). However, the idea of global downscaling during sleep is not fully supported by biological data (6). For example, serial electron microscopic measurements of cortical neuronal synapses suggest that only a subset of synapses undergo size reductions following a period of

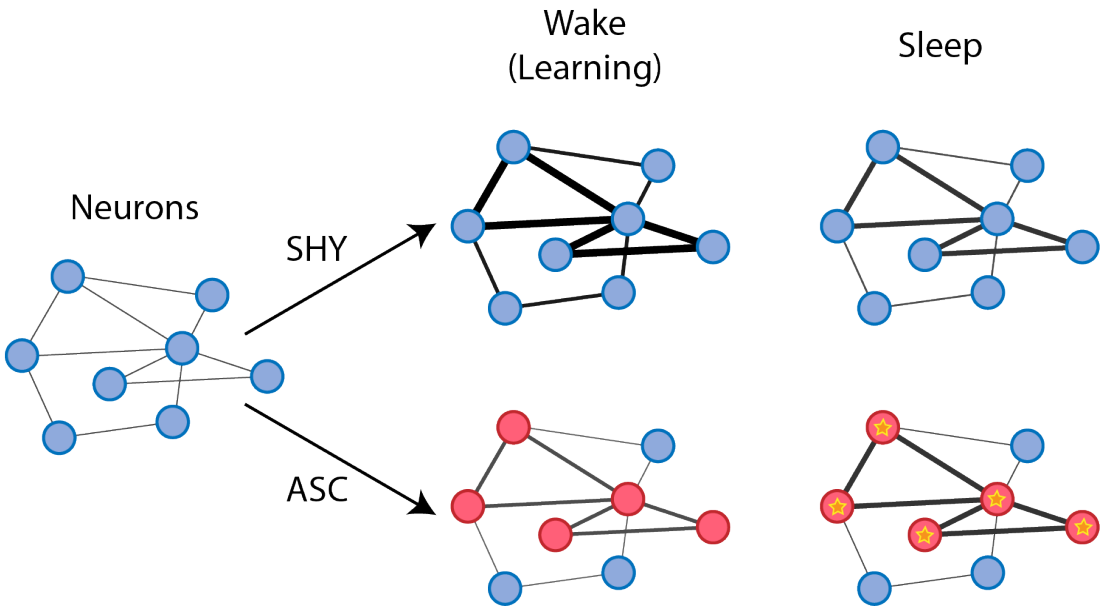

Figure 1.1 Illustration of two hypotheses for sleep-dependent memory consolidation. Homeostasis hypothesis (SHY) proposes that there the connections are strengthened during wakefulness and downscaled during sleep, resulting in an enhanced signal-to-noise ratio, and benefits on memory. Active systems consolidation (ASC) posits that newly acquired memory representations get reactivated during sleep, thus the connections are strengthened within the network, favoring the formation of a more persistent, long term memory.

sleep (compared with a similar period of sleep disruption) (7). Moreover, at the same time, longitudinal imaging of cortical neurons' synapses has suggested that dendritic spine formation is actually increased selectively during periods of post-learning sleep (8). Futhermore, longitudinal in vivo electrophysiological recordings from hippocampus and cortex showed that neurons actually present non-uniform changes in firing rate across sleep bouts (9, 10).

Another prevailing hypothesis regarding sleep's role in memory, active systems consolidation (ASC), posits that newly acquired memory representations – i.e., the neuronal populations that are activated during initial learning - get reactivated during subsequent sleep. This process is thought to occur particularly during slow wave sleep (SWS), strengthening the synaptic connections among learning-activated neurons within the network, and thus forming a more persistent, long term memory trace (**Figure 1.1**) (11).

While ASC and SHY may seem at first to conflict with each other, another possibility is that these processes work together. ASC may add to SHY, potentially explaining why only a subset of synapses downscale during sleep, while others are strengthened. Below, we will describe the phenomenon of memory trace reactivation in the hippocampus and cortex during post-learning sleep, as well as explore the molecular mechanisms underlying this phenomenon and its role in sleep-dependent memory consolidation.

1.2 Hippocampal place cells and engram cells

Place cells are neurons in the hippocampus that have spatial receptive fields (12). They were first described in the CA1 subregion of rat hippocampus using in vivo (extracellular) electrophysiological recording, but were soon also discovered in hippocampal CA2, CA3, and dentate gyrus (DG) (13). These neurons fire selectively when an animal visits specific locations ("place fields") within the environment it is placed in. These spatially-selective firing patterns are thought to be the foundation for an internal representation of space (14, 15).

Engram cells are neurons in hippocampus or cortex that are selectively activated during a specific sensory or associative learning experience. These neurons undergo enduring cellular changes (usually including immediate-early gene [IEG] mRNA and protein expression) following the experience, which outlast the transient period of elevated firing (16). Because of this elevated IEG expression, engram cells are commonly labeled and manipulated using transgenic mouse lines or transduction with viruses where transgene expression is driven by activity-regulated promoters (**Figure 1.2**) (17, 18). Optogenetic tools have been used in the past decade to demonstrate the role of engram cells in both the hippocampus and cortex in encoding and recall of specific memories. For example, using optogenetics to artificially reactivate a

hippocampal DG engram cell population activated during fear learning (i.e., CFC) produces fear memory (i.e., CFM) retrieval. On the other hand, optogenetically inhibiting the CFC DG engram population prevents the retrieval of CFM (16, 19).

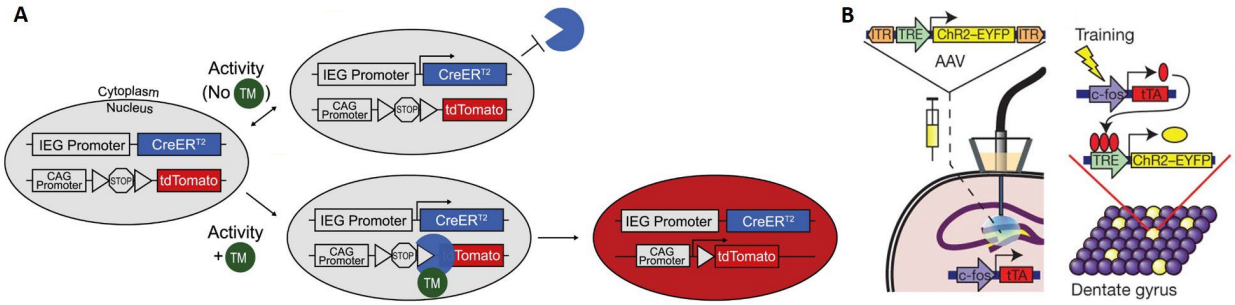

Figure 1.2 Strategies for activity-dependent labeling in mice. A. Targeted recombination in active populations (TRAP). Tamoxifen-dependent recombinase CreER^{T2} is expressed in an activity-dependent manner under the *Fos* immediate early gene promoter. Activated neurons that express CreER^{T2} undergo recombination and express the effector gene (e.g., tdTomato) only when tamoxifen is present. Figure adapted from Guenthner et al., 2013 **B.** The c-fos-tTA mouse was injected with AAV9-TRE-ChR2-EYFP. In the absence of doxycycline, training induces tTA expression. tTA binds to TRE and drives the expression of ChR2-EYFP only in activated cells (yellow). Figure adapted from Liu et al., 2012.

Fluorescent labeling of memory-encoding neurons using IEG-based promoters has also provided new information about memory recall and encoding. For example, within the hippocampal DG, the principal (excitatory) neurons (including place cells and engram cells) are distributed in two separate bands – the suprapyramidal (superior) blade and the infrapyramidal (inferior blade). Recently, it was shown that a wide range of behaviors (including CFM encoding, spatial navigation, socialization, and stress) preferentially activated engram cells of the suprapyramidal blade compared with the infrapyramidal blade (20).

Finally, while the firing activities of both place cells and engram cells are linked to the exploration of a novel context, the exact relationship between the place cells that represent the animal's moment-to-moment location (i.e., their route through the environment) and the engram cell population that represents the contextual memory trace still remains largely unknown.

So far, only one recent study made an effort to directly compare the physiology of the place cell and engram cell populations during contextual memory encoding (21). In this study, Tanaka et al. analyzed tetrode recordings from CA1 pyramidal cells in freely moving c-Fos-tTA (tetracycline-transactivator) transgenic mice and they observed that a large proportion (79.31%) of previously-fluorescently-labeled context-activated engram cells (c-Fos+) had a place field (based on firing pattern) in the re-explored context. Meanwhile, only a small fraction (24.47%) of all active place cells were previously context-labeled c-Fos+ neurons (**Figure1.3 A**). While the peak firing rate of these two populations were similar, the c-Fos+ neurons exhibited higher mean firing rates, had larger place fields, and their spikes carried less spatial information compared with other place cells. Further, the ensemble firing-rate correlations of c-Fos positive place cells reliably discriminated between familiar and novel contexts, whereas the firing rate of the c-Fos negative place cell ensemble did not (**Figure1.3 B, C**). Interestingly, during same-context re-exploration, context-labeled c-Fos+ (engram) cells significantly shifted their preferred firing locations (i.e., place fields) compared with the place cells. These data suggest that c-Fos+ (engram) neurons remained highly context-specific, but did not simply keep their previous place fields. In summary, the research posits that engram cells have lower spatial stability and accuracy compared with other place cells, but nonetheless have the ability to reliably and specifically encode environmental context.

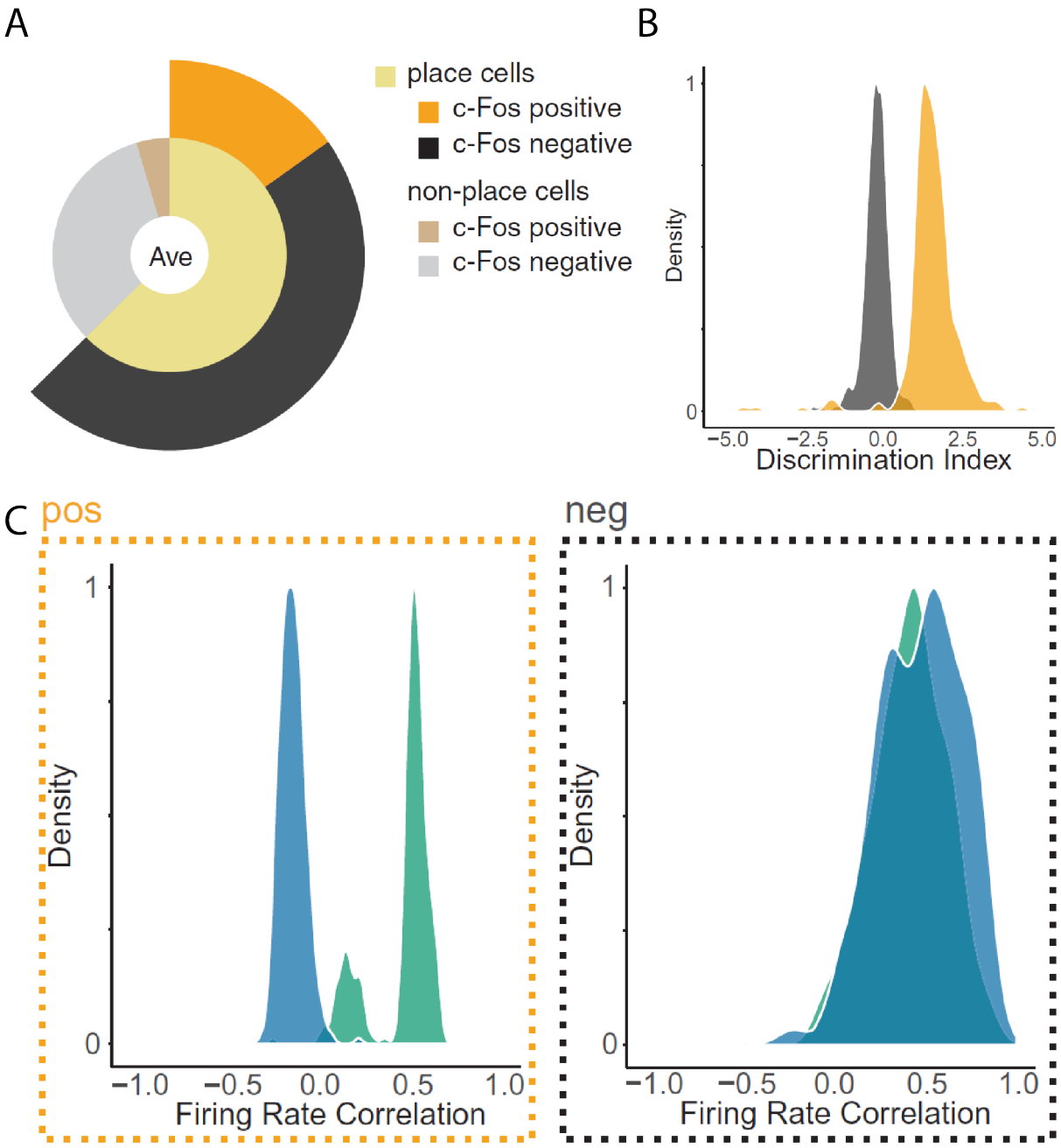

Figure 1.3 cFos+ place cells' ensemble firing-rate correlations discriminated between familiar and novel contexts, but cFos- place cells' ensemble did not. A. Average percentages of each cell type in recorded mice. **B.** Discrimination indexes of cFos+ (orange) or cFos- (black) ensemble firing-rate correlations. **C.** Ensemble firing-rate correlations of cFos+ (orange dashed square) or cFos- (black dashed square) place cells between context A (encoding) to A (recall) (green) vs. A (encoding) to B (novel) (blue). Figure adapted from Tanaka et al., 2018.

1.3 Place cell replay during sleep

The offline replay of place cell firing patterns was first observed by Pavlides and Winson (using in vivo electrophysiological recording) in 1989 (22). They observed that by exposing rats to a given location during wakefulness, the spiking activity of hippocampal CA1 place cells encoding that location in their place field, but not other place cells, significantly increased in the subsequent sleeping states. In 1994, Wilson and McNaughton used simultaneous recordings from ensembles of CA1 place cells to show that cells whose place fields overlapped during spatial tasks had an increased tendency to fire together during subsequent sleep (23). By 1996, this phenomenon was further shown to have preserved a temporal order – the relative timing of the place cells' firing activity during sleep reflected the sequence in which those neurons fired during a previous period of spatial exploration (24). And within a few years, more studies had demonstrated the offline sequential replay of CA1 place cell activity during SWS, which preferentially occurred in close temporal proximity to sharp wave ripples (SPW-Rs) – large periodic depolarizing events initiated by input to CA1 from CA3 (25-27). Intriguingly, the replay of the patterns during sleep (i.e., the relative timing of spiking between individual neurons) was at a much faster speed compared with during the actual experience (28).

Efforts have been made to manipulate, and disrupt, these replay events during SWS to test for the necessity of replay for memory consolidation. Girardeau et al. selectively disrupted hippocampal activity patterns during SPW-Rs using hippocampal commissural stimulation (29). When this disruption was targeted to post-learning sleep, hippocampal spiking activity was silenced transiently, preventing the replay of place cell sequences that were activated during prior spatial memory task training. Performance impairments were observed in rats that received selective elimination of SPW-Rs during post-training sleep. Similar effects were observed

following CA1 cellular activity perturbation during the SPW-Rs in rats (30, 31). Further, optogenetically silencing hippocampal SPW-Rs during post-learning sleep was shown to impair neuronal co-firing pattern reinstatement upon re-exposure to the learning context (32). Together these data suggest that SWS SPW-Rs may promote sleep-dependent spatial memory storage, by promoting reactivation and sequential replay of place cells activated during prior learning.

So far, researchers have been able to 1) show the existence of place cell replay during sleep, especially during SPW-Rs, 2) prolong SPW-Rs ripples to improved hippocampus-dependent memory task performance (33) and 3) disrupt the replay through cellular activity inhibition or SPW-R perturbation to impair spatial memory performance. However, it is worth noting that for technical reasons, the aforementioned studies used interventions that disrupted or changed activity across CA1, rather than only manipulating the activity of place cells or their sequential replays. Thus, there remains a lack of direct evidence for the necessity and sufficiency of place cell replay in spatial (or contextual) memory consolidation.

1.4 Hippocampal engram ensemble reactivation during sleep

DG and CA1 hippocampal engram cells were the first characterized and manipulated engram cell populations in the brain. Compared with the topic of place cell replay during sleep, far fewer studies have investigated sleep-dependent reactivation of engram cells, potentially because of the relatively recent development of genetic tools for labeling and optogenetically manipulating engram cells.

Ghandour et al. analyzed engram cell activity during CFC and post learning sleep in the mouse hippocampal CA1 by tracking in vivo Ca2+ signals (34). Ca2+ transients were recorded during several sessions, including a contextual learning session A, two post-learning non-rapid

eye movement (NREM) sleep sessions B and C, one REM sleep session D, one memory retrieval session E (where mice were re-exposed to the same context), and finally, a different context session F. By comparing the fraction of co-activated CA1 neuronal ensembles in one session vs. another, the authors found that co-activated engram cell sub-ensembles showed a high level of co-activation across various sessions. In contrast, non-engram cells had extremely low and inconsistent co-activation. Further, engram ensembles co-activated during the learning session that were reactivated during subsequent sleep sessions (NREM or REM) were most consistently reactivated during subsequent memory retrieval. By contrast, most non-engram ensembles that were activated during the learning session were not reactivated in the later sessions. This study, which to date has provided the most direct observation of engram cell ensemble activity during learning, subsequent sleep, and retrieval, has shown that sub-ensembles of an engram population that represent a contextual memory trace reactivate during post-learning NREM and REM sleep. However, it remains unclear whether this reactivation is dependent on post-learning sleep, which is essential to many forms of hippocampus-mediated memory storage. Moreover, future studies will be needed to characterize the pattern of activity in CA1 and DG engram populations across time (i.e. during REM and NREM sleep) and to test for necessity and sufficiency of engram ensemble reactivation for memory consolidation.

1.5 Cortex engram ensemble reactivation during sleep

In addition to engram ensembles found in the hippocampus, several recent studies have identified engram populations in the cortex. Similar to observations with hippocampal fear memory engram cell reactivation, reactivation of fear learning-related cortical engram populations are sufficient to elicit a fear response (35-38), while silencing these engram cells

impairs fear memory retrieval (36, 37). While the selectivity of these engram populations for specific memories has been demonstrated, there has been relatively little study of cortical engrams' offline reactivation during post-learning sleep.

Clawson et al. observed that following visually cued learning experience, primary visual cortex (V1) ensembles activated by visual stimuli paired with foot shock (orientation-selective neurons for X°) were reactivated (by observing cFos expression) during subsequent sleep (38) in the TRAP mouse line (17). When sleep-dependent reactivation of those learning-activated V1 ensembles was optogenetically inhibited, mice exhibited generalized fear (i.e. high levels of freezing during presentation of both shock-predictive cues and neutral cues) while control mice (received no optogenetic engram inhibition) successfully discriminated between shock and neutral cues (i.e., freezing more during presentation of the shock cue). This study demonstrated that visual memory consolidation can be disrupted by a lack of proper engram reactivation during sleep.

The authors of another recent study used post-learning optogenetic reactivation of engram ensembles in the retrosplenial cortex (RSC) (39) of cfos-tTA/tetO-ChEF transgenic mice to drive a process known as "systems memory consolidation". After this pattern of stimulation, the memory showed decreased hippocampal dependence, context generalization, and increased cortical activity during memory retrieval. Interestingly, these systems memory consolidation features were only observed when RSC engram cell stimulation was given in sleeping or anesthetized mice, but not in active awake mice, indicating that these memory storage changes are brain state dependent.

1.6 Comparing engram vs. place cell reactivation during sleep

Both place cells and engram cells reactivate during post-learning sleep. However, the observed pattern of reactivation appears to differ between the two populations. The reactivation of place cells recapitulates the sequence of the neurons' relative firing during the context exploration, but often occurs at a much faster (i.e., compressed) speed. On the other hand, engram neurons may be reactivated simultaneously in the form of sub-ensembles. These findings reflect those of Tanaka et al., 2018, which showed that an engram cell population's ensemble firing rate discriminated between familiar and novel contexts, while the corresponding place cell ensemble firing rate failed to do so. Together this indicates that regardless of brain state, compared with place cells, the engram population tends to function as units of (sub)ensembles, and provides a firing rate-based population code to both encode and store memories of specific events. Whether engram cells reactivate during sleep following the same sequential order as their activities during encoding still remains unclear.

1.7 Effects of sleep and sleep loss on engram populations' transcriptomes

In the last few years, there has also been considerable progress in the transcriptomic analysis of learning-related changes in experience-activated engram cells. Transcriptomic profiles of these populations were obtained in the hours following learning using RNA-seq, single-cell (sc), and single-nucleus (sn) RNA-seq from DG, CA1, and cortex areas (40). These studies showed that transcription and chromatin conformation changes occurred in the nucleus of the experience-activated cells during the first 24 h following learning. However, relatively little is known about how post-learning sleep and sleep disruption may affect this process.

One recent study by Delorme et al. profiled a subset of highly active hippocampal neurons that expressed Ser244/247 phosphorylated ribosomal subunit S6 (pS6+; a neuronal activity-regulated phosphorylation event) (41). Ribosome-associated messenger RNA were obtained through translating ribosome affinity purification following CFC and 3 hours of either sleep or SD. The authors found that CFC altered 1908 transcripts in pS6+ neurons in the hippocampus of SD mice, and 2211 transcripts from pS6+ neurons of freely sleeping mice. Only 964 CFC-altered transcripts overlapped between SD and sleep mice, indicating that the effects of learning differed in these pS6+ neurons as a function of subsequent sleep. Further, they observed that SD occluded CFC-induced changes to specific transcripts in pS6+ neurons, which may account for memory consolidation disruption by post-learning SD. However, an important caveat to this study is that the profiled pS6+ neuron population reflects neurons with activity not only driven during learning itself, but during the subsequent 3 hours of sleep or SD. In other words, it is unlikely that this population reflects engram cells activated solely due to learning. Further, this population of neurons' ribosomal RNA was also collected from the whole hippocampus, which may mask hippocampal subregion-specific transcript changes.

So far, no study has examined the effect of sleep and sleep loss on the transcriptome in engram neurons using one of the genetic labeling strategies (transgenic mouse lines or transduction with viruses based on activity-regulated promoters). Future studies comparing the effect of post-learning sleep both between engram and non-engram population, and between different brain regions/subregions, will be important for scientists to understand the molecular and brain circuit-level mechanisms underlying sleep's effects on learning and memory.

1.8 Conclusions

Sleep-dependent neuronal reactivation has long been proposed to play an important role in memory consolidation. The phenomenon has been observed in two different hippocampal cell populations – engram cells and place cells. Engram cells and place cells have intrinsic physiological differences during contextual memory encoding and retrieval. During post-learning NREM and REM sleep, engram cells reactivate in sub-ensembles, while place cells reactivate sequentially during SWS at a much faster rate. There remain quite a few questions for future work. For example, do engram cells' and place cells' reactivation facilitate sleep-dependent memory consolidation? Do they do so through the same or different mechanisms? How does sleep loss affect engram cells' and place cells' transcriptome and epigenome? What does synaptic scaling look like in both populations during sleep? Future work that integrates neuronal network electrophysiological recordings, next generation sequencing, and in vivo imaging will be required to understand how the dynamics of information flow in the hippocampal circuit contributes to the encoding and recall processes it supports.

1.9 Dissertation Outline

The aim of my thesis is to investigate how post-learning sleep loss affects memory consolidation, with a focus on hippocampal subregion-specific memory trace reactivation and regulation of gene and protein expression. I also review current literature on the effect of sleep loss on various subcellular structures and cellular processes in neurons, which likely contributes to the effects of sleep on memory storage.

In Chapter II, I discuss how sleep loss disrupts biosynthetic processes, with a focus on 1) nuclear function of the neurons, transcription, and translation; and 2) other organelles

(mitochondria, Golgi, endoplasmic reticulum) of the neurons and the processes they regulate, such as intracellular transport and metabolism.

In Chapter III, I use targeted recombination in activated populations (TRAP) to label context-encoding engram neurons in the hippocampus, to test whether SD following learning disrupts the reactivation of hippocampal engram neurons in different hippocampal subregions. I use hippocampal subregion-specific profiling of transcripts and proteins to further characterize how learning and subsequent sleep or SD affect hippocampal subregions.

Together, these studies provide a clearer picture of the sleep-dependence of engram neuron reactivation in the context of hippocampal memory storage, the cellular processes that may be affected by post-learning SD, and the spatial distribution of these effects within the hippocampus.

1.10 References

1. B. Rasch, J. Born, About sleep's role in memory. Physiol Rev 93, 681-766 (2013).

2. S. Diekelmann, J. Born, The memory function of sleep. Nat Rev Neurosci 11, 114-126 (2010).

3. L. A. Graves, E. A. Heller, A. I. Pack, T. Abel, Sleep deprivation selectively impairs memory consolidation for contextual fear conditioning. Learn Mem 10, 168-176 (2003).

4. N. Ognjanovski, C. Broussard, M. Zochowski, S. J. Aton, Hippocampal Network Oscillations Rescue Memory Consolidation Deficits Caused by Sleep Loss. Cereb Cortex 28, 3711-3723 (2018).

5. G. Tononi, C. Cirelli, Sleep and the price of plasticity: from synaptic and cellular homeostasis to memory consolidation and integration. Neuron 81, 12-34 (2014).

6. C. Puentes-Mestril, S. J. Aton, Linking Network Activity to Synaptic Plasticity during Sleep: Hypotheses and Recent Data. Front Neural Circuits 11, 61 (2017).

7. L. de Vivo et al., Ultrastructural evidence for synaptic scaling across the wake/sleep cycle. Science 355, 507-510 (2017).

8. G. Yang et al., Sleep promotes branch-specific formation of dendritic spines after learning. Science 344, 1173-1178 (2014).

9. H. Miyawaki, K. Diba, Regulation of Hippocampal Firing by Network Oscillations during Sleep. Curr Biol 26, 893-902 (2016).

10. B. O. Watson, D. Levenstein, J. P. Greene, J. N. Gelinas, G. Buzsaki, Network Homeostasis and State Dynamics of Neocortical Sleep. Neuron 90, 839-852 (2016).

11. J. G. Klinzing, N. Niethard, J. Born, Mechanisms of systems memory consolidation during sleep. Nature Neuroscience 22, 1598-1610 (2019).

12. J. O'Keefe, J. Dostrovsky, The hippocampus as a spatial map. Preliminary evidence from unit activity in the freely-moving rat. Brain Res 34, 171-175 (1971).

13. T. Hartley, C. Lever, N. Burgess, J. O'Keefe, Space in the brain: how the hippocampal formation supports spatial cognition. Philos T R Soc B 369 (2014).

14. E. C. Tolman, Cognitive maps in rats and men. Psychol Rev 55, 189-208 (1948).

15. J. O'Keefe, The hippocampus as a cognitive map (Oxford, 1981).

16. S. A. Josselyn, S. Tonegawa, Memory engrams: Recalling the past and imagining the future. Science 367 (2020).

17. C. J. Guenthner, K. Miyamichi, H. H. Yang, H. C. Heller, L. Luo, Permanent genetic access to transiently active neurons via TRAP: targeted recombination in active populations. Neuron 78, 773-784 (2013).

18. X. Liu et al., Optogenetic stimulation of a hippocampal engram activates fear memory recall. Nature 484, 381-385 (2012).

19. S. Tonegawa, M. D. Morrissey, T. Kitamura, The role of engram cells in the systems consolidation of memory. Nat Rev Neurosci 19, 485-498 (2018).

20. S. R. Erwin et al., A Sparse, Spatially Biased Subtype of Mature Granule Cell Dominates Recruitment in Hippocampal-Associated Behaviors. Cell Rep 31, 107551 (2020).

21. K. Z. Tanaka et al., The hippocampal engram maps experience but not place. Science 361, 392-397 (2018).

22. C. Pavlides, J. Winson, Influences of hippocampal place cell firing in the awake state on the activity of these cells during subsequent sleep episodes. J Neurosci 9, 2907-2918 (1989).

23. M. A. Wilson, B. L. McNaughton, Reactivation of hippocampal ensemble memories during sleep. Science 265, 676-679 (1994).

24. W. E. Skaggs, B. L. McNaughton, Replay of neuronal firing sequences in rat hippocampus during sleep following spatial experience. Science 271, 1870-1873 (1996).

25. A. K. Lee, M. A. Wilson, Memory of sequential experience in the hippocampus during slow wave sleep. Neuron 36, 1183-1194 (2002).

26. K. Diba, G. Buzsaki, Forward and reverse hippocampal place-cell sequences during ripples. Nat Neurosci 10, 1241-1242 (2007).

27. T. J. Davidson, F. Kloosterman, M. A. Wilson, Hippocampal replay of extended experience. Neuron 63, 497-507 (2009).

28. G. Findlay, G. Tononi, C. Cirelli, The evolving view of replay and its functions in wake and sleep. Sleep Adv 1, zpab002 (2020).

29. G. Girardeau, K. Benchenane, S. I. Wiener, G. Buzsaki, M. B. Zugaro, Selective suppression of hippocampal ripples impairs spatial memory. Nat Neurosci 12, 1222-1223 (2009).

30. V. Ego-Stengel, M. A. Wilson, Disruption of ripple-associated hippocampal activity during rest impairs spatial learning in the rat. Hippocampus 20, 1-10 (2010).

31. I. Gridchyn, P. Schoenenberger, J. O'Neill, J. Csicsvari, Assembly-Specific Disruption of Hippocampal Replay Leads to Selective Memory Deficit. Neuron 106, 291-300 e296 (2020).

32. G. M. van de Ven, S. Trouche, C. G. McNamara, K. Allen, D. Dupret, Hippocampal Offline Reactivation Consolidates Recently Formed Cell Assembly Patterns during Sharp Wave-Ripples. Neuron 92, 968-974 (2016).

33. A. Fernandez-Ruiz et al., Long-duration hippocampal sharp wave ripples improve memory. Science 364, 1082-1086 (2019).

34. K. Ghandour et al., Orchestrated ensemble activities constitute a hippocampal memory engram. Nat Commun 10, 2637 (2019).

35. K. K. Cowansage et al., Direct reactivation of a coherent neocortical memory of context. Neuron 84, 432-441 (2014).

36. C. Meissner-Bernard, Y. Dembitskaya, L. Venance, A. Fleischmann, Encoding of Odor Fear Memories in the Mouse Olfactory Cortex. Curr Biol 29, 367-380 e364 (2019).

37. T. Kitamura et al., Engrams and circuits crucial for systems consolidation of a memory. Science 356, 73-78 (2017).

38. B. C. Clawson et al., Causal role for sleep-dependent reactivation of learning-activated sensory ensembles for fear memory consolidation. Nat Commun 12, 1200 (2021).

39. A. F. de Sousa et al., Optogenetic reactivation of memory ensembles in the retrosplenial cortex induces systems consolidation. Proc Natl Acad Sci U S A 116, 8576-8581 (2019).

40. M. Fuentes-Ramos, M. Alaiz-Noya, A. Barco, Transcriptome and epigenome analysis of engram cells: Next-generation sequencing technologies in memory research. Neurosci Biobehav Rev 127, 865-875 (2021).

41. J. Delorme et al., Hippocampal neurons' cytosolic and membrane-bound ribosomal transcript profiles are differentially regulated by learning and subsequent sleep. Proc Natl Acad Sci U S A 118 (2021).

Chapter 2 Ultrastructural Analyses Reflect the Effects of Sleep and Sleep Loss on Neuronal Cell Biology

This chapter includes the review article: Wang, L., & Aton, S. J. (2022). Perspective–ultrastructural analyses reflect the effects of sleep and sleep loss on neuronal cell biology. *Sleep*, *45*(5), zsac047.

2.1 Introduction

Sleep loss affects brain function in numerous ways, including disrupting both working and long term memory, attention, and decision making (1). While the last two decades have provided new insights into how sleep loss affects neural activity (2-6), gene expression (7-9), and protein translation (10-12), a complete understanding of the cell biological effects of sleep deprivation (SD) in the brain is still lacking. Recent electron microscopic analyses of neurons in the *Drosophila* and rodent brain demonstrate that acute or chronic sleep loss can alter the structures of various organelles, including mitochondria, nucleus, and Golgi apparatus. Here, we discuss these ultrastructural changes in the context of biochemical findings from the sleep deprived brain, to clarify how these morphological changes may relate to altered cellular processes like transcription, translation, intracellular transport, and metabolism. A better understanding of these effects will have broad implications for understanding the biological importance of sleep, and the relationship of sleep loss to neuropathology.

2.2 Effects of sleep loss on neuronal nuclear function

A recent serial block-face electron microscopy (SBEM) study showed that in *Drosophila* brain Kenyon cells, both 11-h and 35-h of SD significantly increased the number and density of electron-dense "dark clusters" of chromatin within the nucleus (13), which suggests possible epigenetic changes to neurons as a function of sleep loss. A similar phenomenon was reported using EM - with electron-dense clusters observed in rat hippocampal neurons' nuclei after chronic (14-day) sleep restriction, with or without caffeine administration (14). Although the exact driver of cluster formation is still unclear, such clusters likely reflect the same process of heterochromatin formation observed in mammals in the context of both cellular senescence (15) and neuronal plasticity (16). The increased number and density of heterochromatin clusters after longer-duration SD suggests that long-term sleep loss may disrupt patterns of transcriptionally-active DNA in neurons. Several lines of evidence support this idea (**Figure 2.1**). For example, one recent study using an assay for transposase-accessible chromatin with sequencing (ATAC-seq) to identify transcriptionally-accessible regions of DNA showed that SD rapidly (within as little as 3 h) and dramatically changes chromatin accessibility in the mouse cerebral cortex. Surprisingly, however, the vast majority of the differentially accessible DNA sites showed increased, rather than decreased, accessibility after SD (17) - which is more typical of euchromatin. SD may also affect transcription by altering DNA methylation. Studies using methylated DNA immunoprecipitation in rat cortex (18) and 5 mC and 5 hmC arrays in mouse cortex (19) have demonstrated altered methylation patterns after as little as 3-6 h of SD, which are associated with bidirectional changes in gene transcription. SD may also affect histone acetylation, which increases DNA accessibility to transcription factors. Recent findings suggest that both acute and chronic SD increase histone deacetylase activity, reducing levels of histone

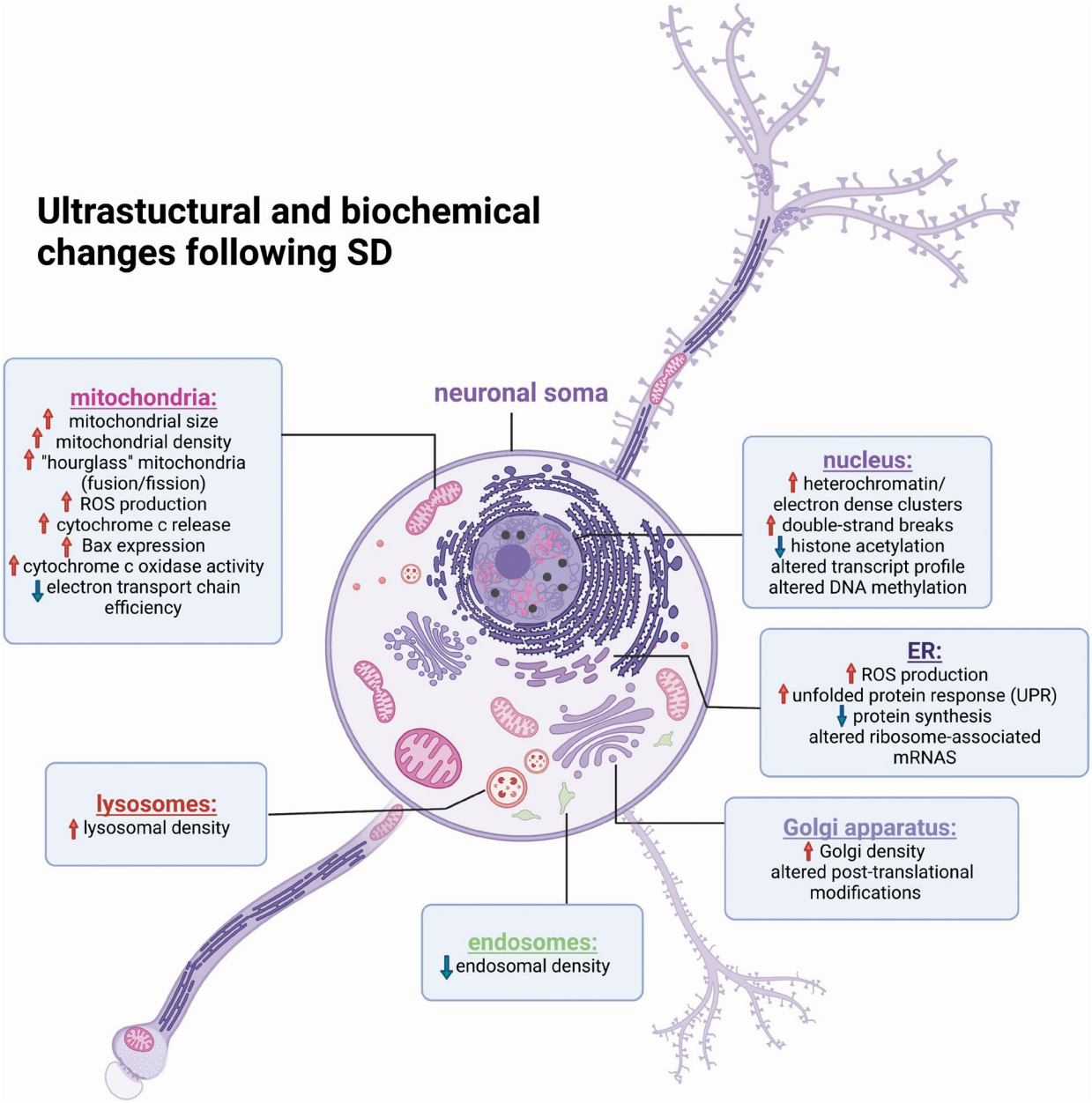

Figure 2.1 Summary of both morphological and biochemical alterations to neuronal organelles following SD. While many organelles such as mitochondria, Golgi, and ER are also present in axons and dendrites, it is unclear how morphology changes in those structures with SD. It is also unclear whether biochemical/functional changes to organelles are cell compartment-specific. Figure was created with BioRender.com.

H3 and H4 acetylation in mouse and rat brain (20-22). Treating animals with histone deacetylase inhibitors rescued both SD-induced cognitive disruption (20, 22) and late long-term potentiation (LTP) impairments caused by SD (20). Histone deacetylation could drive formation of heterochromatin, and thus the formation of electron-dense nuclear clusters reported by Flores et al. and Xie et al (14, 23).

However, another possibility is that these dark clusters reflect sites of DNA damage, such as those occurring during senescence (15). It is thought that heterochromatin regulation after DNA damage is important for silencing damaged genes, maintaining genomic stability (24). Prolonged wake induces double-strand breaks in DNA within *Drosophila* neurons (**Figure 2.1**), and SD can disrupt repair of these breaks (25). More recent work in zebrafish has shown that sleep facilitates neuronal chromosome rearrangements essential for DNA repair, while SD disrupts these mechanisms (26). One possibility is that DNA damage accumulation during SD (through generation of reactive oxygen species; ROS (27, 28), or other mechanisms) ultimately leads to neuronal senescence and cell death. Indeed, recent data suggest that neurodegeneration can be triggered in the mammalian brain through this SD-driven mechanism (29).

Thus, a critical unanswered question from these observations centers on clarifying the precise nature of these electron-dense nuclear clusters. Understanding how their formation reflects DNA damage, repair, and transcriptional regulation will be essential for understanding how SD affects the most fundamental cell biological processes of neurons - i.e., central dogma (DNA→mRNA→protein) and cell survival.

2.3 Sleep deprivation, cellular energetics, and mitochondrial function

Mitochondria produce energy for the brain in the form of ATP. This bioenergetic function is regulated by sleep-wake cycles, with higher levels of ATP in wake-active regions of the brain during spontaneous sleep, and ATP reduction during SD (30). As a byproduct of ATP production, mitochondria generate ROS. Alterations in mitochondrial function could thus couple sleep loss to oxidative stress-mediated DNA damage. Multiple studies across species have found that ROS are generated at higher levels in the brain during prolonged SD (31-33) (**Figure 2.1**). This is despite (or perhaps, due to) the fact that prolonged sleep disruption reduces efficiency of the ATP-generating mitochondrial electron transport chain. Critically, this reduction persists in some regions of the brain even after the opportunity for recovery sleep (34). In turn, generation of ROS in mitochondria is directly coupled to sleep homeostatic responses in sleep regulating neurons in the *Drosophila* brain (28, 31).

Beyond the effects of SD on mitochondrial energetics, long-term sleep disruption has also been shown to increase Bax expression in mitochondria in the hippocampus, and release of cytochrome c from mitochondria into the cytoplasm (35) (**Figure 2.1**). These changes have been linked to both reduced excitability in hippocampal neurons (likely due to reduced ATP (35)) and initiation of neuronal apoptosis and neurodegeneration (36).

Available data suggest that at least in the first hours of sleep loss, neuronal mitochondria respond to this energetic challenge in several ways. Mitochondria in the mammalian neocortex show upregulation of cytochrome c oxidase expression and activity (37-39) and antioxidant responses (32) after 3-12 h of SD (**Figure 2.1**). The morphological changes described in Flores et al. after more prolonged SD in flies (23), and described in de Vivo et al. in mice (40), may also be an adaptive response to SD-driven disruption of mitochondrial metabolic function. One

possibility is increasing mitochondrial abundance in neuronal somata is essential for neurons to survive SD-induced disruption of electron transport chain efficiency. This process could be driven by *de novo* organelle biogenesis (41), mitochondrial transportation to the soma from other cellular compartments (i.e., neurites) (42), or increased mitochondrial biogenesis through fission (43). The recent report of an increased proportion of "hourglass"-shaped mitochondria after SD in mouse pyramidal neurons (40) (**Figure 2.1**) suggests that either mitochondrial fission or fusion may be enhanced by sleep loss. Reported increases in "hourglass"-shaped mitochondria, the presence of "extra-large" mitochondria (40), and a trend toward higher proportion of hyperfused mitochondria (23) after prolonged SD may also reflect the formation of so-called "megamitochondria" through membrane fusion. Megamitochondrial formation likely reflects a process aimed at combating the unfavorable cellular environments and decreasing intracellular ROS level (44) following acute or prolonged SD. While both fission and fusion can be adaptive cellular responses to mitochondrial stress, it is important to note that both are also an essential feature of apoptosis (44, 45).

Other morphological changes to neuronal mitochondria themselves have been reported after prolonged SD - e.g., decreased relative volume of intercristal space, which have been reported in both rat hippocampus and neocortex (46).These intra-organelle morphological changes may relate to SD-driven changes in mitochondrial cristae functions - e.g. changes in cytochrome c storage or electron transport chain activity (46-48). Taken together, the reported effects of SD on mitochondrial morphology suggest a major impact of sleep loss on neuronal energy production, and potentially also on neuronal viability.

2.4 Neuronal proteostasis, and intraneuronal transport - effects of sleep loss on Golgi, endoplasmic reticulum (ER), endosomes, and lysosomes

Recent SBEM data from *Drosophila* brain Kenyon cells also showed a non-significant trend for increased density of Golgi apparatus per Kenyon cell body after longer-duration SD (23). While previous mouse cortex EM data did not directly measure Golgi or ER, they did report significant increases in pyramidal neurons' lysosomal size and density with acute and chronic SD, respectively, and reductions in endosomal density with chronic SD (40). Because the ER, Golgi, lysosomes, and endosomes mediate membrane-associated protein production, trafficking and quality control, together these ultrastructural findings could reflect SD-induced alterations to intracellular transport and proteostasis.

Across species, biochemical (8, 49-52), transcriptomic (7, 53), and ribosome profiling (8, 12) data suggest that protein translation/quality control and transport are affected by acute sleep loss. For example, in nematodes, *Drosophila*, and mice (49, 51), a brief period of SD leads to an enhanced unfolded protein response (UPR; the cellular stress response to accumulation of misfolded protein in the ER lumen) (**Figure 2.1**). Early SD-induced UPR effects in the brain include suppression of protein translation (10), post-translational modification (54), and increased expression of molecular chaperones (52, 55, 56). While these changes may aid in normalizing protein quality under conditions of cellular stress, sustained UPR activation engages pro-apoptotic pathways (57, 58), ultimately leading to neurodegeneration.

Disruption of ER function also impacts nuclear function. Critically, another site of potentially DNA-damaging ROS production in neurons is the ER, where ROS are made in the process of chaperone-assisted protein folding (59, 60). Thus, one possibility is that some of the

increased ROS observed in the brain with SD are generated by changes to biochemical processes within the ER (**Figure 2.1**).

Changes in Golgi density, lysosomal size and density, and endosome density after SD all suggest that neuronal transport and quality control of membrane-associated protein cargo may change with sleep loss. Critically, however, analysis of these structures within the cell body alone cannot give a complete picture of how sleep loss affects protein synthesis, quality control, and transport. Moreover, to date, there is no data on how sleep loss affects the subcellular distribution of the Golgi, ER, lysosomes, or endosomes in neurons. Appropriate subcellular localization and organization of these organelles is essential for spatial regulation of both protein and mRNA, which in neurons plays vital roles in neurotransmission, synaptic plasticity, and information storage (8, 61, 62). Beyond these essential functions, the presence of Golgi and ER in neurites plays additional roles, including local calcium buffering, regulation of synaptic extracellular glycoproteins, and lipid biogenesis (63, 64). A recent study from our lab, using neuronal compartment-specific ribosome profiling, demonstrates that mRNAs translated in these membrane-bound organelles vary dramatically with both prior learning and subsequent sleep or SD (8). Understanding how sleep and SD affect intra-neuronal movement of these organelles and their functions in neurites will be essential to understanding how sleep and sleep loss affect neuronal cell biology.

2.5 Future directions

As is true with transcriptomic and biochemical responses to sleep loss, available data suggest that cellular structures changes may also be conserved in neurons across species. This raises a biologically important question – what do these structural changes indicate with respect

to the physiological and metabolic processes occurring within neurons? It will be vital for future studies to explore the relationships between the morphological changes present in neuronal organelles after SD, the biochemical and physiological changes occurring within those organelles, and the neuronal and brain-level functional changes due to sleep disruption. Moreover, studies of how organelle morphology, function, and transport within axonal and dendritic cell compartments are affected by sleep and SD will be vital to clarify how brain states affect the cell biology of these essential neuronal structures. Finally, further work is needed to understand 1) what aspects of sleep and SD control these basic mechanisms and 2) how neuronal cellular changes affect the brain and cognition. Progress on these fronts should yield clues to essential, evolutionarily-conserved, sleep functions.

2.6 References

1. P. Alhola, P. Polo-Kantola, Sleep deprivation: Impact on cognitive performance. *Neuropsychiatr Dis Treat* **3**, 553-567 (2007).

2. C. Puentes-Mestril, S. J. Aton, Linking network activity to synaptic plasticity during sleep: hypotheses and recent data. *Frontiers in Neural Circuits* **11**, doi: 10.3389/fncir.2017.00061 (2017).

3. C. Puentes-Mestril, J. Roach, N. Niethard, M. Zochowski, S. J. Aton, How rhythms of the sleeping brain tune memory and synaptic plasticity. *Sleep* **42**, pii: zsz095 (2019).

4. V. V. Vyazovskiy *et al.*, Cortical firing and sleep homeostasis. *Neuron* **63**, 865-878 (2009).

5. J. Delorme *et al.*, Sleep loss drives acetylcholine- and somatostatin interneuron-mediated gating of hippocampal activity, to inhibit memory consolidation. *Proc Natl Acad Sci USA* **118** (2021).

6. N. Niethard *et al.*, Sleep-Stage-Specific Regulation of Cortical Excitation and Inhibition. *Curr Biol* **26**, 2739-2749 (2016).

7. M. Mackiewicz *et al.*, Macromolecule biosynthesis - a key function of sleep. *Physiol. Genomics* **31**, 441-457 (2007).

8. J. Delorme *et al.*, Hippocampal neurons' cytosolic and membrane-bound ribosomal transcript profiles are differentially regulated by learning and subsequent sleep. *Proc Natl Acad Sci USA* **118** (2021).

9. C. Cirelli, C. M. Gutierrez, G. Tononi, Extensive and divergent effects of sleep and wakefulness on brain gene expression. *Neuron* **41**, 35-43 (2004).

10. J. C. Tudor *et al.*, Sleep deprivation impairs memory by attenuating mTORC1-dependent protein synthesis. *Sci Signal* **9**, ra41 (2016).

11. S. B. Noya *et al.*, The Forebrain Synaptic Transcriptome Is Organized by Clocks but Its Proteome Is Driven by Sleep *Science* **366** (2019).

12. L. C. Lyons, S. Chatterjee, Y. Vanrobaeys, M. E. Gaine, T. Abel, Translational changes induced by acute sleep deprivation uncovered by TRAP-Seq. *Mol Brain* **13** (2020).

13. C. C. Flores *et al.*, Identification of ultrastructural signatures of sleep and wake in the fly brain. *Sleep* **45** (2022).

14. G. Xie, X. Huang, H. Li, P. Wang, P. Huang, Caffeine-related effects on cognitive performance: Roles of apoptosis in rat hippocampus following sleep deprivation. *Biochemical and Biophysical Research Communications* **534**, 632-638 (2021).

15. A. Penagos-Puig, M. Furlan-Magaril, Heterochromatin as an Important Driver of Genome Organization. *Frontiers in Cell and Developmental Biology* **8** (2020).

16. D. A. Gallegos, U. Chan, L.-F. Chen, A. E. West, Chromatin Regulation of Neuronal Maturation and Plasticity. *Trends in Neuroscience* **41**, 311-324 (2018).

17. C. N. Hor *et al.*, Sleep-wake-driven and circadian contributions to daily rhythms in gene expression and chromatin accessibility in the murine cortex. *Proc Natl Acad Sci USA* **116**, 25773-25783 (2019).

18. O. Ventskovska, T. Porkka-Heiskanen, N. N. Karpova, Spontaneous sleep–wake cycle and sleep deprivation differently induce Bdnf1, Bdnf4 and Bdnf9a DNA methylationand transcripts levels in the basal forebrain and frontal cortex in rats. *J Sleep Res* **24**, 124-130 (2015).

19. R. Massart *et al.*, The genome-wide landscape of DNA methylation and hydroxymethylation in response to sleep deprivation impacts on synaptic plasticity genes. *Translational Psychiatry* **4** (2014).

20. L.-W. Wong, Y. S. Chong, W. L. E. Wong, S. Sajikumar, Inhibition of Histone Deacetylase Reinstates Hippocampus-Dependent Long-Term Synaptic Plasticity and Associative Memory in Sleep-Deprived Mice. *Cereb Cortex* **30**, 4169-4182 (2020).

21. R. B. Varela *et al.*, Role of epigenetic regulatory enzymes in animal models of mania induced by amphetamine and paradoxical sleep deprivation *Eur J Neurosci* **53**, 649-662 (2021).

22. R. Duan *et al.*, Histone Acetylation Regulation in Sleep Deprivation-Induced Spatial Memory Impairment *Neurochem Res* **41**, 2223-2232 (2016).

23. C. C. Flores *et al.*, Identification of Ultrastructural Signatures of Sleep and Wake in the Fly Brain *Sleep* **Online ahead of print** (2021).

24. A. Fortuny *et al.*, Imaging the response to DNA damage in heterochromatin domains reveals core principles of heterochromatin maintenance. *Nat Communications* **12** (2021).

25. M. Bellesi, D. Bushey, M. Chini, G. Tononi, C. Cirelli, Contribution of sleep to the repair of neuronal DNA double-strand breaks: evidence from flies and mice. *Sci Rep* **6** (2016).

26. D. Zada, I. Bronshtein, T. Lerer-Goldshtein, Y. Garini, L. Appelbaum, Sleep increases chromosome dynamics to enable reduction of accumulating DNA damage in single neurons. *Nat Communications* **10** (2019).

27. A. Vaccaro *et al.*, Sleep Loss Can Cause Death through Accumulation of Reactive Oxygen Species in the Gut. *Cell* **181**, 1307-1328 (2020).

28. V. M. Hill *et al.*, A bidirectional relationship between sleep and oxidative stress in Drosophila *PLoS Biology* **16** (2018).

29. J. Zhang *et al.*, Extended wakefulness: compromised metabolics in and degeneration of locus ceruleus neurons. *J Neurosci* **34**, 4418-4431 (2014).

30. M. Dworak, R. W. McCarley, T. Kim, A. V. Kalinchuk, R. Basheer, Sleep and brain energy levels: ATP changes during sleep *J Neurosci* **30**, 9007-9016 (2010).

31. A. Kempf, S. M. Song, C. B. Talbot, G. Miesenbock, A potassium channel β-subunit couples mitochondrial electron transport to sleep. *Nature* **568**, 230-234 (2019).

32. L. Ramanathan, S. Hu, S. A. Frautschy, J. M. Siegel, Short-term total sleep deprivation in the rat increases antioxidant responses in multiple brain regions without impairing spontaneous alternation behavior *Behav Brain Res* **207**, 305-309 (2010).

33. L. Ramanathan, S. Gulyani, R. Nienhuis, J. M. Siegel, Sleep deprivation decreases superoxide dismutase activity in rat hippocampus and brainstem. *Neuroreport* **13**, 1387-1390 (2002).

34. A. C. Andreazza *et al.*, Impairment of the mitochondrial electron transport chain due to sleep deprivation in mice. *J Psychiatr Res* **44**, 775-780 (2010).

35. R.-H. Yang *et al.*, Paradoxical sleep deprivation impairs spatial learning and affects membrane excitability and mitochondrial protein in the hippocampus. *Brain Research* **1230**, 224-232 (2008).

36. J. E. Owen *et al.*, Late-in-life neurodegeneration after chronic sleep loss in young adult mice. *Sleep* **44** (2021).

37. C. Cirelli, G. Tononi, Differences in gene expression between sleep and waking as revealed by mRNA differential display *Brain Res Mol Brain Res* **56**, 293-305 (1998).

38. E. V. Nikonova *et al.*, Changes in Components of Energy Regulation in Mouse Cortex with Increases in Wakefulness. *Sleep* **33**, 889-900 (2010).

39. E. V. Nikonova *et al.*, Differences in activity of cytochrome C oxidase in brain between sleep and wakefulness. *Sleep* **28**, 21-27 (2005).

40. L. de Vivo *et al.*, Loss of sleep affects the ultrastructure of pyramidal neurons in the adolescent mouse frontal cortex. . *Sleep* **39**, 861-874 (2016).

41. I. G. Onyango *et al.*, Regulation of neuron mitochondrial biogenesis and relevance to brain health. *Biochimica et Biophysica Acta (BBA)-Molecular Basis of Disease* **1802**, 228-234 (2010).

42. Z. H. Sheng, Q. Cai, Mitochondrial transport in neurons: impact on synaptic homeostasis and neurodegeneration. *Nat Rev Neurosci* **13**, 77-93 (2012).

43. D. C. Chan, Mitochondria: dynamic organelles in disease, aging, and development *Cell* **125**, 1241-1252 (2006).

44. T. Wakabayashi, Megamitochondria formation - physiology and pathology. *J Cell Mol Med* **6**, 497-538 (2002).

45. D. C. Chan, Fusion and Fission: Interlinked Processes Critical for Mitochondrial Health. *Annu Rev Genet* **46**, 265-287 (2012).

46. Z. Lu *et al.*, Topological reorganizations of mitochondria isolated from rat brain after 72 hours of paradoxical sleep deprivation, revealed by electron cryo-tomography *Am J Physiol Cell Physiol* **321**, C17-25 (2021).

47. G. C. Garcia *et al.*, Mitochondrial morphology provides a mechanism for energy buffering at synapses. *Sci Rep* **9**, 18306 (2019).

48. R.-S. Zhao, S. Jiang, L. Zhnag, Z.-B. Yu, Mitochondrial electron transport chain, ROS generation and uncoupling (Review). *Int J Mol Med* **44**, 3-15 (2019).

49. N. Naidoo, W. Giang, R. J. Galante, A. I. Pack, Sleep deprivation induces the unfolded protein response in mouse cerebral cortex. *J Neurochem* **92**, 1150-1157 (2005).

50. N. Naidoo, M. Ferber, M. Master, Y. Zhu, A. I. Pack, Aging Impairs the Unfolded Protein Response to Sleep Deprivation and Leads to Proapoptotic Signaling. *J Neurosci* **28**, 6539-6548 (2008).

51. J. Sanders, M. Scholz, I. Merutka, D. Biron, Distinct unfolded protein responses mitigate or mediate effects of nonlethal deprivation of C. elegans sleep in different tissues. *BMC Biology* **15** (2017).

52. P. J. Shaw, C. Cirelli, R. J. Greenspan, G. Tononi, Correlates of sleep and waking in Drosophila melanogaster. *Science* **287**, 1834-1837 (2000).

53. P. J. Shaw, G. Tononi, R. J. Greenspan, D. F. Robinson, Stress response genes protect against lethal effects of sleep deprivation in Drosophila. *Nature* **417**, 287-291 (2002).

54. Y. Lee *et al.*, Sleep deprivation impairs learning and memory by decreasing protein O-GlcNAcylation in the brain of adult zebrafish *FASEB J* **34**, 853-864 (2020).

55. N. Naidoo, V. Casiano, J. Cater, J. Zimmerman, A. I. Pack, A role for the molecular chaperone protein BiP/GRP78 in Drosophila sleep homeostasis. *Sleep* **30**, 557-565 (2007).

56. M. K. Brown *et al.*, Aging induced endoplasmic reticulum stress alters sleep and sleep homeostasis. *Neurobiol Aging* **35**, 1431-1441 (2014).

57. H. Zinszner *et al.*, CHOP is implicated in programmed cell death in response to impaired function of the endoplasmic reticulum. . *Genes Development* **12**, 982-995 (1998).

58. I. Tabas, D. Ron, Integrating the mechanisms of apoptosis induced by endoplasmic reticulum stress. *Nat Cell Biol* **13**, 184-190 (2011).

59. H. M. A. Zeeshan, G. H. Lee, H.-R. Kim, H.-J. Chae, Endoplasmic Reticulum Stress and Associated ROS. *Int J Mol Sci* **17** (2016).

60. S. S. Cao, R. J. Kaufman, Endoplasmic Reticulum Stress and Oxidative Stress in Cell Fate Decision and Human Disease. *Antioxid Redox Signal* **21**, 396-413 (2014).

61. P. G. Donlin-Asp, C. Polisseni, R. Klimek, A. Heckel, E. M. Schuman, Differential regulation of local mRNA dynamics and translation following long-term potentiation and depression. *Proc Natl Acad Sci USA* **118** (2021).

62. S. Giandomenico, B. Alvarez-Castelao, E. M. Schuman, Proteostatic regulation in neuronal compartments. *Trends in Neuroscience* **45**, 41-52 (2022).

63. Z. Ozturk, C. J. O'Kane, J. J. Perez-Moreno, Axonal Endoplasmic Reticulum Dynamics and Its Roles in Neurodegeneration. *Front Neurosci* **14** (2020).

64. A. P. Govind *et al.*, Activity-dependent Golgi satellite formation in dendrites reshapes the neuronal surface glycoproteome. *eLife* **10** (2021).

Chapter 3 Reactivation of Memory-encoding Dentate Gyrus Neurons During Memory Consolidation is Associated with Subregion-specific, Learning- and Sleep-mediated Biosynthetic Changes

This chapter includes the manuscript: Wang, L., Park, L., Wu, W., King, D., Medina, A.V., Raven, F., Martinez, J.D., Ensing, A., McDonald, K., Yang, Z., Jiang, S. and Aton, S. (2023). Reactivation of memory-encoding dentate gyrus neurons during memory consolidation is associated with subregion-specific, learning- and sleep-mediated biosynthetic changes. Submitted to *Nature Communications*.

3.1 Abstract

Post-learning sleep plays an important role in hippocampal memory processing, including contextual fear memory (CFM) consolidation. Here, we used targeted recombination in activated populations (TRAP) to label context-encoding engram neurons in the hippocampal dentate gyrus (DG) in male mice and assessed reactivation of these neurons during post-learning sleep. We find that post-learning sleep deprivation (SD), which impairs CFM consolidation, selectively disrupts reactivation in inferior blade DG engram neurons. This change was linked to more general suppression of neuronal activity markers in the inferior, but not superior, DG blade by SD. To further characterize how learning and subsequent sleep or SD affect these (and other) hippocampal subregions, we used subregion-specific spatial profiling of transcripts and proteins. We found that transcriptomic responses to sleep loss differed greatly between hippocampal regions CA1, CA3, and DG inferior blade, superior blade, and hilus – with activity-driven transcripts, and those associated with cytoskeletal remodeling, selectively suppressed in the inferior blade. Critically, learning-driven transcriptomic changes, measured 6 h following contextual fear learning, were limited to the two DG blades, differed dramatically between the blades, and were absent from all other regions. These changes suggested an increase in

glutamatergic receptor signaling, and a decrease in GABA receptor signaling, during memory consolidation. Protein abundance across hippocampal subregions was also differentially impacted by sleep vs. SD and by prior learning, with the majority of alterations to protein expression restricted to DG. Together, these data suggest that the DG plays an essential role in the consolidation of hippocampal memories, and that the effects of sleep and sleep loss on the hippocampus are highly subregion-specific, even within the DG itself.

3.2 Introduction

Hippocampal memory consolidation is affected by the amount and quality of post-learning sleep (1-4). In both animal models and human subjects, sleep deprivation (SD) negatively impacts consolidation of hippocampus-dependent memories (5-7). For example, in mice, consolidation of contextual fear memory (CFM), a canonical form of Pavlovian conditioning (8) is disrupted by SD in the first 5-6 h following single-trial contextual fear conditioning (CFC; pairing exploration of a novel context with a foot shock) (9-13). Recent studies have shown that SD can alter basic features of hippocampal network function, including oscillatory patterning of network activity (11), intracellular signaling (10, 14, 15), transcription and translation (12, 16-19), and excitatory-inhibitory balance (20, 21). However, the precise mechanisms responsible for SD-driven disruption of hippocampal memory storage remain unknown.

Growing evidence suggests that CFM is encoded via activation of a sparse population of hippocampal engram neurons (22). Natural cue-driven memory recall (i.e., upon return to the conditioning context) can reactivate at least some of the same neurons active during CFC in hippocampal structures including DG (23, 24). Optogenetic reactivation of these so-called

engram neurons drives fear memory retrieval (25, 26). Based on these findings, offline reactivation of engram neurons is widely hypothesized to serve as the mechanistic basis of memory trace storage. Indeed, recent data suggest that consolidation is associated with, and requires, sleep-associated reactivation of engram populations in neocortex (27, 28) and hippocampal area CA1 (29). However, we have recently found that SD profoundly disrupts network activity in DG (12, 17, 20, 21). This effect is mediated in part through acetylcholine-dependent activation of somatostatin-expressing interneurons in DG - which in turn suppress activity among DG granule cells (20). DG is a critical input structure to the hippocampus (receiving input from neocortex via the entorhinal cortex), and DG engram neurons' activity is necessary and sufficient for CFM recall (25, 26, 30). Thus, a critical unanswered question is how post-CFC sleep and SD affect post-learning engram neuron reactivation in the context of CFM consolidation.

We first addressed this question using targeted recombination in activated populations (TRAP) (31) to label CFC-activated engram neurons in dorsal hippocampal DG. We find that these TRAP-labeled engram neurons selectively reactivate over the first few hours following CFC. Post-learning SD disrupts this offline reactivation in a region-specific manner, preventing reactivation specifically in inferior blade DG granule cells. These findings suggest a subregion-specific, instructive, sleep-dependent mechanism for CFM consolidation, which selectively drives engram neuron reactivation in one subregion (inferior blade of DG). To identify subregion-specific cellular mechanisms associated with this phenomenon, we used spatial transcriptomics to identify transcript changes associated with CFC and subsequent sleep or SD in subregions of DG, CA1, and CA3. Surprisingly, SD-driven transcriptomic changes differed substantially between these subregions and varied dramatically between the two DG blades.

Many of the changes occurring in the inferior blade with SD could play a causal role in preventing engram neuron reactivation during SD, or the functional consequence of engram neuron activity disruption – including changes to pathways involved in regulating synaptic structure. Moreover, learning-associated transcriptomic changes: 1) were present only in the two DG blades 6 h following CFC, 2) were absent from all other subregions profiled at this timepoint, and 3) differed significantly between the blades. Further characterization of hippocampal subregions with spatial protein and phosphoprotein profiling again showed distinct, subregion-specific effects of both learning and subsequent sleep vs SD. Together, these findings reveal previously uncharacterized heterogeneity and subregion-specificity in the effects of both learning and sleep on the hippocampus. The present data provide new insights into mechanisms by which post-learning sleep contributes to hippocampal memory consolidation.

3.3 Results

3.3.1 Hippocampal engram neuron reactivation during post-learning sleep is subregion-specific.

To visualize neurons activated in the hippocampus by a learning experience, we used a genetic strategy recently used to identify visual memory engram neurons in mouse primary visual cortex (V1) (27). To identify context-activated neurons with TRAP (31), *cfos-CRE^{ER}* transgenic mice were crossed to a *tdTomato* reporter line (*cfos::tdTomato*). At lights on (i.e, the beginning of the rest phase; Zeitgeber time [ZT]0), *cfos::tdTomato* mice were placed in a novel context (Context A) for 15 min of free exploration, immediately after which they were administered 4-hydroxytamoxifen (4-OHT) to label context-activated hippocampal neurons with tdTomato. 6 days later at ZT0, the mice were either returned to Context A (A to A) or placed in a

dissimilar Context B (A to B) for 15 min. 90 min after the second period of exploration (**Figure 3.1a**), mice were perfused and hippocampal cFos expression was quantified to assess neuronal activity. In agreement with previous reports using a different transgenic strategy (24)(26), TRAPed tdTomato+ neuronal cell bodies in the DG granule cell layers were more likely to be reactivated during Context A re-exposure than during exploration of Context B (**Figure 3.1b-c**). Conversely, a larger proportion of A to A cFos+ neurons were tdTomato+ compared with A to B cFos+ neurons (**Figure 3.1e**). We next compared the specificity of Context A engram neuron activation in the superior vs. inferior blades' granule cell layer within DG. In the superior blade, but not the inferior blade, the proportion of cFos+ tdTomato+ neurons was significantly higher in the A to A group compared with A to B (**Figure 3.1d**,**f**), despite the average proportion of cFos+ tdTomato+ neurons being similar between the two blades for animals in the same experimental condition (e.g., A to A). These differences between the A to A and A to B were not due to either the number of total tdTomato+ neurons or total cFos+ neurons, which were similar between the two groups, both across the entire granule cell population (**Supplemental Figure S3.1a-b**) and within each of the two blades (**Supplemental Figure S3.1c-d**). However, consistent with previous reports (31, 32), tdTomato+ and cFos+ neuron numbers were consistently higher in the superior vs. inferior blade (**Supplemental Figure S3.1c-d**). Together, these data suggest that TRAPed engram cells in DG granule cell layer - particularly in the superior blade - are reliably reactivated upon re-exposure to the same context.

We next tested how reactivation of DG engram populations was affected by context-associated CFC. Male *cfos::tdTomato* mice explored either Context A or dissimilar Context B at ZT0, and were administered 4-OHT to label context-activated neurons. 6 days later at ZT0, mice from both groups underwent single-trial CFC in Context A and were perfused 90 min later to

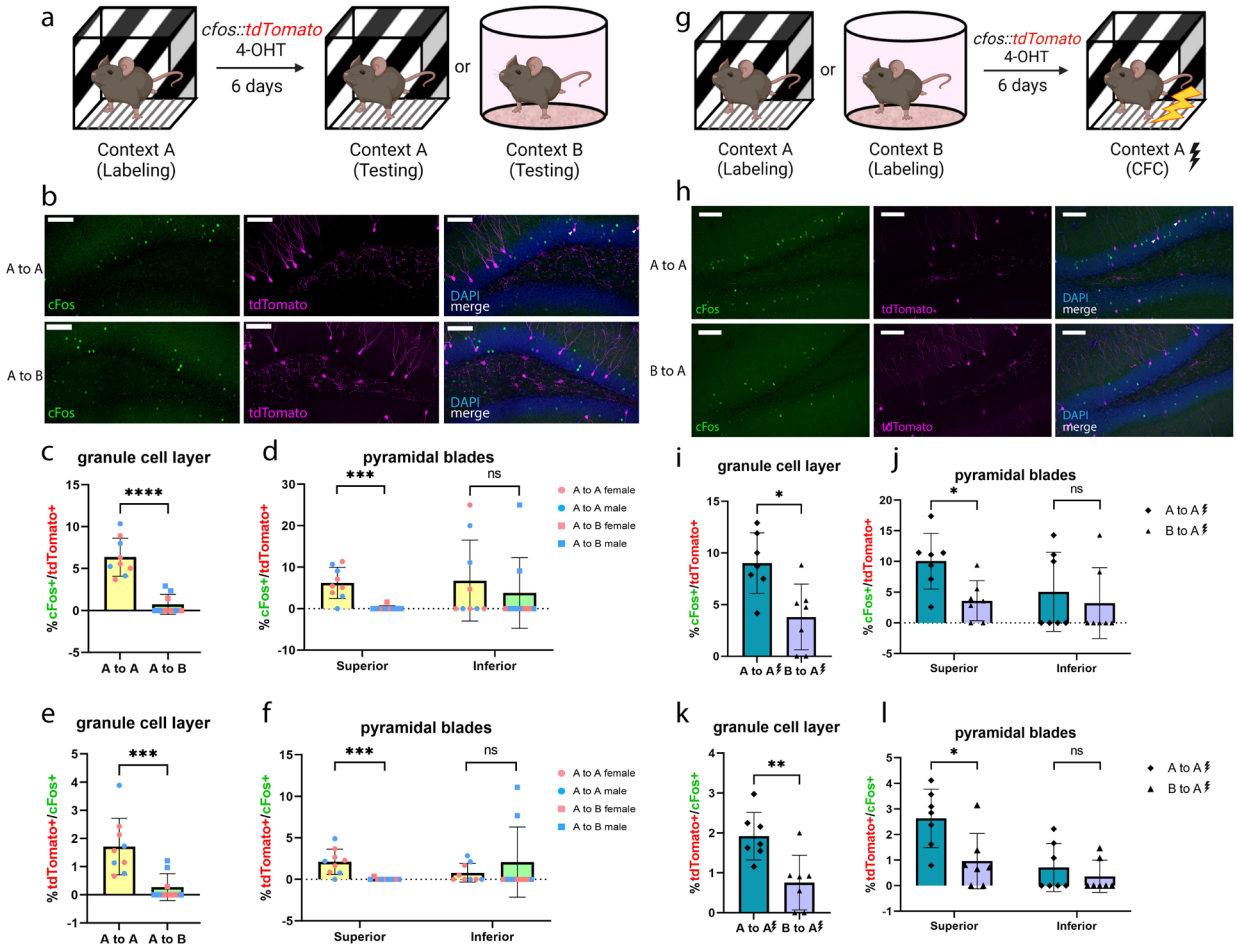

Figure 3.1 Contextual fear conditioning (CFC) reactivates context-labeled neurons. a, Male and female *cfos::tdTomato* mice were injected with 4-hydroxytamoxifen (4-OHT) following Context A exploration. 6 d later, mice were either re-exposed to Context A (A to A) or were placed in a dissimilar Context B (A to B) prior to tissue harvest. **b,** Representative images showing overlap of tdTomato (magenta) and cFos protein (green). Examples of colocalization within a neuron is indicated with a white arrowhead. Scale bar =100 µm. **c,** Percentage of cFos+/tdTomato+ cells in the DG granule cell layer is significantly higher in A to A (n = 9; 4 males and 5 females) compared with in A to B (n = 9; 5 males and 4 females). **** indicates $p < 0.0001$, Mann Whitney test. **d,** cFos+/tdTomato+ overlap percentage differed between conditions in the superior blade (*** indicates $p = 0.0006$, Mann Whitney test) but not the inferior blade (ns = not significant). **e,** Percentages of tdTomato+/cFos+ cells in the DG granule cell layer. *** indicates $p = 0.0009$, Mann Whitney test. **f,** tdTomato+/cFos+ overlap percentage differed between conditions in the superior (*** indicates $p = 0.0004$, Mann Whitney test) and inferior (ns = not significant) blade of DG granule cell layer. **g,** Male *cfos::tdtomato* mice were injected with 4-OHT following either Context A or Context B exploration. 6 d after labeling, all mice received contextual fear conditioning (CFC) in Context A prior to tissue harvest. **h,** Representative images showing overlap of tdTomato (magenta) and cFos protein (green). Examples of colocalization within a neuron is indicated with a white arrowhead. Scale bar = 100 µm. **i,** Percentages of cFos+/tdTomato+ cells in the DG granule cell layer is significantly higher in A to A (n = 7) than B to A (n = 7). * indicates $p = 0.0256$, Mann Whitney test. **j,** The cFos+/tdTomato+ overlap percentage is significantly higher in the superior blade (* indicates $p = 0.0256$, Mann Whitney test) but not the inferior blade (ns, not significant). **k,** Percentages of tdTomato+/cFos+ cells in the DG granule cell layer. ** indicates $p = 0.007$, Mann Whitney test. **l,** Percentages of tdTomato+/cFos+ cells in the superior (* indicates $p = 0.0256$, Mann Whitney test) and inferior (ns = not significant) blade of DG granule cell layer. All bars indicate mean ± s.d.

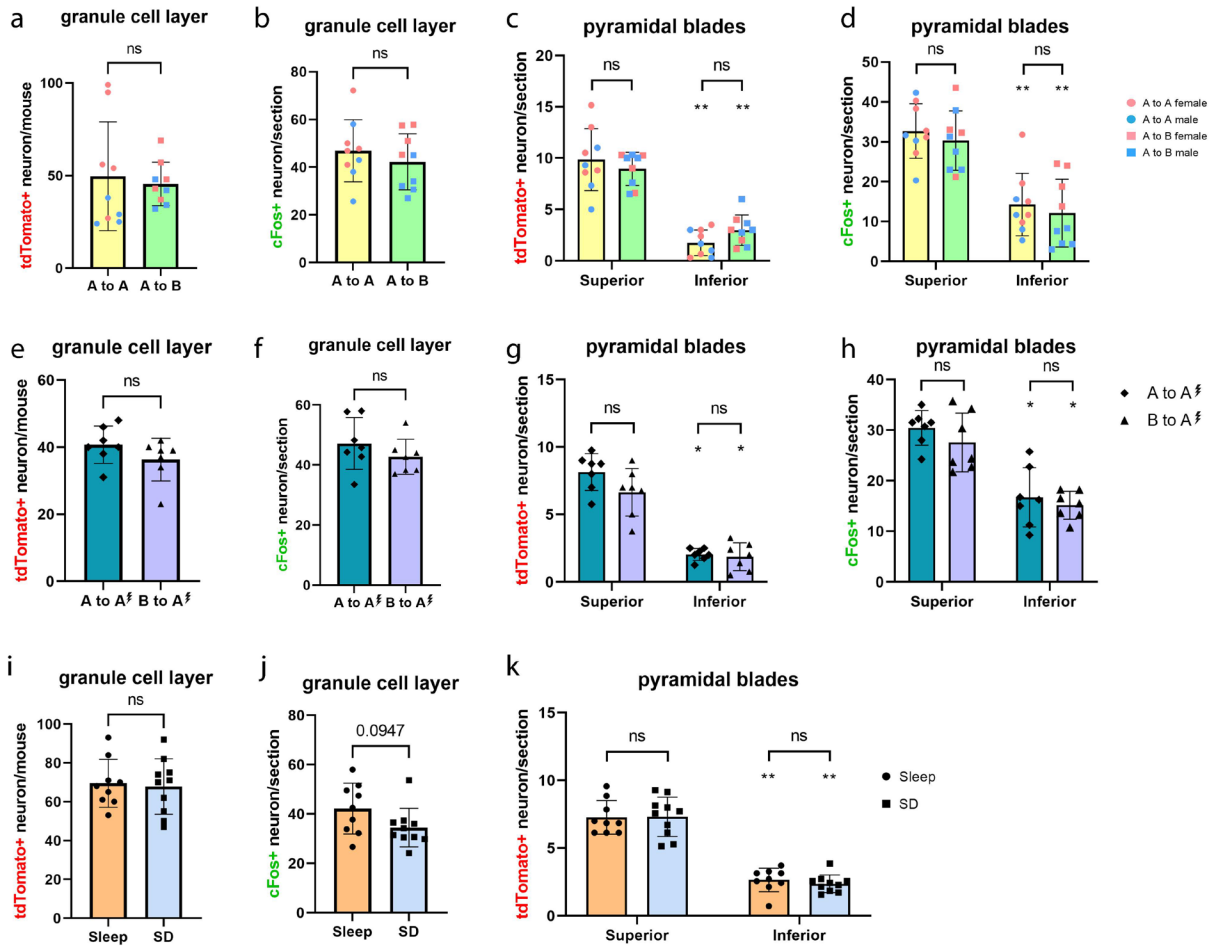

Supplemental Figure S 3.1 Numbers of tdTomato+ and cFos+ neurons in the DG granule cell layer. **a,** Numbers of tdTomato+ and (**b**) cFos+ neurons in the DG granule cell layer were similar in A to A and A to B mice. Values indicate mean ± s.d.. **c,** tdTomato+ neuron densities in A to A and A to B mice were similar for comparisons within the same blade, e.g. superior A to A vs. superior A to B. For both A to A and A to B scenarios, the inferior blade had fewer tdTomato+ neurons compared the superior blade (** ** indicates p = 0.0039 and p = 0.0039, respectively, Wilcoxon matched-pairs signed rank test). **d,** cFos+ neuron densities in A to A and A to B scenarios showed a similar pattern, with the inferior blade having fewer cFos+ neurons than the superior blade (** indicates p = 0.0039 and p = 0.0078, respectively, Wilcoxon matched-pairs signed rank test). **e,** Numbers of tdTomato+ and **f**, cFos+ neurons in the DG granule cell layer were similar in A to A-CFC and A to B-CFC mice. Values indicate mean ± s.d.. **g-h,** tdTomato+ and cFos+ neuron densities in the superior and inferior blades were comparable in A to A-CFC and A to B-CFC mice. Again, the inferior had fewer tdTomato+ neurons (* indicates p = 0.0156 and p = 0.0156, respectively, Wilcoxon matched-pairs signed rank test) and fewer cFos+ neurons compared the superior blade (* indicates p = 0.0156 and p = 0.0156, respectively, Wilcoxon matched-pairs signed rank test), in both scenarios. **i,** Numbers of tdTomato+ and **j**, cFos+ neurons in the DG granule cell layer were similar in Sleep and SD mice. **k**, tdTomato+ neuron densities in the superior blade or inferior blade were comparable in Sleep and SD mice. The inferior blade had fewer tdTomato+ neurons compared the superior blade under both Sleep and SD conditions (** indicates p = 0.0039 and ** p = 0.0020, respectively, Wilcoxon matched-pairs signed rank test). Values indicate mean ± s.d..

quantify CFC-driven neuronal activation (**Figure 3.1g**). Again, a greater proportion of Context A-activated tdTomato+ DG granule cells (vs. Context B-activated tdTomato+ neurons) were cFos+ following CFC in Context A (A to A vs. B to A; **Figure 3.1h-i**), and a higher percentage of cFos+ neurons were previously TRAPed tdTomato+ neurons in the A to A paradigm vs. the B to A paradigm (**Figure 3.1k**). As was observed previously, in the superior blade, but not the inferior blade, the proportion of cFos+ tdTomato+ neurons was higher following the A to A CFC paradigm compared with B to A CFC paradigm (**Figure 3.1 j,l**). Again, the total numbers of tdTomato+ cFos+ neurons were similar between groups (**Supplemental Figure S3.1e-f**), and were more numerous in the superior vs. inferior blades (**Supplemental Figure S3.1g-h**). Thus, CFC selectively reactivates specific context-encoding granule cells in the DG superior blade.

Across experimental groups, we also observed a very small number of tdTomato+ neurons in the DG hilus. These TRAPed hilar neurons were morphologically distinct from labeled granule cells (**Supplemental Figure S3.2a**). We found that numbers of cFos+ and tdTomato+ hilar neurons were comparable between A to A and A to B re-exposure paradigms, as well as between A to A and B to A CFC paradigms. No significant differences were observed for cFos+ tdTomato+ overlap between the paradigms (**Supplemental Figure S3.2a-g**), although this may be attributable to the low overall tdTomato+ cell numbers in hilus.

We (11-13) and others (9, 10) have previously shown that sleep deprivation (SD) over the hours immediately following CFC results in disrupted CFM consolidation. We confirmed these disruptive effects in the *cfos::tdTomato* mouse line. At ZT0, all mice underwent single-trial CFC in Context A, after which they were returned to their home cage for either 6 h of SD by gentle handling (followed by recovery sleep) or *ad lib* sleep (**Figure 3.2a**). At ZT0 the following day,

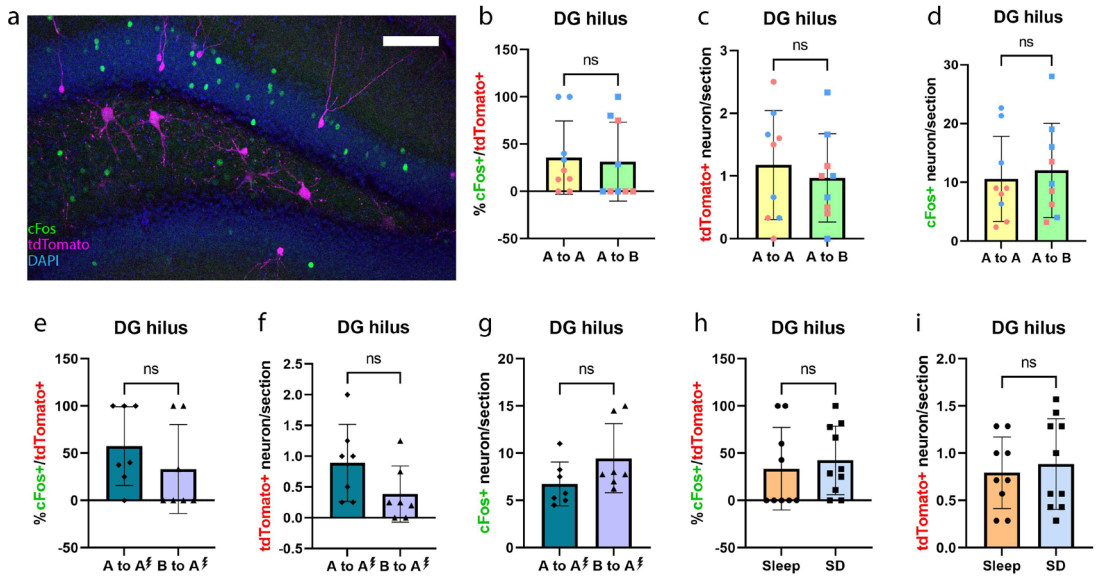

Supplemental Figure S 3.2 Hippocampal hilus cFos+ tdTomato+ overlap showed no significant difference between any of the paradigms. a, Representative image of TRAPed hilar tdTomato+ neurons. Neuronal morphology for TRAPed hilar neurons was distinct from labeled granule cells. **b,** Percentage of cFos+/tdTomato+ cells in the DG hilus, as well as the numbers of (**c**) tdTomato+ and (**d**) cFos+ neurons, were similar between A to A and A to B mice. **e,** Percentage of cFos+/ tdTomato+ cells in the DG hilus, as well as the numbers of (**f**) tdTomato+ and (**g**) cFos+ neurons, were similar in A to A-CFC and A to B-CFC mice. **h,** Percentage of cFos+/tdTomato+ cells in the DG hilus, as well as the numbers of (**i**) tdTomato+ neurons, were similar in Sleep and SD mice. Values indicate mean ± s.d..

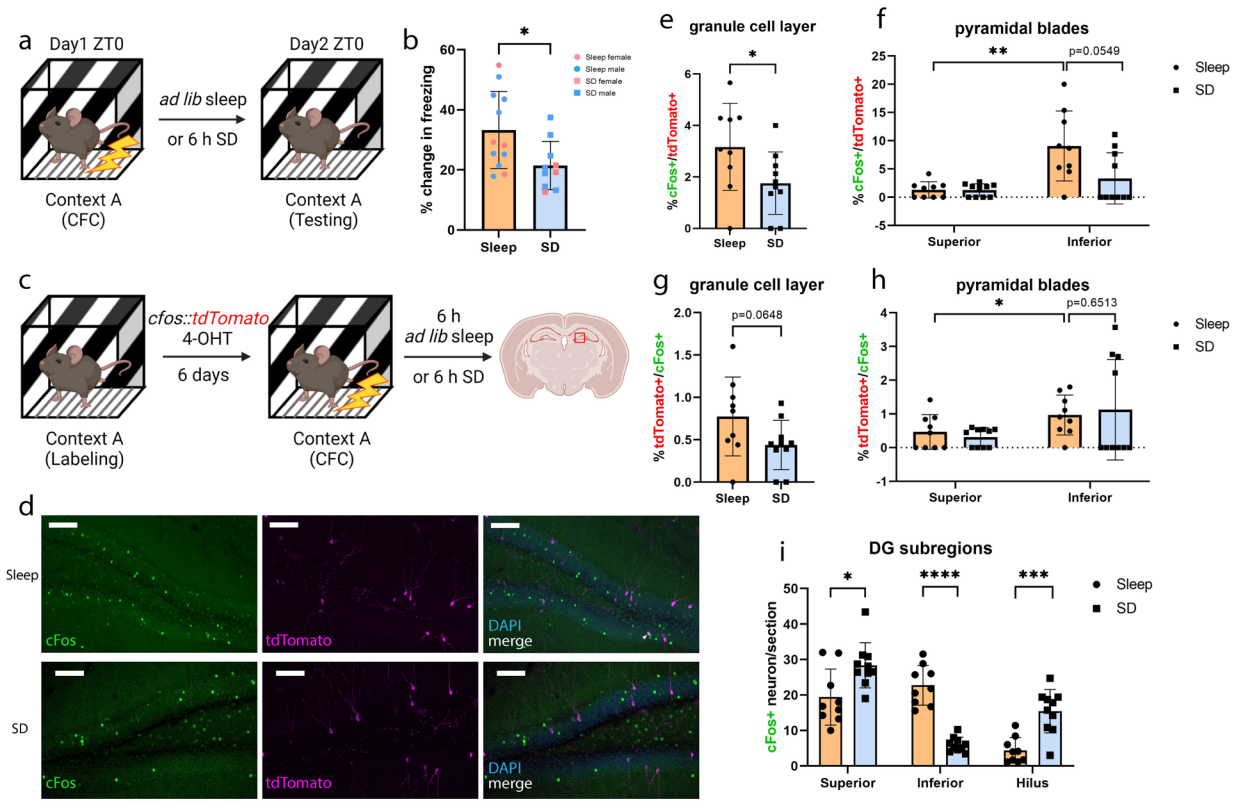

Figure 3.2 Post-learning SD disrupts reactivation of dentate gyrus engram neurons in a subregion-specific manner. a, Experimental procedures. Male and female mice underwent single-trial CFC at ZT0 and were either allowed *ad lib* sleep (n = 12, 8 males and 4 females) or underwent SD (n = 10, 7 males and 3 females) for the first 6 h after CFC; CFM testing occurred at ZT0 next day. **b,** CFM consolidation (measured as the change in context-dependent freezing from baseline) was significantly reduced after SD. * indicates p = 0.0198, Student's t test. **c,** Male *cfos::tdtomato* mice were injected with 4-OHT following Context A exploration. 6 d later, all mice received contextual fear conditioning (CFC) in Context A and were either allowed *ad lib* sleep or were sleep deprived (SD) for 6 h prior to tissue harvest. **d,** Representative images showing overlap of tdTomato (magenta) and cFos protein (green). Examples of colocalization within a neuron is indicated with a white arrowhead. Scale bar = 100 µm. **e,** Percentage of cFos+/tdTomato+ cells in the DG granule cell layer is significantly higher following sleep (n = 9) than SD (n = 10). * indicates p = 0.0347, Mann Whitney test. **f,** Sleep mice had a significantly larger percentage of cFos+/tdTomato+ neurons in the inferior blade compared with the superior blade (** indicates p = 0.0078, Wilcoxon matched-pairs signed rank test), and a strong trend (p = 0.0549, Mann Whitney test) for more cFos+/tdTomato+ overlap in the inferior blade compared with the SD mice. **g,** Percentage of tdTomato+/cFos+ cells in the DG granule cell layer have a strong trend (p = 0.0648, Mann Whitney test) for being higher following sleep (n = 9) than SD (n = 10). **h,** Sleep mice had a significantly larger percentage of tdTomato+/cFos+ neurons in the inferior blade compared with the superior blade (* indicates p = 0.0391, Wilcoxon matched-pairs signed rank test). No significant difference (p = 0.6513, Mann Whitney test) between sleep and SD mice in the inferior blade. **i,** SD increased cFos+ cell number in the superior blade (* indicates p = 0.035, Mann Whitney test) and the hilus (*** indicates p = 0.0009, Mann Whitney test), and reduced cFos+ cell numbers in the inferior blade (**** indicates $p < 0.0001$, Mann Whitney test). All data are presented as mean ± s.d..

mice were returned to Context A to test CFM recall. Consistent with prior results, SD significantly reduced context-specific freezing during the CFM test (**Figure 3.2b**).

We next tested the effect of post-learning SD on the activity of CFC-activated engram neurons in DG in the hours following CFC (i.e., on engram neuron reactivation during consolidation). Naive *cfos::tdTomato* mice were allowed to explore Context A at ZT0, and DG context-activated neurons were labeled via 4-OHT administration. 6 days later at ZT0, mice underwent single-trial CFC in Context A, and were then returned to their home cage for either 6 h of SD or 6 h of *ad lib* sleep, after which they were perfused (**Figure 3.2c**). No significant differences were observed between freely-sleeping and SD mice for total numbers of tdTomato+ or cFos+ tdTomato+ DG hilar neurons (**Supplemental Figure S3.2h-i**). However, consistent with observations of ensemble reactivation in the hippocampus [25] and neocortex [23], reactivation of Context A tdTomato+ DG granule cells was evident 6 h after CFC (albeit at a slightly lower rate than activation of Context A neurons during Context A CFC; **Figure 3.1g-i**) (**Figure 3.2d-e**). Moreover, a higher ratio of Context A tdTomato+ granule cells were cFos+ at this timepoint in freely-sleeping vs. SD mice (**Figure 3.2d-e**). Surprisingly (and in contrast to effects of reexposure to context alone), this difference appeared to be driven largely by higher reactivation rates among TRAPed inferior blade granule cells during sleep (**Figure 3.2f**). Freely-sleeping mice, but not SD mice, had a significantly larger proportion of cFos+ tdTomato+ granule cells in the inferior blade compared with the superior blade **(Figure 3.2f,h)**. Freely-sleeping mice also showed a strong trend ($p = 0.0549$) for more cFos+ tdTomato+ granule cells in the inferior blade compared with the SD mice (**Figure 3.2f**). Together, these data suggest that post-CFC sleep could promote consolidation of CFM by reactivating DG engram neurons in a subregion-specific manner that is spatially distinct from how these neurons are reactivated during

waking experience, More specifically, they suggest that while superior blade DG engram neurons are preferentially activated by context during memory encoding, inferior blade engram neurons are preferentially reactivated in the hours following CFC, during sleep-dependent CFM consolidation.

Prior studies using a tTA-based system identified extensive immediate-early gene (IEG)-driven transgene expression among CA1 neurons after context exposure (26). However, consistent with prior reports using TRAP (31), we observed very sparse tdTomato expression among neurons in the CA1 and CA3 pyramidal cell layers after Context A exposure in *cfos::tdTomato* mice (**Supplemental Figure S3.3a-b**). In contrast to what was observed in DG, following Context A CFC, tdTomato+ cells in CA1 showed a higher level of cFos expression after post-CFC SD than following *ad lib* sleep (**Supplemental Figure S3.3c-d**). In comparison, there was no difference in the level of cFos expression among CA3 neurons between SD and Sleep mice (**Supplemental Figure S3.3e-f**). Together with data suggesting that manipulating activity among putative CA1 engram neurons does not affect CFM encoding (26), these findings suggest that reactivation of DG engram neurons in the hours following CFC might play a uniquely instructive role during sleep-dependent CFM consolidation.

3.3.2 Post-learning SD selectively suppresses activity of DG inferior blade granule cells.

Our data suggest subregion-specific changes in DG engram neuron reactivation in *cfos::tdTomato* mice after sleep vs. SD. Moreover, our previous findings (17, 20, 21) suggest that overall neuronal activity levels might differ between DG and other hippocampal structures as a function of sleep vs. SD. To clarify how post-CFC sleep affects network activity across hippocampal subregions, we next compared expression of IEG proteins cFos and Arc among neurons in DG, CA1, and CA3 in C57BL/6J mice following post-CFC sleep vs. SD.

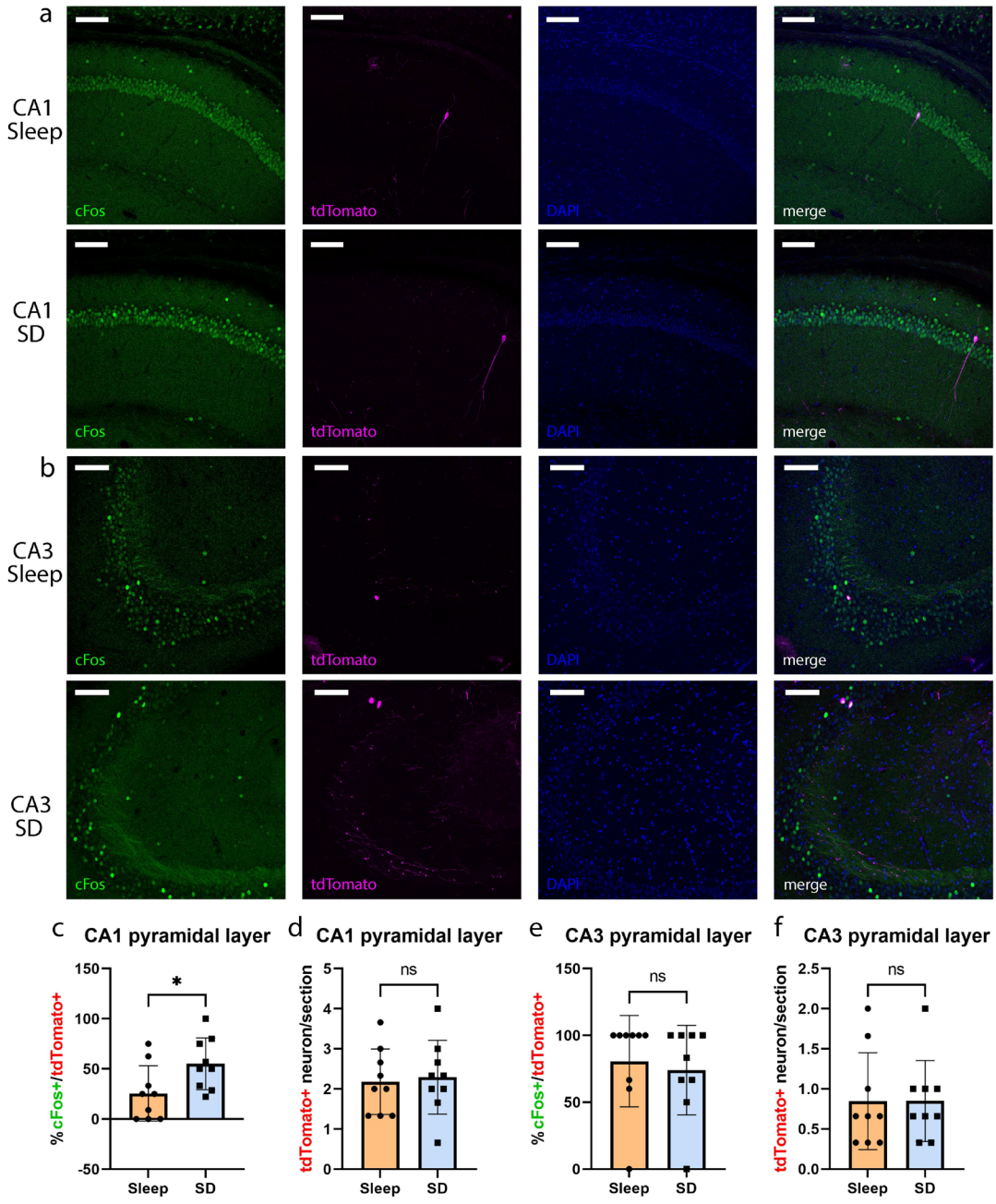

Supplemental Figure S 3.3 Post-learning SD increased cFos+ tdTomato+ overlap in the hippocampal CA1 but not CA3. a, Representative images showing overlap of tdTomato (***magenta***) and cFos protein (***green***) in the pyramidal layer of CA1 and **b,** CA3. Scale bar = 100 µm. **c,** Percentage of cFos+/tdTomato+ cells in the CA1 pyramidal layer was significantly higher following SD (n = 9) than sleep (n = 9). * indicates p = 0.0367, Mann Whitney test. **d,** Numbers of tdTomato+ neurons in the CA1 pyramidal layer were similar in sleep and SD mice. **e,** Percentage of cFos+/tdTomato+ cells in the CA3 pyramidal layer, as well as **f,** the numbers of tdTomato+ neurons, were similar in Sleep and SD mice. Values indicate mean ± s.d..

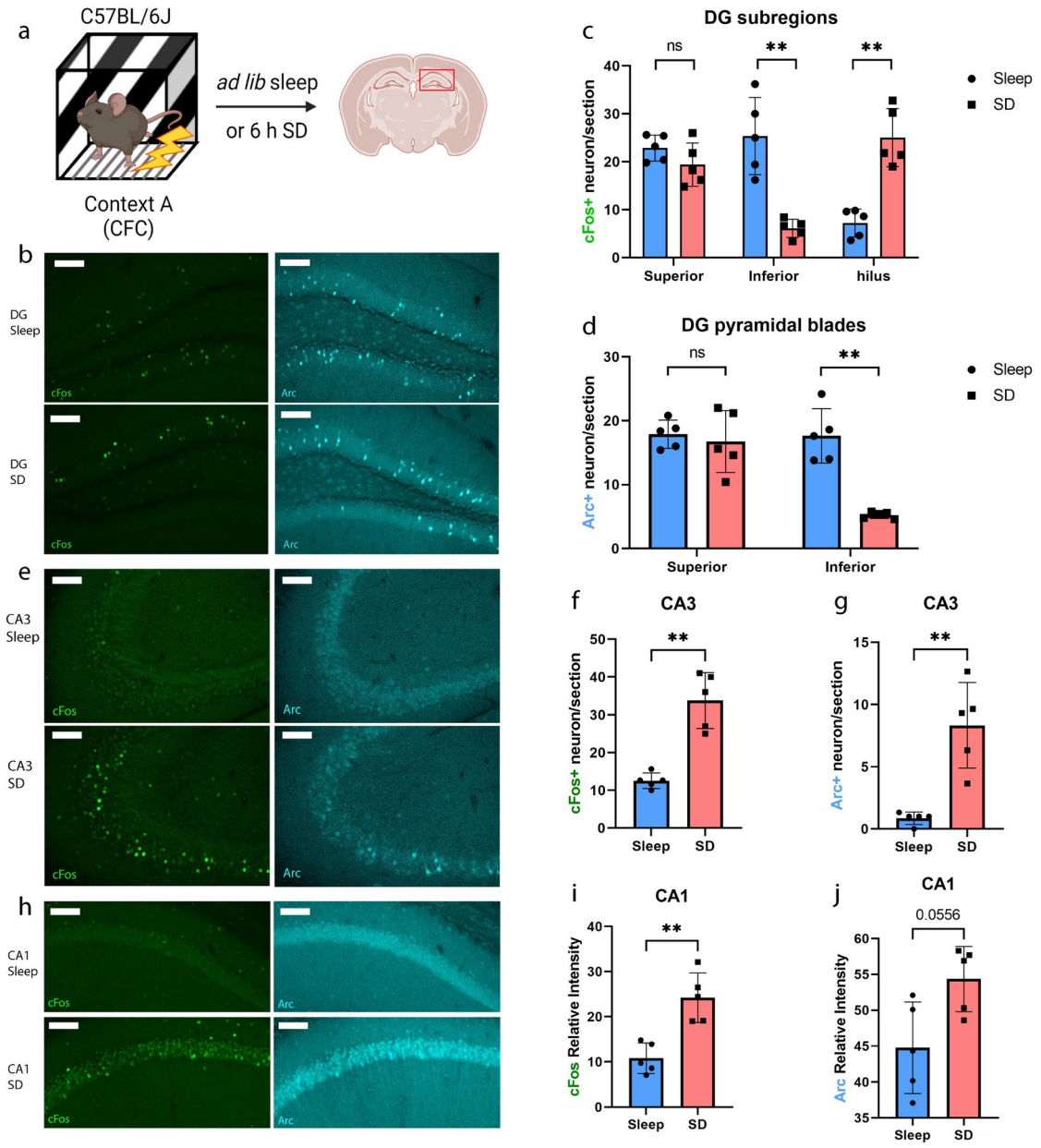

Figure 3.3 Post-learning SD selectively suppresses activity of DG inferior blade granule cells. a, Experimental procedure. C57BL/6J mice underwent single-trial CFC in Context A and were either allowed ad lib sleep or were sleep deprived (SD) for 6 h prior to tissue harvest. **b,** Representative images showing cFos (green) and Arc protein (cyan) following sleep or SD in the dentate gyrus. Scale bar = 100 µm. **c,** SD did not change cFos+ cell number in the superior blade in C57BL/6J mice (p = 0.3095, Mann Whitney test) but increased the cFos+ cell the hilus (** indicates p = 0.0079, Mann Whitney test), and reduced cFos+ cell number in the inferior blade (** indicates p = 0.0079, Mann Whitney test). **d,** SD reduced Arc+ cell numbers in the inferior blade compared with sleep. ** indicates p = 0.0079, Mann Whitney test. **e,** Representative images showing cFos (green) and Arc protein (cyan) following sleep or SD in the CA3. Scale bar = 100 µm. **f,** SD increased cFos+ (**indicates p = 0.0079, Mann Whitney test) and (**g**) Arc+ (** indicates p = 0.0079, Mann Whitney test) cell number in the CA3. Data are presented as mean ± s.d. **h,** Representative images showing cFos (green) and Arc protein (cyan) following sleep or SD in the CA1. Scale bar = 100 µm. **i,** SD increased cFos protein relative intensity (** indicates p = 0.0079, Mann Whitney test) in the CA1 pyramidal layer and (**j**) had a strong trend of increasing Arc (p = 0.0556, Mann Whitney test). All data are presented as mean ± s.d.

When single-trial CFC in Context A was followed by 6 h of SD (**Figure 3.3a**), both cFos and Arc expression were significantly decreased among inferior blade granule cells (**Figure 3.2i; Figure 3.3a-d**). However, expression in the superior blade was either unchanged or increased after SD (**Figure 3.2i, Figure 3.3c-d**), and expression of cFos in the hilus was dramatically increased after SD (**Figure 3.2i, Figure 3.3c**). Moreover, SD significantly increased cFos+ and Arc+ cell numbers in the CA3 pyramidal cell layer (**Figure 3.3 e-g**), as well as relative cFos and Arc staining intensity in the CA1 pyramidal cell layer (**Figure 3.3 h-j**). Taken together, these data are consistent with previous reports that SD drives alterations in DG activity that differ from those reported elsewhere in the brain (17, 20, 21) . They also suggest that following CFC, SD-mediated disruption of CFM consolidation could be caused by selectively disrupted activity (and associated engram neuron reactivation) in the DG inferior blade.

3.3.3 SD causes diverse and subregion-specific alterations in hippocampal gene expression, and drives distinctive responses in the DG blades.

Our preliminary findings (**Figures 3.1-3**) suggest that post-CFC sleep may have differential effects on granule cell, and more specifically, engram neuron activation between the two DG blades. These subregion-specific effects may be linked to sleep-dependent CFM consolidation. We have recently shown that learning and subsequent sleep or sleep loss differentially affect ribosome-associated mRNA profiles in different hippocampal cell types (12, 21). Based on our observation of subregion-specific changes in cFos and Arc expression and engram neuron reactivation following post-CFC sleep or SD (**Figures 3.2**, **3**), we speculated that learning and sleep could independently alter biosynthetic processes that impinge on synaptic plasticity in a subregion-specific manner. More specifically, we hypothesized that CFC and subsequent sleep vs. SD could differentially impact important neurobiological processes

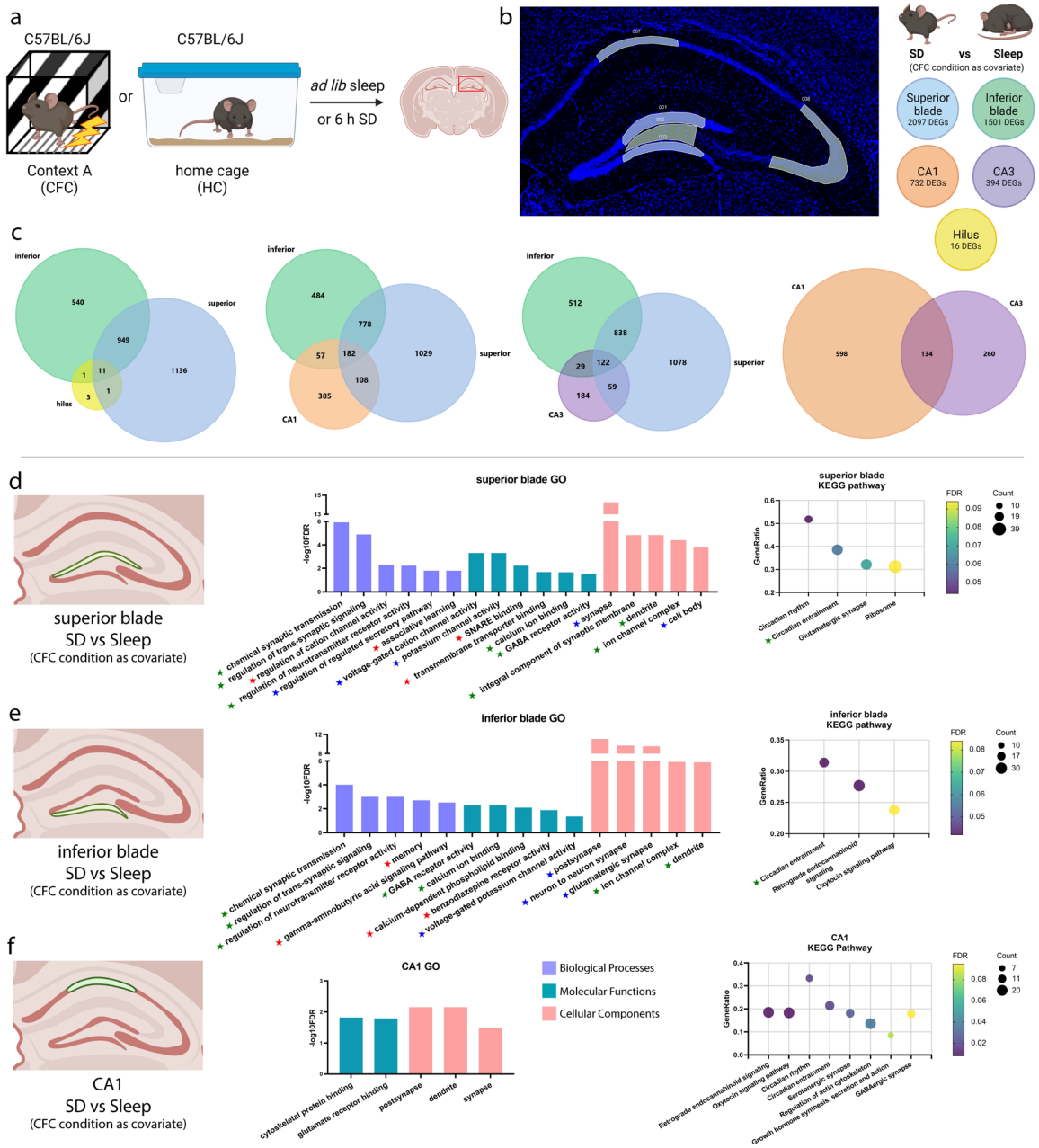

Figure 3.4 SD causes subregion-specific alterations in hippocampal gene expression. a, C57BL/6J mice were either left undisturbed in their home cage (HC) or underwent single-trial CFC in Context A (CFC). Over the next 6 h, mice in CFC and HC groups were either allowed ad lib sleep or underwent SD in their HC prior to perfusion. **b,** (***Left***) Representative image of (region of interest) ROI selection using NanoString's GeoMx Digital Spatial Profiler (DSP). (***Right***) Illustration of the comparison and number of DEGs for SD vs Sleep in each hippocampal subregion. **c,** Venn diagrams reflect the number of SD vs Sleep DEGs and their overlap in the DG superior blade, inferior blade, hilus, CA1, and CA3. **d,** The most significant gene ontology terms, ranked by FDR value, and KEGG pathways enriched for transcripts altered by SD alone in the superior blade, (**e**) inferior blade, and (**f**) CA1. Red stars highlight GO terms uniquely mapped to one blade only, blue stars indicate the presence of related (parent/child) terms in both blades, and green stars highlight GO terms and KEGG pathways overrepresented in both superior and inferior blades.

in the DG inferior blade vs. other hippocampal substructures, including the superior blade.

To test this hypothesis, we separately profiled mRNAs in various subregions within the dorsal hippocampus using NanoString GeoMx Digital Spatial Profiler (DSP). At ZT 0, mice were either left undisturbed in their home cage (HC) or underwent single-trial CFC in Context A (CFC). Over the next 6 h, mice in both the CFC and HC groups were either allowed *ad lib* sleep or underwent SD in their home cage prior to perfusion (**Figure 3.4a**). This 2 × 2 experimental design structure (resulting in 4 experimental groups) allowed us to separately test for effects of learning and sleep on transcript levels within each subregion. Brain sections from each experimental group were stained with nuclear label Syto 13 to identify borders of the DG hilus, the superior and inferior blade granule cell layers of DG, and the pyramidal cell body layers of CA1 and CA3 (example regions of interest [ROIs] shown in **Figure 3.4b**). From each mouse (n = 3-4 mice/group) either bilateral or unilateral hippocampal subregions were sampled for DSP transcript measurement (1-2 regional samples/mouse, each subregion sample corresponding to one biological replicate). In total, 11508 gene targets from the mouse Whole Transcriptome Atlas (WTA) passed target filtering and were quantified for each sample. As expected, principal component analysis (PCA) revealed clear separation of CA1, CA3, DG hilus, and DG pyramidal blades' gene expression profiles (**Supplemental Figure S3.4a**).

We first assessed the effects of SD itself on each hippocampal subregion. For this, we included data from all mice, and used the learning condition (CFC or HC) as a covariate. This structure allowed us to 1) determine effects that are driven by SD, regardless of prior learning, and 2) make comparisons with related data sets from whole-hippocampus RNAseq data, which used a similar study design (21). Transcripts affected by SD (i.e., differentially-expressed genes [DEGs] for the SD vs. Sleep conditions; n = 7 and n = 8 mice, respectively) were then

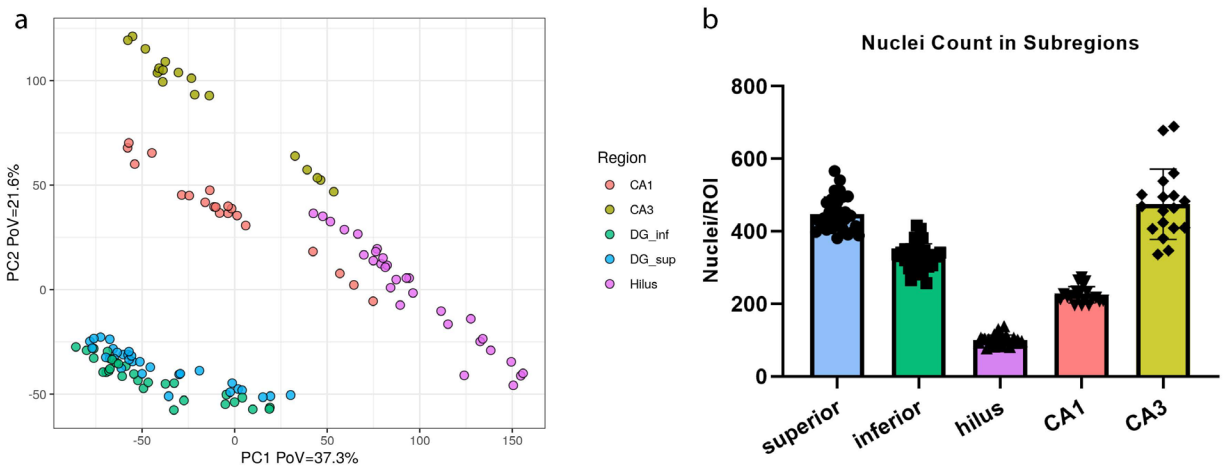

Supplemental Figure S 3.4 Principal component analysis and nuclei count for all regions of interest. **a,** Principal component analysis of all transcripts showing regions of interest (ROIs) strongly stratified according to hippocampal subregion, regardless of treatment group. **b,** Nuclei count in hippocampal subregions as number of nuclei per region of interest (ROI) from GeoMx Digital Spatial Profiler.

compared between hippocampal subregions (**Figure 3.4b, c**). Within DG, SD significantly altered (FDR < 0.1) 2097 transcripts in the superior blade and 1501 transcripts in the inferior blade; of these, 960 altered transcripts overlapped between the two blades (**Figure 3.4c**). Comparatively fewer transcripts were altered by SD in the DG hilus, although this may be due to the relatively small ROI size (in terms of contributing cell number) for the hilus when compared with granule cell layers (**Supplemental Figure S3.4b**). Of the 16 SD-altered genes identified in the hilus, 11 ((*Rbm3* (↓)*, Cirbp* (↓)*, Pdia6* (↑)*, Hspa5* (↑)*, Fam163b* (↓)*, Sdf2l1* (↑)*, R3hdm4* (↓), *Xbp1* (↑)*, Btf3l4* (↓)*, Dtnb* (↓)*,* and *Sqstm1* (↓); arrows indicate increased or decreased abundance after SD) were similarly altered by SD in both the superior and inferior blades (**Figure 3.4c**). For CA1 and CA3 pyramidal layers, 732 genes and 394 SD DEGs, respectively, were identified; of these, only 134 were similarly altered by SD in both subregions (**Figure 3.4c**). While many SD DEGs overlapped between different hippocampal subregions (with the largest overlap between superior and inferior blades), the majority of SD DEGs was unique to individual subregions (**Supplemental Figure S3.5a-b**). This was true for transcripts that were either upregulated or downregulated after SD (**Supplemental Figure S3.5c-d**). 53 DEGs were altered by SD across CA1, CA3, DG superior and inferior blades, and these were consistently either upregulated or downregulated by SD across all four of these subregions (**Supplemental Figure S3.5e**). Somewhat surprisingly, only five transcripts in total (*Rbm3* (↓)*, Pdia6* (↑)*, Hspa5* (↑)*, Sdf2l1* (↑)*,* and *Dtnb* (↓)) were consistently altered by SD across all five hippocampal subregions measured. These pan-hippocampal transcript changes included transcripts encoding components of the ER chaperone complex **(Supplemental Figure S3.6)**, consistent with previous findings (33) that SD activates the ER stress response, both in the hippocampus (12, 16) and elsewhere in the brain (34).

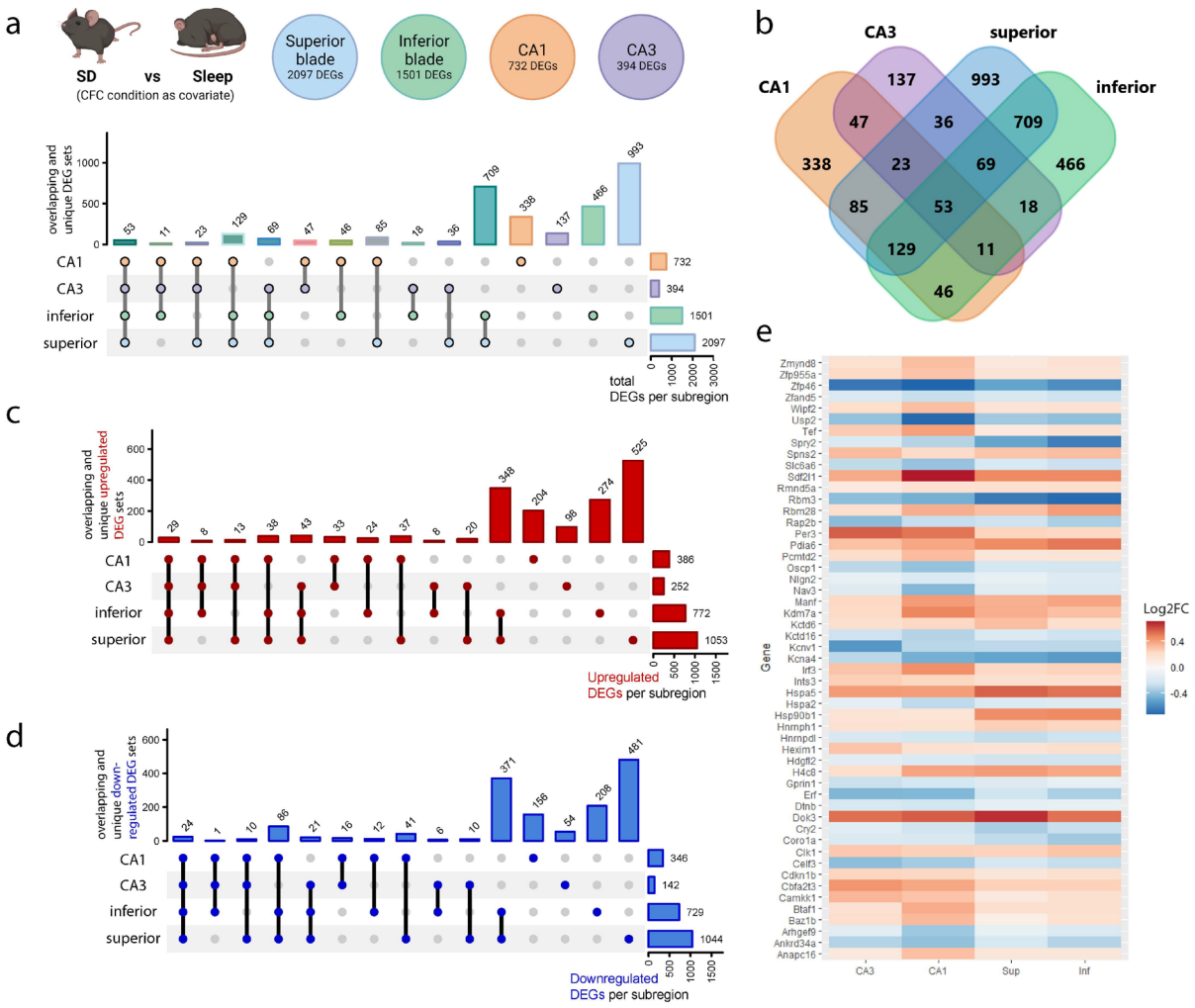

Supplemental Figure S 3.5 Overlap of SD-altered DEGs in the superior and inferior blade of DG, CA1, and CA3. a, UpSet plot and **b,** Venn diagram of overlapping SD-altered DEGs between each of the 4 principal cell body subregions (CA1, CA3, Inferior blade, Superior blade). The number of total DEGs for each subregion is shown on the right side of the UpSet plot. Dots with connecting lines indicate overlap of DEGs between one or more subregions, and the corresponding overlap can be found in the Venn diagram. Individual dots with no connecting lines indicate DEGs only affected in the specific subregion. The number of DEGs for a specific overlap is shown on the top of the UpSet plot. **c,** UpSet plot of only SD-upregulated DEGs between each hippocampal subregion. **d,** UpSet plot of only SD-downregulated DEGs between each hippocampal subregion. **e,** Heatmap of the 53 DEGs altered by SD across CA1, CA3, DG superior and inferior blades.

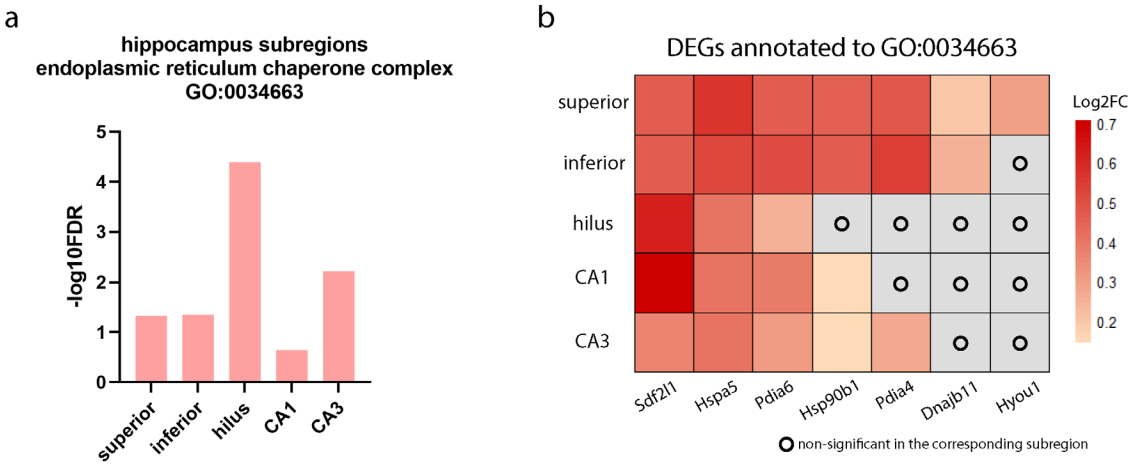

Supplemental Figure S 3.6 SD-impacted gene ontology term ER chaperone complex. a, Gene ontology cellular component term, ER chaperone complex (GO:0034663), was significantly impacted in the DG superior, inferior blade, hilus, and CA3 following SD. **b,** Expression level of SD vs Sleep DEGs annotated to GO:0034663 in superior blade, inferior blade, hilus, CA1, and CA3.

To better understand cellular mechanisms affected by these subregion-specific transcriptomic changes, we used gene ontology (GO) classifiers of biological process, molecular functions, and cellular component annotation of SD-altered transcripts in each subregion (**Figure 3.4 d-f**). We first compared the two DG blades' responses to SD against each other. Several GO terms were either overrepresented among transcripts altered by SD in both the DG superior and inferior blades (marked with green stars in **Figure 3.4 d-e**), or shared parent/child terms for transcripts altered by SD in both blades (blue stars). These included transcripts encoding synaptic and dendritic components of neurons, and those involved in regulation of GABA receptors, voltage-gated channels, and synaptic transmission. A few GO terms were uniquely altered by SD in each blade (red stars). For example, transcripts annotated as mediators of memory (GO:0007613; smallest common denominator-corrected $p_{adj} = 0.002$) were overrepresented among transcripts altered by SD in the inferior blade only. In contrast, transcripts annotated as mediators of associative learning (GO:0008306; $p_{adj} = 0.016$) were selectively altered by SD in the superior blade. While these two biological processes are often linked together conceptually, the number of transcripts present in both annotation categories was only 318, from a total of 3,140 and 1,545, respectively. Critically, however, in both cases, the vast majority of SD DEGs mapped to these processes were downregulated after SD. We also compared KEGG database pathway mapping for SD-altered transcripts from superior and inferior blade, to identify cellular pathways differentially affected by SD in the two blades. The circadian entrainment (KEGG: 04713) pathway was affected by SD in both DG superior (FDR-corrected $p_{adj} = 0.060$) and inferior ($p_{adj} = 0.042$) blades. In the superior blade only, circadian rhythm (KEGG: 04710; $p_{adj} = 0.044$), glutamatergic synapse (KEGG: 04724; $p_{adj} = 0.070$), and ribosome (KEGG: 03010; $p_{adj} = 0.094$) pathways were overrepresented among SD-altered transcripts. DEGs in the glutamatergic

synapse pathway were primarily downregulated, with a few notable (and likely physiologically-important) exceptions including *Grm1*, *Grm2*, *Cacna1c*, *Gria1*, and *Grin2a*, which were all upregulated after SD (**Supplemental Figure S3.7a**). Interestingly, among ribosome pathway DEGs from the superior blade, SD upregulated those annotated as mitochondrial ribosome components, while downregulating those annotated as non-mitochondrial ribosome components, with no exceptions (**Supplemental Figure S3.7a**). This suggests strong and opposing effects of SD on mitochondrial vs. non-mitochondrial biogenesis, and supports recent work suggesting effects of SD on mitochondrial structure and function in neurons (35). In contrast to pathways identified in superior blade, inferior blade SD-altered transcripts overrepresented retrograde endocannabinoid signaling (KEGG: 04723; $p_{adj} = 0.042$) and oxytocin signaling (KEGG: 04921; $p_{adj} = 0.084$) pathway components. For both pathways, DEGs were generally downregulated after SD, with only a few exceptions (**Supplemental Figure S3.7b**).

For comparison with the DG blades, we identified GO and KEGG pathways overrepresented among CA1 SD-altered transcripts (**Figure 3.4f**). Several pathways identified in this analysis were also mapped to SD DEGs from the DG blades – i.e., retrograde endocannabinoid signaling (KEGG: 04723; $p_{adj} = 0.008$), oxytocin signaling (KEGG: 04921; $p_{adj} = 0.008$), circadian rhythm (KEGG: 04710; $p_{adj} = 0.019$), and circadian entrainment (KEGG: 04713; $p_{adj} = 0.019$). As was true in DG, transcripts in these pathways were generally downregulated after SD, with the exception of circadian rhythm, where most transcripts were upregulated. Additional KEGG-annotated pathways with transcripts enriched among CA1 SD DEGs included serotonergic synapse (where serotonin receptor-encoding transcripts were generally upregulated after SD; KEGG: 04726; $p_{adj} = 0.027$), regulation of actin cytoskeleton (where transcripts were generally downregulated after SD; KEGG: 04810; $p_{adj} = 0.036$),

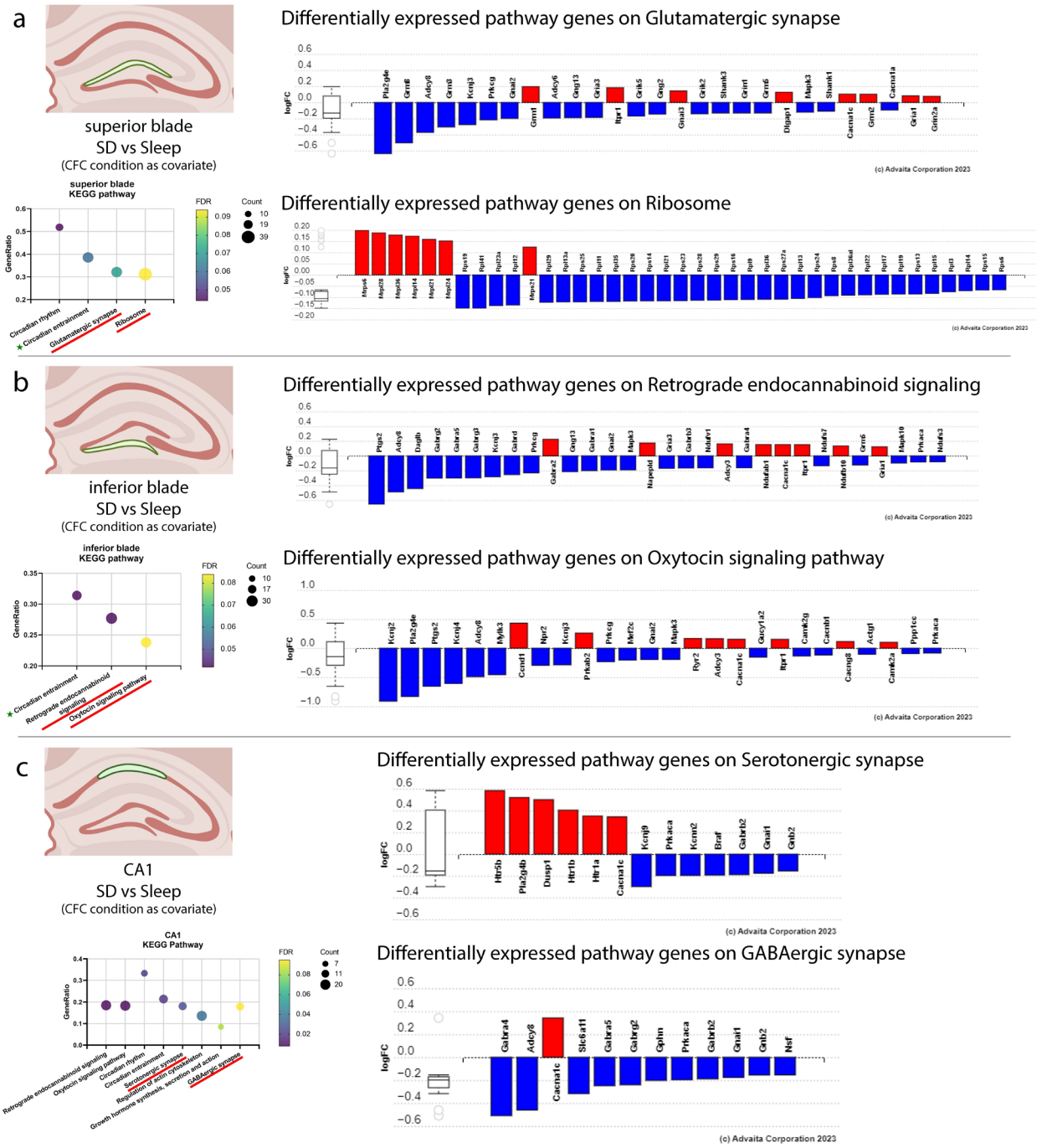

Supplemental Figure S 3.7 Differentially expressed pathway genes for SD-impacted pathways in hippocampal subregions. a, SD altered DEGs annotated to Glutamatergic synapse and Ribosome pathways in the superior blade of DG. **b,** SD altered DEGs annotated to Retrograde endocannabinoid signaling and Oxytocin signaling pathways in the inferior blade of DG. **c,** SD altered DEGs annotated to Serotonergic synapse and GABAergic synapse in the CA1.

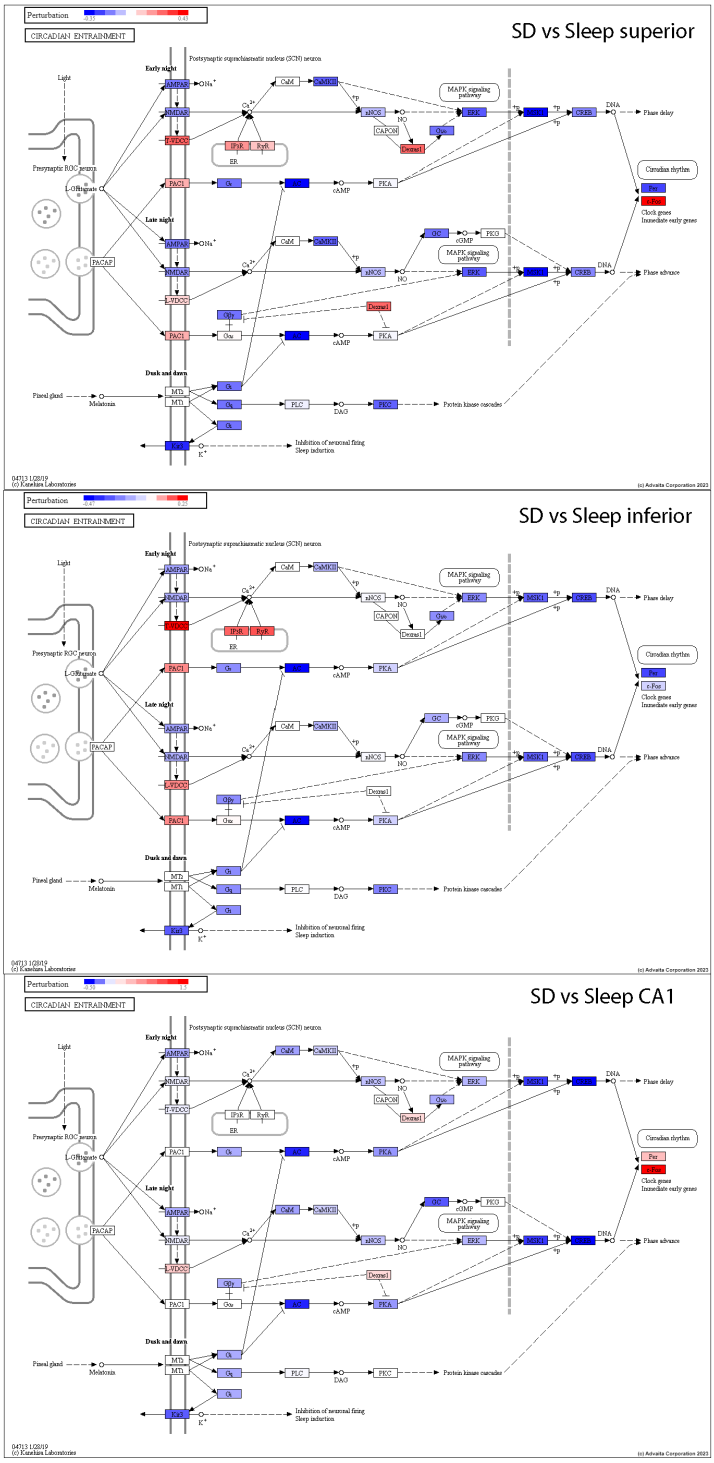

Supplemental Figure S 3.8 Diagrams of SD-impacted Circadian entrainment KEGG pathway (KEGG: 04713) in the superior blade, inferior blade, and CA1. The perturbation accounts both for the gene's measured fold change, and for the computed accumulated perturbation propagated from fold changes to any significantly altered upstream regulator genes, with the highest negative perturbation shown in dark blue, and the highest positive perturbation shown in dark red. The legend describes the values on the gradient for each subregion.

growth hormone synthesis, secretion and action (KEGG: 04935; p_{adj} = 0.084), and GABAergic synapse (where most transcripts were downregulated after SD; KEGG: 04727; p_{adj} = 0.095) (**Supplemental Figure S3.7c**). Circadian entrainment (KEGG: 04713) was the only KEGG pathway mapped for SD DEGs in all three subregions (DG superior blade, inferior blade, and CA1). Pathway diagrams of circadian entrainment showed a consistent SD-induced negative perturbation of calcium-calmodulin kinase (CaMKII) and mitogen-activated protein kinase (MAPK) signaling pathway components across three subregions, which is consistent with prior studies showing that SD attenuates kinase signaling and CREB-mediated gene transcription (10, 21, 36). Surprisingly, although MAPK and CREB signaling components upstream of clock genes were negatively regulated by SD in all three regions, clock gene and IEG transcripts were differentially perturbed across the three regions (**Supplemental Figure S3.8**). These findings, consistent with our observations in **Figures 3.2** and **3.3**, indicate that multiple regulatory mechanisms drive differential SD-driven IEG expression changes across the hippocampal subregions.

To further characterize cellular pathways regulating SD-mediated changes, we performed predicted upstream regulator analysis of SD DEGs within each subregion (**Table 3.1**). For superior blade DEGs, this analysis predicted inhibition of upstream regulators encoded by *Cask*, *Lin7b*, *Lin7c*, *Lin7a*, *Apba1*, and *Unc13b* transcripts (FDR = 0.007), due to downregulation of *Ppfia4*, *Cplx1*, *Tspoap1*, *Rab3a*, *Stx1a*, *Syn1*, *Snap25*, and *Ppfia2* transcripts. Collectively, these downregulated transcripts encode multiple receptor tyrosine phosphatases and active zone vesicular trafficking and release regulating proteins after SD. The expression for two of these upstream regulators, *Lin7b* (encoding lin-7 homolog B, crumbs cell polarity complex component – which normally coordinates their activity in the presynaptic terminal) and *Apba1* (encoding

amyloid beta precursor protein binding family A, member 1), were measured to be downregulated by SD (**Table 3.1**). These findings suggest that presynaptic biogenesis may be decreased within the DG superior blade after a period of SD.

Similar analysis of SD DEGs within CA1 suggested that regulators encoded by *Rab18* (encodes a member of the Ras-related small GTPases, which regulate membrane trafficking in organelles and transport vesicles), *Rab3gap2,* and *Rab3gap1* (RAB3 GTPase activating protein subunit 1 and 2) were predicted as inhibited upstream regulators, and miRNAs *mmu-miR-27a-3p* and *mmu-miR-27b-3p* were predicted as activated miRNAs (**Table 3.2**).

3.3.4 DG transcriptional responses to SD can oppose those in CA1 and CA3, and suggest selective disruption of DG inferior blade activity.

For several SD-altered transcripts, expression levels changed in opposite directions when comparing the two DG blades with other hippocampal subregions. For example, the expression of *Arc* was upregulated by SD in hilus but downregulated by SD in the inferior blade **(Figure 3.5b)**. *Zmat3* (encoding a zinc finger domain transcription factor)*, C1ql3* (encoding an extracellular regulator of excitatory synapses)*,* and *Sf3b6* (encoding an mRNA splicing factor) were upregulated by SD in superior blade but downregulated in CA1; *Per1, Kctd12* (encoding an auxiliary subunit of GABA-B receptors)*, D830031N03Rik* (a.k.a., *Macf1;* microtubule-actin crosslinking factor 1)*,* ephrin receptor-encoding *Epha10,* small GTPase-encoding *Rasl11b, Ets2* (encoding a telomerase-regulating transcription factor)*, Mbnl1* (encoding a pre-mRNA splicing factor)*, Gga3* (encoding a trans-Golgi network sorting and trafficking protein)*,* and *Ier5* (which encodes an immediate early response protein that may mediate transcriptional responses to heat shock) were upregulated by SD in CA1 but downregulated in superior blade **(Figure 3.5c)**. This suggests that nuclear and cytoplasmic processes, and regulators of both glutamatergic and

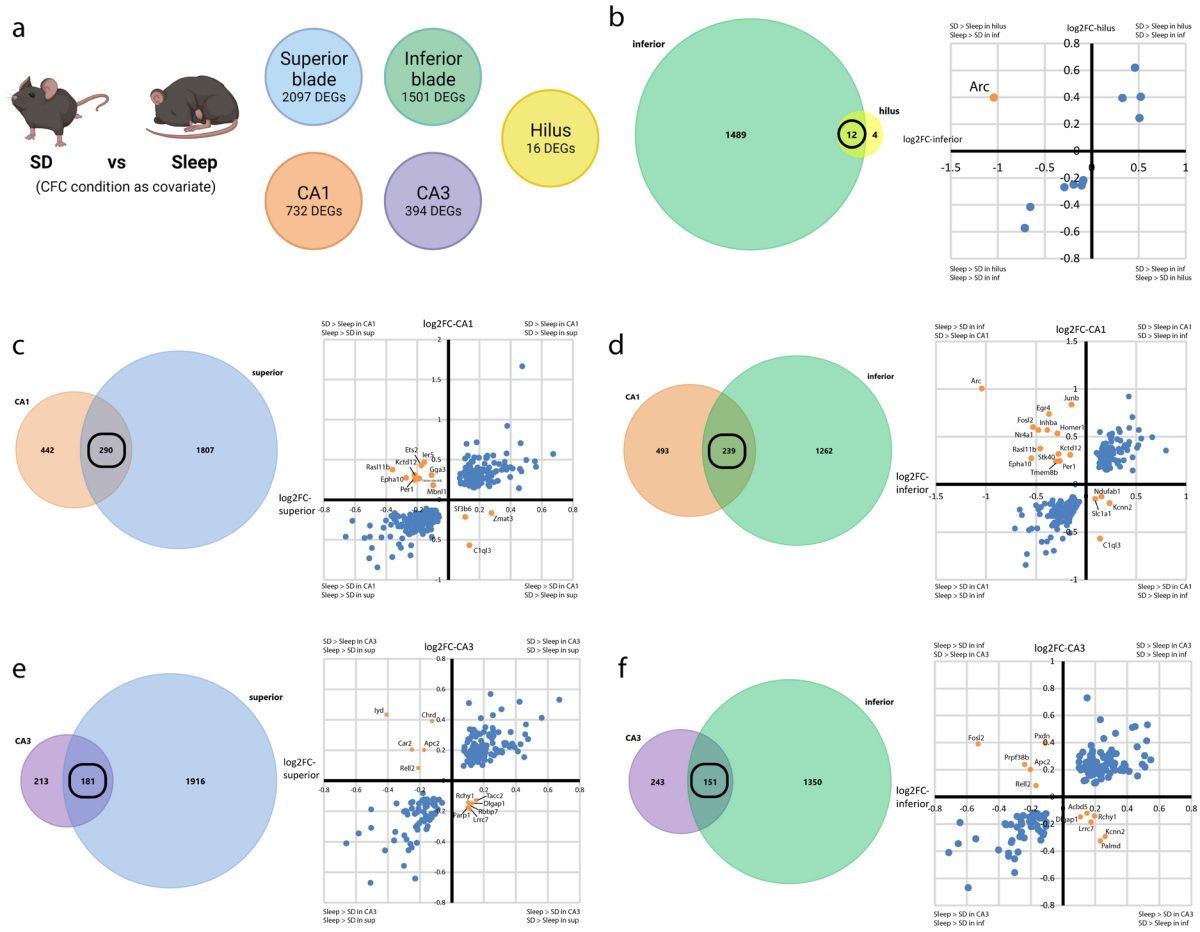

Figure 3.5 Select SD-altered transcripts' levels were altered in opposite directions across hippocampal subregions. a, Illustration of the comparison and number of DEGs for SD vs Sleep in each hippocampal subregion. **b,** Expression level of the 12 overlapping DEGs between inferior blade and hilus. Blue dots represent SD-altered DEGs that are consistently enriched in one of the two subregions. Orange dot represents the gene (Arc) that is upregulated by SD in hilus but downregulated by SD in DG inferior blade. **c,** Expression level of the 290 overlapping DEGs between superior blade and CA1. 3 DEGs were upregulated by SD in DG superior blade but downregulated in CA1 and 9 were upregulated by SD in CA1 but downregulated in superior blade. **d,** Expression level of the 239 overlapping DEGs between inferior blade and CA1. Of these, 4 were upregulated by SD in the inferior blade but downregulated in CA1 and 13 were upregulated by SD in CA1 but downregulated in the inferior blade. **e,** Expression level of the 181 overlapping DEGs between superior blade and CA3. 6 were upregulated by SD in the superior blade but downregulated in CA3 and 5 were upregulated by SD in CA3 but downregulated in the superior blade. **f,** Expression level of the 151 overlapping DEGs between inferior blade and CA3. 6 were upregulated by SD in the inferior blade but downregulated in CA3 and 5 were upregulated by SD in CA3 but downregulated in the inferior blade. Blue dots represent SD-altered DEGs that are consistently enriched in one of the two subregions. Orange dots represent DEGs that are regulated in opposite directions by SD in the subregions.

GABAergic synapses, are differentially regulated between CA1 and superior blade in response to SD. Chromatin remodeling factor *Rbbp7, Lrrc7* (encoding a protein required for glutamate receptor localization and synaptic plasticity), postsynaptic scaffold encoding *Dlgap1, Parp1* (encoding a chromatin-associated enzyme critical for DNA damage repair)*, Rchy1* (encoding an E3 ubiquitin ligase)*,* and *Tacc2* (encoding a regulator of nuclear structure) were upregulated by SD in superior blade but downregulated in CA3. These differences may reflect differential disruption of nuclear and cytoplasmic functions between the two regions, resulting in increased engagement of nuclear and cytoplasmic quality control mechanisms in the superior blade. On the other hand, *Chrd* (encoding secreted factor chordin), *Car2* (encoding carbonic anhydrase), *Apc2* (encoding a negative regulator of the Wnt signaling pathway), *Rell2* (encoding a collagen-binding activator of the MAPK pathway), and *Iyd* (encoding a tyrosine deiodinating enzyme) were upregulated by SD in CA3 but downregulated in superior blade **(Figure 3.5e)**.

Consistent with our immunohistochemical data **(Figure 3.3)**, expression of many IEGs, including *Arc, Fosl2, Homer1, Nr4a1, Junb, and Egr4*, was differentially affected by SD in CA1 vs. inferior blade, indicating opposite changes in neuronal activation patterns during SD in these structures. Similar to the superior blade, expression of *Epha10, Per1, Rasl11b,* and *Kctd12* were decreased after SD in the inferior blade, and simultaneously increased by SD in CA1. In addition, *Tmem8b* (encoding a cell matrix adhesion protein)*, Stk40* (encoding a serine-threonine protein kinase)*, Inhba* (encoding a protein involved in hormone secretion) were downregulated by SD in the inferior blade, and upregulated by SD in CA1. On the other hand, *Ndufab1* (encoding part of mitochondrial respiratory complex 1), *Kcnn2* (encoding a calcium-activated potassium channel that prolongs action potential afterhyperpolarization, and would be predicted to reduce neuronal firing rates), *C1ql3* (encoding an extracellular regulator of excitatory

synapses), and *Slc1a1* (encoding a high-affinity glutamate transporter) were upregulated by SD in the inferior blade but downregulated in CA1 **(Figure 3.5d)**. Taken together, these transcriptomic changes are consistent with an overall reduction of neuronal activity during SD that occurs selectively in the DG inferior blade. *Kcnn2, Lrrc7, Dlgap1, Rchy1, Palmd* (encoding paralemmin-like protein, which is predicted to be involved in dendritic remodeling), and *Acbd5* (encoding an Acyl-CoA binding protein) were upregulated by SD in inferior blade but downregulated in CA3, in large part mirroring differences between superior blade and CA3. *Prpf38b* (encoding a pre-mRNA splicing factor), *Pxdn (*encoding a peroxidase involved in extracellular matrix formation), AP-1 transcription factor subunit *Fosl2, Apc2* (a microtubule stabilizing factor, and putative negative regulator of Wnt signaling), and *Rell2* were upregulated by SD in CA3 but downregulated in the inferior blade (**Figure 3.5f**). These differences suggest that transcripts associated with neuronal activity and synaptic and structural plasticity are simultaneously upregulated in CA3 and downregulated in the inferior blade after SD.

In contrast to the differential regulation of individual transcripts between the DG blades and CA1/3 subregions after SD, no transcripts were regulated in different directions when comparing the hilus, CA1, and CA3 DEGs against each other (**Supplemental Figure S3.9**). Together, these data support the conclusions that: 1) SD differentially affects granule cells in the two DG blades vs. pyramidal cells of CA3 and CA1, and 2) selective effects of SD on the inferior blade's transcript profile may reflect the selective suppression of activity in the inferior blade during SD.

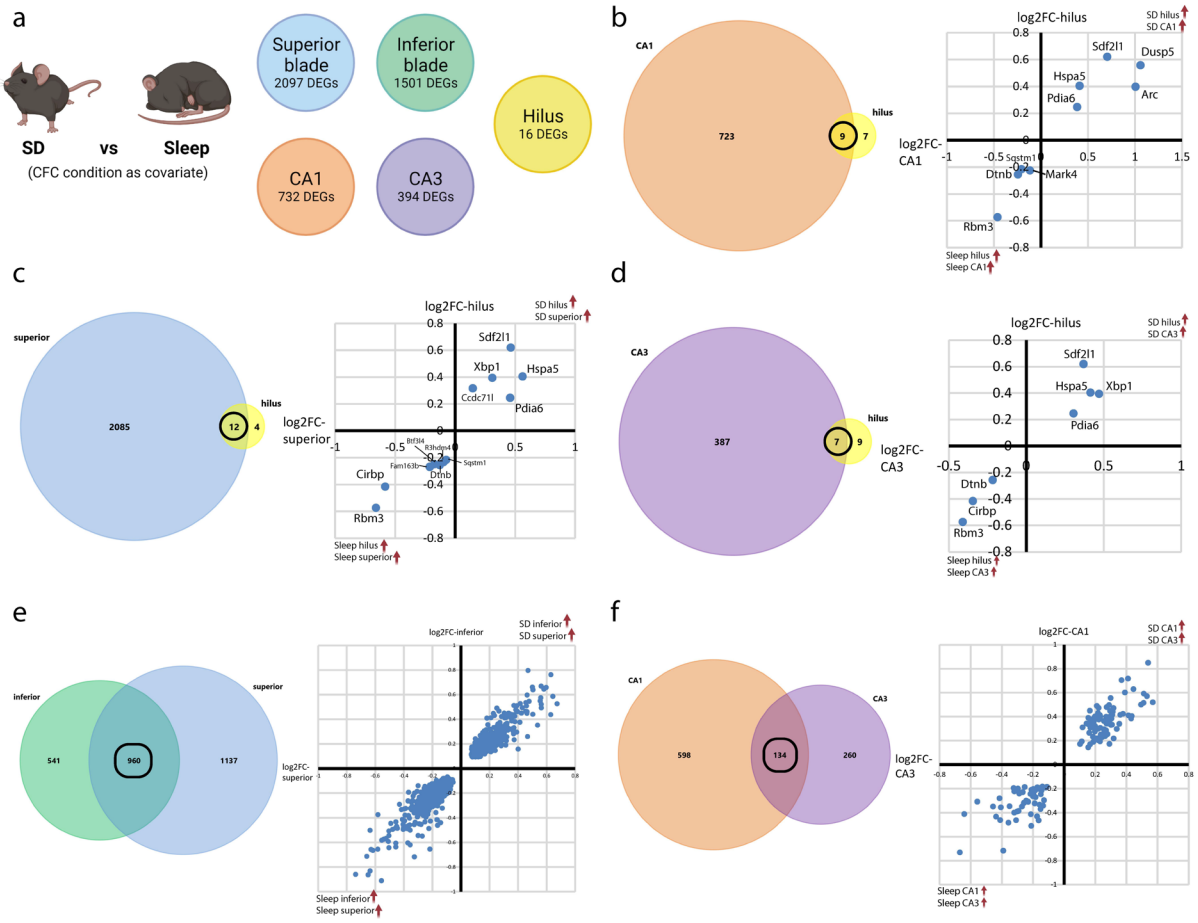

Supplemental Figure S 3.9 SD vs. Sleep DEG overlap between hippocampal subregions. a, Illustration of the comparison and number of DEGs for SD vs Sleep in each hippocampal subregion. **b,** 9 DEGs overlapped between CA1 and hilus, all of them were regulated in the same direction (i.e., were similarly up or downregulated) by SD. **c,** 12 DEGs overlapped between superior blade and hilus; all were regulated in the same direction by SD. **d,** 7 DEGs overlapped between CA3 and hilus; all were regulated in the same direction by SD. **e**, 960 DEGs overlapped between superior and inferior blades; all were regulated in the same direction by SD. **f,** 134 DEGs overlapped between CA1 and CA3; all were regulated in the same direction by SD.

3.3.5 Transcriptomic differences between superior and inferior DG blades are altered by SD vs. sleep.

Because we observed differences in engram neuron context selectivity and sleep-associated reactivation between the DG inferior blade and superior blades (**Figures 3.1** and **3.2**), we directly compared how gene expression differed between the two blades (Inferior vs. Superior DEGs) after sleep vs. SD, again using prior learning condition (CFC/HC) as a covariate. 580 genes were differentially expressed between inferior and superior blade in freely-sleeping mice (Sleep Inferior vs. Sleep Superior), while 750 genes were differentially expressed between the blades in SD mice (SD Inferior vs. SD Superior). 251 Inferior vs. Superior DEGs overlapped between Sleep and SD conditions (**Figure 3.6a**), of which 249 were consistently expressed at a higher level in either the inferior or superior blades (**Figure 3.6b**). For example, *Penk, Fst, Pmepa1, Npy, Col6a1,* and 156 other DEGs were consistently enriched in the superior blade while *Sema5b, Lhx9, Myo5b, Gpc3* and 84 additional DEGs were consistently enriched in the inferior blade (**Figure 3.6b**); these likely represent differences in cellular constituents between the blades, some of which have been previously characterized. For example, several DEGs we identified as enriched in the superior blade, including *Penk, Rgs4*, *Col6a1*, and *Nefm*, may be attributed to a recently-identified subcluster of *Penk*-expressing granule cells located in the DG superior blade (32, 37). These differentially-expressed transcripts thus likely reflect true (constitutive) genetic differences between the two blades.

A few Inferior vs. Superior DEGs showed very dramatic alterations as a function of Sleep vs. SD. For example, consistent with our immunohistochemical results (**Figure 3.3**), *Fos* and *Arc* showed higher expression levels in the superior blade than the inferior blade after SD, but did not differ between the blades in freely-sleeping mice. Interestingly, some transcripts were

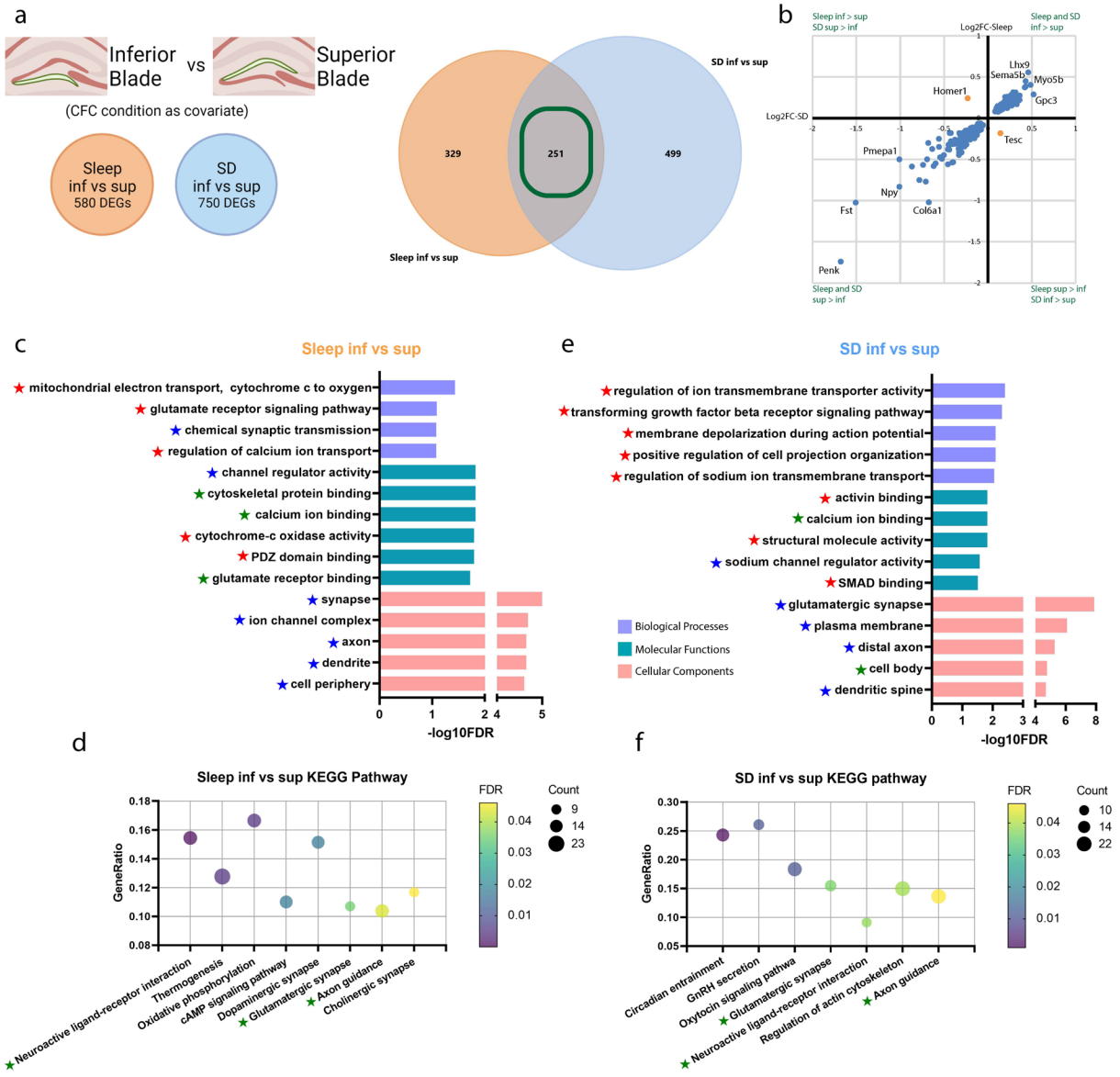

Figure 3.6 Transcriptomic differences between superior and inferior DG blades. a, (***Left***) Illustration of the inferior blade vs superior blade comparison and the number of DEGs under either Sleep or SD condition. (***Right***) Venn diagram reflects the overlap (251 transcripts) of inferior vs superior blade DEGs under Sleep or SD condition. **b,** 249 (blue dots) of the 251 DEGs were consistently expressed at a higher level in either the inferior or superior blades. *Homer1* was enriched in the superior blade in SD mice but enriched in the inferior blade in Sleep mice, while *Tesc* was enriched in the inferior blade in SD mice but enriched in the superior blade in Sleep mice. **c, e,** The most significant gene ontology terms and **d, f** KEGG pathways - ranked by FDR values - mapped for inferior vs superior DEGs in (**c, d)** Sleep mice (**e, f**) and SD mice. Red stars highlight GO terms uniquely mapped under either Sleep or SD condition, blue stars indicate the presence of parent/child terms for both conditions, and green stars highlight GO terms and KEGG pathways overrepresented in both Sleep and SD conditions.

differentially enriched in one blade vs. the other as a function of sleep condition. For example, *Homer1* (encoding an activity-regulated protein involved in synaptic growth and hippocampal plasticity) (38, 39) expression was higher in the superior blade after SD, but with *ad lib* sleep, its expression was higher in the inferior blade (**Figure 3.6b**). On the other hand, *Tesc* (encoding a calcium-binding protein implicated in dendritic growth and neuronal survival) (40) expression was higher in the inferior blade with SD, but with *ad lib* sleep, its expression was higher in the superior blade (**Figure 3.6b**).

We performed GO and biological pathway analysis on Inferior vs. Superior DEGs to further explore how the two blades' function differed under Sleep and SD conditions (**Figure 3.6 c-f**). Most cellular component terms had partially overlapping parent/child terms mapped under either the Sleep or the SD condition (blue stars), while biological process and molecular function had more terms uniquely mapped under either the Sleep or the SD condition, with no direct parent/child relationships (red stars). For example, Sleep was associated with Inferior vs. Superior DEGs enriched for PDZ domain binding molecular function (GO:0030165; smallest common denominator-corrected $p_{adj} = 0.016$) – typically membrane-associated synaptic signaling molecules. Within this molecular class, after *ad lib* sleep, the inferior blade had lower expression of some transcripts, including *Cit* (encoding citron, an actin cytoskeleton-associated serine/threonine kinase activating protein), *Cntnap2*, and MAGUK family members *Mpp3* and *Dlg3*, but higher expression of others, including glutamate receptor components *Grid2*, *Grik2*, and *Gria2*, AMPA receptor regulator *Shisa9*, and voltage-gated calcium channel subunit *Cacng3*. Several pathways were identified using KEGG analysis as differentially regulated between the two DG blades after sleep, including glutamatergic synapse (KEGG: 04724; FDR-corrected $p_{adj} = 0.035$), neuroactive ligand-receptor interaction (KEGG: 04080; $p_{adj} = 8.171e\text{-}5$), axon guidance

(KEGG: 04360; p_{adj} = 0.043), thermogenesis (KEGG: 04714; p_{adj} = 0.005), oxidative phosphorylation (KEGG: 00190; p_{adj} = 0.005), cAMP signaling pathway (KEGG: 04024; p_{adj} = 0.017), dopaminergic synapse (KEGG: 04728; p_{adj} = 0.017), and cholinergic synapse (KEGG: 04725; p_{adj} = 0.046). For all of these pathways, most or all DEG components were expressed at significantly lower levels in the inferior blade, relative to the superior blade, after sleep.

In SD mice, Inferior vs. Superior DEGs enriched for components of the circadian entrainment (KEGG: 04713; p_{adj} = 9.796e-4), GnRH secretion (KEGG: 04929; p_{adj} = 0.011), oxytocin signaling (KEGG: 04921; p_{adj} = 0.011), glutamatergic synapse (KEGG: 04724; p_{adj} = 0.036), neuroactive ligand-receptor interaction (KEGG: 04080; p_{adj} = 0.038), regulation of actin cytoskeleton (KEGG: 04810; p_{adj} = 0.039), and axon guidance (KEGG: 04360; p_{adj} = 0.046) pathways. Only three of these pathways also mapped to Inferior vs. Superior DEGs in the freely-sleeping mice (green stars; **Figure 3.6d, f**). Interestingly, Inferior vs. Superior DEGs enriched for regulation of actin cytoskeleton only in the SD condition. The vast majority of DEGs in this pathway were expressed at lower levels in the inferior blade vs. superior blade after SD, including *Mylk3* (encoding myosin light chain kinase 3), *Myh10* (myosin heavy polypeptide 10, involved in postsynaptic cytoskeleton reorganization), *Arpc2*, *3*, and *4* (actin related protein 2/3 complex, subunits 2, 3, and 4; subunit 2 positively regulates actin polymerization and localize to glutamatergic synapses), *Actr2* (Arp2 actin-related peptide 2, which localizes to the actin cap), *Arhgef4* (Rho guanine nucleotide exchange factor 4, thought to be involved in filopodium assembly), *Pfn1* and *Pfn2* (profilin-1 and profilin-2, regulators that bind to actin and affect the structure of the cytoskeleton), and *Pak1* (P21/RAC1 Activated Kinase 1, a cytoskeletal regulator of cell motility and morphology) (**Supplemental Figure S3.10**). The selective downregulation of these pathway components in the inferior blade after SD likely results in disruption of structural

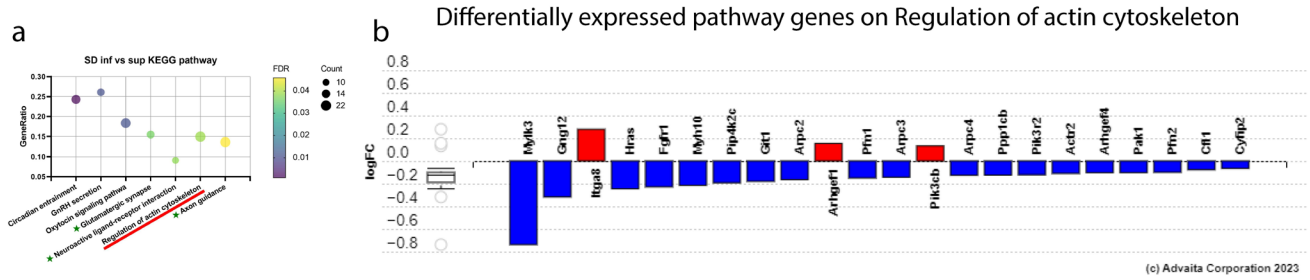

Supplemental Figure S 3.10 Inferior vs. Superior blade differentially expressed genes annotated to the Regulation of actin cytoskeleton KEGG pathway. a, Inferior vs. Superior blade KEGG pathways under SD condition. **b,** Inferior vs. Superior blade differentially expressed pathway genes in the Regulation of actin cytoskeleton pathway.

plasticity in inferior blade neurons. This idea is supported by recent data showing that SD selectively reduces dendritic spine density in inferior blade granule cells, while leaving superior blade granule cells relatively unaffected (41).

Upstream regulator analysis (**Table 3.3**) further predicted that after SD (but not after *ad lib* sleep), upstream regulators *Exosc10, Mtrex, C1d,* and *Bud23* would be inhibited in the inferior blade. This is based on downstream downregulated expression of many transcripts encoding ribosomal protein components (*Rps2,6,7,9,* and *14,* and *Rpl3, 4, 5, 19, 27a,* and *38*) in the inferior blade relative to the superior blade after SD. These transcripts are known to be directly transcriptionally coregulated by two nucleolar factors, *Exosc10* (exosome component 10) and *Mtrex* (Mtr4 exosome RNA helicase), although neither *Exosc10* nor *Mtrex* transcript was differentially expressed between the two DG blades after SD. Another upstream regulator predicted to be suppressed in the inferior blade after SD was *Wasl* (WASP like actin nucleation promoting factor). Consistent with this prediction, a number of transcripts encoding actin-regulating factors (*Arpc2, 3,* and *4*, and *Atcr2*) were all selectively downregulated in the inferior blade relative to the superior blade after SD (but not after *ad lib* sleep), although expression levels for *Wasl* itself did not differ between the blades after SD.

Because *de novo* protein synthesis and actin cytoskeleton rearrangement are thought to be critical for synaptic plasticity and memory consolidation, the selective disruption of these two cellular pathways in the inferior blade after SD may lead to SD-mediated memory consolidation deficits. Taken together, these analyses identify numerous functional differences between the superior and inferior blades which appear specifically under SD conditions. These SD-driven changes are likely to disrupt synaptic and structural plasticity in inferior blade granule cells, and are consistent with the selective disruption of engram neuron reactivation in the inferior blade

during SD. These transcriptomic differences may either represent either an upstream cause, or a downstream consequence, of this subregion-specific activity disruption.

3.3.6 CFC-induced transcriptomic effects in the hours following learning are restricted to the hippocampal DG.

Recent findings using translating ribosome affinity purification (TRAP) seq have revealed that transcriptomic effects of CFC vary with cell type in the hippocampus, and are almost exclusively restricted to ribosomes associated with neuronal cell and organellar membranes (12). To understand how CFC affects transcripts in different hippocampal subregions, we quantified transcriptomic effects of learning (comparing CFC vs. HC) using data from all mice, using sleep condition (Sleep or SD) as a covariate (**Figure 3.7a**). In dramatic contrast to the more widespread effects of Sleep vs. SD (**Figure 3.4c**), CFC itself had no significant effects on transcripts measured 6 h later in CA3 or CA1 pyramidal cell layers, or in the DG hilus. CFC altered the most transcripts (784 CFC vs. HC DEGs) within the DG superior blade. We identified two cellular component GO terms - synaptic membrane (GO:0097060, smallest common denominator-corrected $p_{adj} = 0.016$) and GABA receptor complex (GO:1902710, $p_{adj} = 0.045$) - that had constituent transcripts significantly enriched among DEGs altered in the superior blade by CFC (**Figure 3.7c**). 45 DEGs mapped to the synaptic membrane term. Transcripts downregulated in the superior blade after CFC included GABAA receptor subunit-encoding genes *Gabra3, Gabrg3,* and *Gabra2, Rims3* (encoding a presynaptic regulator of exocytosis), *Dcc* (encoding a protein with pre and postsynaptic roles in excitatory synapse plasticity), *Lrfn5* (encoding a cell surface regulator of synapse assembly), *Ache* (encoding acetylcholinesterase), *L1cam* (encoding an presynaptic cell surface adhesion regulator),

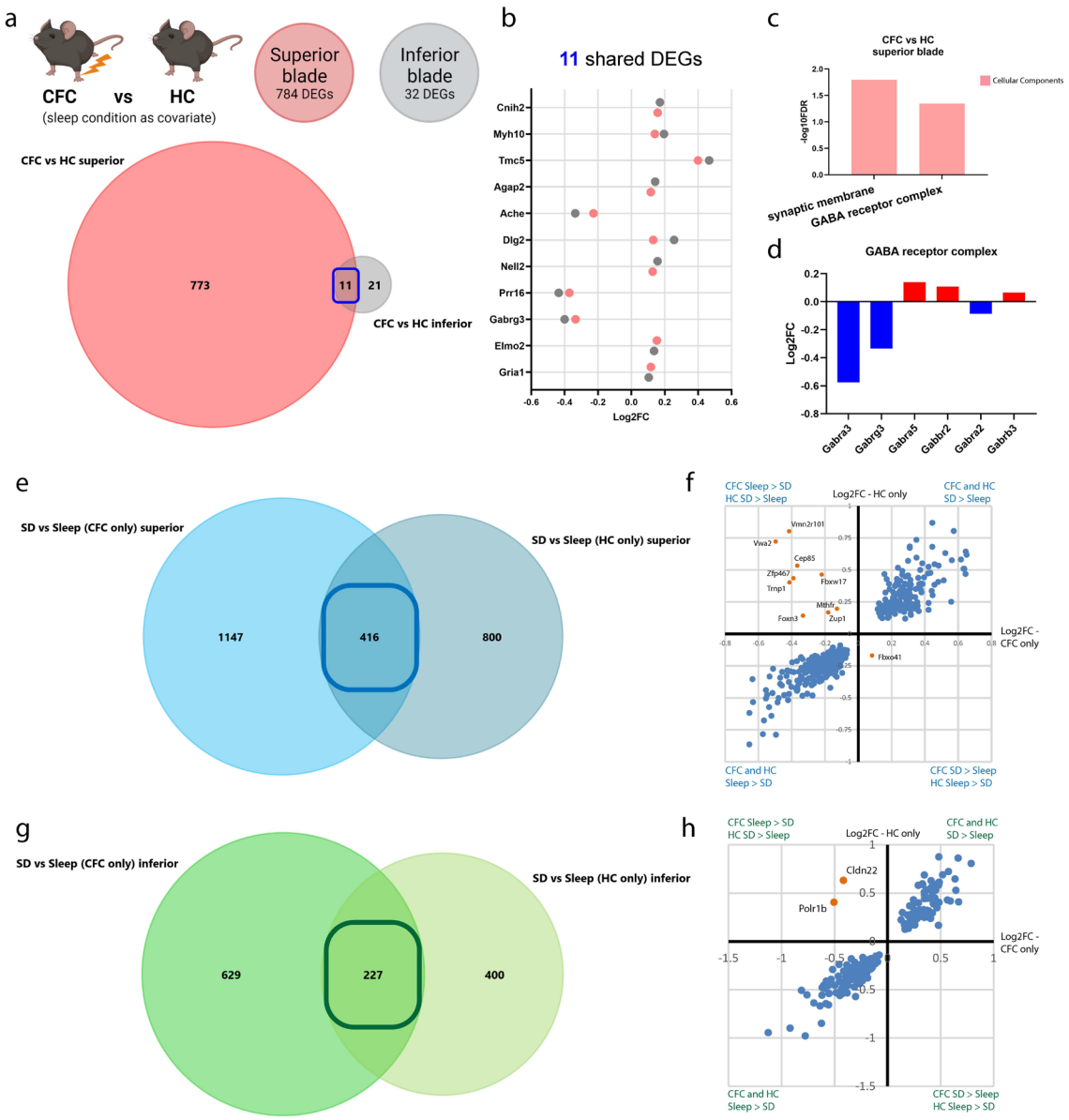

Figure 3.7 Learning (CFC)-induced transcriptomic effects are restricted to the hippocampal DG. a, Illustration of the CFC vs HC comparison and the number of DEGs in superior blade and inferior blade. There are no DEGs found in the CA1, CA3, and hilus for the CFC vs HC comparison. Venn diagram reflects the overlap (11 transcripts) for CFC vs HC. **b,** CFC altered 11 transcripts significantly in both superior (red) and inferior blade (gray). **c,** Significant GO terms mapped for the DEGs altered by CFC in the superior blade. **d,** DEGs altered by CFC mapped for the GABA receptor complex GO term. **e,** In mice that received CFC, 1563 transcripts were altered by subsequent SD in the superior blade while in HC mice, the number was 1216. 416 of them overlapped. **f,** Expression level of the 416 overlapping SD-altered DEGs between CFC-only and HC-only mice. Blue dots represent transcripts that are consistently enriched in the two groups following either sleep or SD. Orange dots represent genes that are regulated in opposite directions by SD in the two groups of mice. **g,** In CFC mice, 856 transcripts were altered by subsequent SD in the inferior blade while in HC mice, the number was 627. 227 of them overlapped. **h,** Expression level of the 227 overlapping SD-altered DEGs between CFC-only and HC-only mice. Polr1b and Cldn22 (orange dots) were upregulated by SD in HC mice, but downregulated by SD in CFC mice.

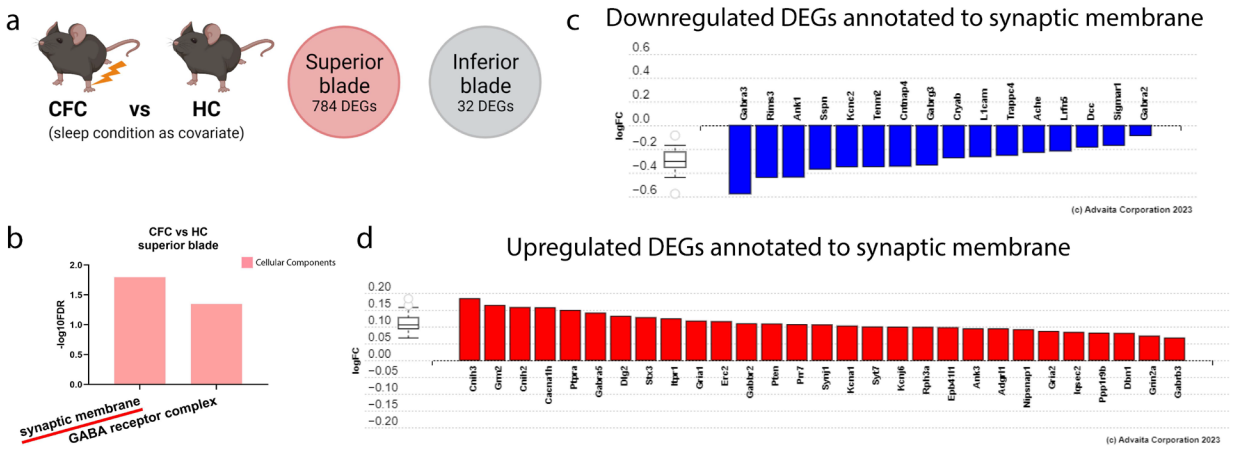

Supplemental Figure S 3.11 CFC-altered DEGs annotated to gene ontology term synaptic membrane. a, Illustration of the CFC vs HC comparison. **b,** Significant GO terms mapped for the DEGs altered by CFC in the superior blade. **c,** CFC downregulated DEGs annotated to synaptic membrane. **d,** CFC upregulated DEGs annotated to synaptic membrane.

Trappc4 (trafficking protein particle complex 4, which is involved in dendrite development and endosome regulation), *Kcnc2* (encoding voltage-gated potassium channel Kv3.2), *Tenm2* (teneurin transmembrane protein 2), *Cntnap4* (contactin associated protein-like 4, a regulator of GABAA receptor localization and transmission), and *Ank1* (which links synaptic membrane proteins to the spectrin cytoskeleton) (**Supplemental Figure S3.11c**). Many more transcripts in the GO term were upregulated in the superior blade after CFC, including those encoding both metabotropic (*Grm2*) and ionotropic (*Gria1*, *Gria2*, *Grin2a*) glutamate receptor subunits, two cornichon family members (*Cnih2* and *Cnih3,* auxiliary AMPA receptor subunits that promote receptor transmission), components of the presynaptic vesicle release machinery (*Erc2*, *Stx3, Syt7*), potassium (*Kcna1*, encoding voltage gated delayed rectifier Kv1.1, and *Kcnj6*, encoding presynaptic inward rectifier GIRK2) and calcium channels (*Cacna1h*, encoding T-type voltage gated Ca(v) 3.2), metabotropic GABA receptor 2 (*Gabbr2*), regulator of postsynaptic receptor internalization synaptojanin (*Synj1*), postsynaptic MAGUK scaffold protein discs large 2 (*Dlg2*), inositol 1,4,5-trisphosphate receptor 1 (*Itpr1*), *Dbn1* (encoding drebrin1, a postsynaptic actin and profilin interacting protein that positively regulates dendritic spine morphogenesis and glutamatergic receptor localization), *Rph3a* (rabphilin 3a, which retains NMDA receptors at the postsynaptic density), and *Ank3* (which anchors transmembrane proteins at both synaptic structures and the axon initial segment). CFC also upregulated transcripts encoding synaptic membrane proteins with less well-characterized function, but which have been identified as risk genes for autism in genome-wide screens (*Nipsnap1*, *Iqsec2, Adgrl1*, *Epb41l1,* and *Pten*) (**Supplemental Figure S3.11d**). Six CFC vs. HC DEGs were also associated with the GABA receptor complex term, including *Gabra3*, *Gabrg3*, *Gabra5*, *Gabbr2*, *Gabra2*, *Gabrb3* (**Figure 3.7d**). The overall profile of transcript changes - with downregulated transcripts related to

GABAergic signaling and upregulated transcripts related to structural remodeling and glutamatergic signaling - suggests that excitatory-inhibitory balance may change in the superior blade following learning. Together, these data support the same conclusion as our prior work (12) – that CFC strongly affects membrane-associated and synaptic components of neurons – and indicates that these post-learning synaptic and structural changes are present for many hours post-CFC across the DG superior blade.

In comparison with the relatively large number of CFC vs. HC DEGs in the DG superior blade, only 32 transcripts were altered by CFC in the inferior blade (**Figure 3.7a**). Of these, 11 transcripts (*Cnih2* (↑), *Myh10* (↑), *Tmc5* (↑), *Agap2* (↑), *Ache* (↓), *Dlg2* (↑), *Nell2* (↑), *Prr16* (↓), *Gabrg3* (↓), *Elmo2* (↑), and *Gria1* (↑)) were similarly altered in both superior and inferior blades after CFC vs. HC (**Figure 3.7b**). While fewer in number, this set of transcript changes is nonetheless consistent with effects on synaptic plasticity and changing excitatory-inhibitory balance, which may be present in both DG blades following learning.

To further characterize the possible interactions between learning and subsequent sleep or SD, we next assessed the effects of SD separately in the DG blades of CFC and HC mice. In CFC mice (n = 4 for CFC-Sleep and n = 4 for CFC-SD), SD significantly altered expression of 1563 and 856 transcripts in the superior and inferior blades, respectively, while in HC mice (n = 4 for HC-Sleep and n = 3 for HC-SD), SD altered 1216 and 627 transcripts in the superior and inferior blades, respectively **(Figure 3.7e, g)**. Of these, only 416 SD DEGs overlapped between CFC and HC mice in the superior blade, and 10 of those 416 overlapping transcripts were differentially regulated based on prior learning (**Figure 3.7f**). These included *Vmn2r101* (encoding a putative g protein-coupled receptor), *Vwa2* (encoding an extracellular matrix protein), and a number of factors involved in DNA regulation: *Cep85* (centrosomal protein 85),

Zfp467 (zinc finger protein 467), *Trnp1* (TMF1 regulated nuclear protein 1, a putative euchromatin DNA-binding factor), *Fbxw17* (F-box and WD-40 domain protein 17), *Foxn3* (a member of the forkhead/winged helix transcription factor family), *Mthfr* (methylenetetrahydrofolate reductase), and *Zup1* (zinc finger containing ubiquitin peptidase 1, thought to be involved in regulating DNA repair), which were upregulated by SD in HC mice but downregulated by SD in CFC mice, and *Fbxo41* (encoding a neuron-specific F-box protein), which was upregulated by SD in CFC mice but downregulated in HC mice (**Figure 3.7f**). Similarly, in the inferior blade, only 227 SD-altered transcripts overlapped between CFC and HC mice. *Polr1b* (RNA polymerase I polypeptide B) and *Cldn22* (claudin 22) were upregulated by SD in HC mice, but downregulated by SD in CFC mice (**Figure 3.7h**). While the function of these differential transcriptomic responses to SD is a matter of speculation, one possibility is that DNA repair and transcription regulatory mechanisms are differentially engaged by SD, depending on whether a memory has been recently encoded. What is clear is that for the above genes, the effects of sleep loss are dependent on prior learning experiences.

3.3.7 SD and learning differentially affect protein and phosphoprotein abundance between hippocampal subregions

To clarify the relationship between changing transcript levels and protein abundance, we next used DSP to profile select protein and phosphoprotein levels in each hippocampal subregion. A total of 87 proteins were quantified, using panels of antibodies targeting markers of neural and glial cell types, autophagy, cell death, MAPK and PI3K/AKT signaling pathways, and Alzheimer's and Parkinson's disease pathologies. Statistical comparisons between treatment groups and subregions mirrored those used for WTA. We first assessed the effects of SD itself

(comparing SD vs. Sleep) with learning condition (CFC/HC) as a covariate. We observed increased levels of phosphorylated S6 (S235/S236) and phosphorylated ERK1/2 (42/44 MAPK; T202/Y204) across CA1, CA3, and DG hilus following SD, consistent with IEG expression changes we observed in these structures (**Figure 3.3**). Together with our previous findings [17], these data suggest elevated activity in these subregions after SD. Additional SD-driven changes present in these regions include increased phosphorylated p90 RSK (T359/S363) and decreased phosphorylated Tau (T231) in CA1, increased phosphorylated Tau (S214) in both the hilus and CA3, and increased beta-secretase 1 (BACE1) and decreased myelin basic protein and S100B within CA3 only (**Figure 3.8a**). Somewhat surprisingly, no significant changes due to Sleep vs. SD were observed for proteins quantified in either of the DG blades when the learning condition was used as a covariate.

We then compared protein expression between DG inferior and superior blades (Inferior vs. Superior), again using the learning condition (CFC/HC) as a covariate. 34 proteins differed between the blades in freely-sleeping mice; 38 were differentially expressed between the blades following SD (**Figure 3.8c**). 30 differentially-expressed proteins overlapped between SD and Sleep conditions (**Figure 3.8c**). In freely-sleeping mice, 5 of the 34 differentially-expressed proteins had corresponding transcript-level differences by WTA, although the direction of expression differences between blades for transcript vs. protein did not always correspond. For example, pan-AKT and phosphorylated AKT1 (S473) levels were higher after sleep in the inferior blade, while *Akt1* transcript levels were higher in the superior blade. Phosphorylated GSK3A (S21) and GSK3B (S9) proteins were similarly expressed at higher levels in the inferior blade, while the *Gsk3a* transcript was more abundant in the superior blade. One plausible explanation for the differences in transcript vs. protein abundance is that these

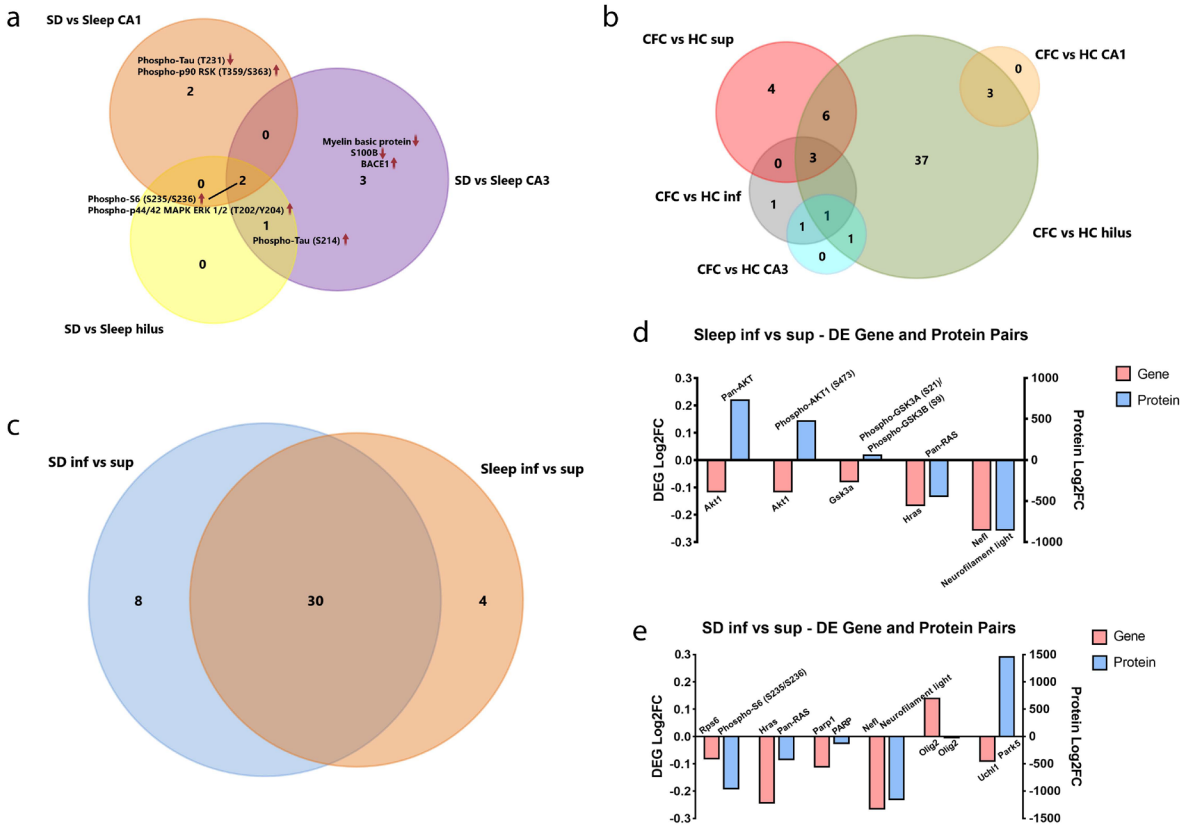

Figure 3.8 Learning and subsequent sleep or SD differentially affect protein expression in hippocampal subregions. a, Venn diagram of SD-altered proteins in CA1, hilus, and CA3. **b,** Venn diagram of CFC-altered proteins in hippocampal subregions. **c,** Venn diagram reflects the overlap (30 proteins) of inferior vs superior blade differentially expressed proteins under Sleep or SD condition. **d,** Log2FC of proteins differentially expressed between inferior and superior blade in the sleep mice and their corresponding DEGs for the same comparison in the WTA analysis. **e,** Log2FC of proteins differentially expressed between inferior and superior blade in the SD mice and their corresponding DEGs for the same comparison.

reflect differences in the rate of protein synthesis of transcripts between the blades. (**Figure 3.8d**).

In SD mice, 6 of the 38 proteins differentially expressed between the two DG blades also had transcript-level differences by WTA. Here again, the differences in protein and transcript levels occasionally moved in opposite directions. For example, Olig2 (a transcription factor that regulates oligodendrocyte, interneuron, and motor neuron development) protein was expressed at higher levels in the superior blade while the *Olig2* transcript was more abundant in the inferior blade. Park5 (ubiquitin C-terminal hydrolase L1) protein levels were higher in the inferior blade after SD, while corresponding transcript *Uchl1* was more abundant in the superior blade (**Figure 3.8e**). As might be expected for SD mice (based on engram neuron reactivation and IEG expression levels; **Figures 3.2** and **3.3**), phosphorylated S6 (S235/S236) and its corresponding transcript *Rps6* were both present at higher levels in the superior blade vs. inferior blade following SD. Similarly, pan-RAS GTPase, DNA repair enzyme poly-ADP-ribose polymerase (PARP), and neurofilament light, as well as corresponding transcripts *Hras, Parp1*, and *Nefl*, were all expressed at higher levels in the superior vs. inferior blade in SD mice. (**Figure 3.8e**). Of these, pan-Ras and neurofilament light were consistently enriched in the superior blade regardless of the sleep state, indicating a plausible constitutive difference between the two blades (**Figure 3.8d-e**).

Lastly, we quantified changes in protein levels that were due to learning (comparing CFC vs. HC), using sleep condition (Sleep/SD) as a covariate (**Figure 3.8b**). Three proteins were altered by learning in CA1 (neurofilament light, autophagy protein beclin 1, and MER tyrosine kinase) and in CA3 (Tau, phosphorylated Tau [T231], and apolipoprotein A-I). Learning altered slightly more proteins in the superior and inferior blades (13 and 6, respectively). Of these, 3

were significantly increased after learning in the inferior blade only (Tau, phosphorylated Tau [T199], phosphorylated Tau [T231]), and 10 were altered by learning in the superior blade only (including increases in ERK1/2, NeuN [a neuronal nuclear protein that regulates synaptic plasticity], MAP2, and Park5, and decreases in the amyloid-β regulating enzyme neprilysin, phosphorylated GSK3A [S21] and GSK3B [S9], phospho-AMPK-alpha [T172], phospho-PRAS40 [T246], p53, and beta-secretase 1). Surprisingly, the subregion with the most significantly-altered proteins after learning was the hilus, where (despite the lack of transcripts altered by CFC) 51 proteins were affected. 3 of these protein-level changes overlapped among all three DG subregions (superior, inferior blade and hilus) after CFC: MEK1 was significantly upregulated, while pan-RAS and phosphorylated ERK1/2 (42/44 MAPK; T202/Y204) were significantly downregulated.

Taken together, these data suggest that as is true for transcriptomic changes following learning and subsequent sleep or SD, protein abundance is also differentially affected by these processes within each dorsal hippocampal subregion. While the number of proteins and phosphoproteins profiled here was limited, these changes included effects on components of signaling pathways involved in activity-dependent plasticity, protein synthesis and ubiquitination, and responses to neuronal stress. These effects were also subregion-specific, with changes due to sleep vs. SD alone (regardless of prior learning) most prominent in CA1 and CA3 (and absent from the DG blades), and changes due to learning (regardless of subsequent sleep or SD) most prominent in the DG.

Table 3.1 SD vs Sleep Upstream Regulator - Genes

Subregion	Comparison	Symbol	Entrez	LogFC	adjpv	Predicted as	FDR
CA1	SD vs Sleep	Rab18	19330	-0.049	0.759	inhibited	0.001
CA1	SD vs Sleep	Rab3gap2	98732	0.037	0.861	inhibited	0.001
CA1	SD vs Sleep	Rab3gap1	226407	0.095	0.623	inhibited	0.001
superior	SD vs Sleep	Cask	12361	0.068	0.454	inhibited	0.007
superior	SD vs Sleep	Lin7b	22342	-0.175	0.014	inhibited	0.007
superior	SD vs Sleep	Lin7c	22343	0.043	0.5	inhibited	0.007
superior	SD vs Sleep	Lin7a	108030	-0.022	0.845	inhibited	0.007
superior	SD vs Sleep	Apba1	319924	-0.126	0.012	inhibited	0.007
superior	SD vs Sleep	Unc13b	22249	-0.016	0.913	inhibited	0.007
hilus	SD vs Sleep	Atf6	226641	-0.036	0.902	activated	3.91E-06
hilus	SD vs Sleep	Ufm1	67890	0.021	0.962	activated	0.023
hilus	SD vs Sleep	Xbp1	22433	0.395	0.007	activated	0.03
hilus	SD vs Sleep	Zfx	22764	0.095	0.844	inhibited	0.018
hilus	SD vs Sleep	Ppa1	67895	-0.07	0.857	inhibited	0.018

LogFC and adjpv are measured fold change and adjusted p-value for the particular gene's expression.
FDR indicates the p-value corrected for multiple comparisons for the upstream refulator prediction.
Blue highlights the downregulated gene that is consistent with the inhibition prediction.
Red highlights the upregulated gene that is consistent with the activation prediction.

Table 3.2 SD vs Sleep Upstream Regulator - miRNAs

Subregion	Comparison	miRNA Name	FDR
CA1	SD vs Sleep	mmu-miR-27a-3p	0.013336492
CA1	SD vs Sleep	mmu-miR-27b-3p	0.013336492

Table 3.3 inf vs sup Upstream Regulator

Condition	Comparison	Symbol	Entrez	LogFC	adjpv	Predicted as	FDR
SD	inf vs sup	Exosc10	50912	0.022	0.912	inhibited	0.006
SD	inf vs sup	Mtrex	72198	-0.079	0.497	inhibited	0.006
SD	inf vs sup	C1d	57316	0.025	0.872	inhibited	0.006
SD	inf vs sup	Wasl	73178	-0.046	0.617	inhibited	0.006
SD	inf vs sup	Bud23	66138	-0.039	0.865	inhibited	0.024

LogFC and adjpv are measured fold change and adjusted p-value for the particular gene's expression. FDR indicates the p-value corrected for multiple comparisons for the upstream refulator prediction.

3.4 Discussion

Our results demonstrate that post-learning DG engram neuron reactivation is state-dependent and occurs in a subregion-specific manner during post-learning sleep (**Figures 3.1-2**). We also find that while most hippocampal subregions (DG hilus, CA1, and CA3) are more active during SD than during sleep, activation of DG inferior blade granule cells is selectively suppressed (**Figure 3.3**). These subregion-specific findings inspired us to explore how the transcriptome within these regions is affected by single-trial CFC, and as a function of sleep vs. SD (**Figures 3.4-7**). Our spatial transcriptomic analysis demonstrates that transcripts affected by learning and subsequent sleep state differ substantially between CA1, CA3, and DG subregions. We also find that when measured 6 h following CFC, learning-driven transcript changes are detectable only within the DG superior and inferior blade (despite persistent, and subregion-specific, changes in select proteins' abundance in all regions). Together these findings present a picture of the hippocampus as a diverse landscape, where sleep loss has distinct effects in each region, and where following learning, persistent sleep-dependent, activity-driven gene expression changes are restricted to the DG.

This study adds to what is known about the function of hippocampal engram ensembles during memory encoding and consolidation, and more specifically how sleep contributes to this process. Engram neurons in DG are thought to be critical for contextual memory encoding [36] and recall (25, 26). Our data **(Supplemental Figure S3.1)** agree with recent findings that context-associated behaviors preferentially activate suprapyramidal blade DG granule cells [28, 29]. We find that context-activated neurons in the superior blade are preferentially reactivated during context re-exposure and same-context CFC **(Figure 3.1d** and **j)**. Together, these findings

suggest that context is more selectively encoded in DG by superior blade neurons than by inferior blade neurons.

Sleep-associated reactivation of engram neurons has been hypothesized as an important mechanism for memory consolidation (2, 3, 42). However, only a few recent studies have focused on the functional role of engram populations in the hours following learning (12, 28, 29). Here we find evidence for sleep-associated reactivation of DG engram neurons, with post-CFC sleep required for reactivation in the inferior blade (**Figure 3.2e-f**). Because our data suggest that the inferior blade engram population is less selective for context than superior blade TRAP-labeled neurons, it is tempting to speculate that reactivation of inferior blade neurons during sleep provides mnemonic information about other aspects of the CFM engram – for example, the emotional salience of the context, rather than the context itself. This would be consistent with the phenotype observed after experimental post-CFC sleep disruption – i.e., a reduction in freezing behavior, suggesting a lack of fear association with the context (9, 11, 12) (**Figure 3.2b**). Future studies will be needed to clarify the differential functional consequences of offline reactivation in superior vs. inferior blade engram populations. While technically challenging, this could theoretically be addressed by selectively activating or inhibiting one population or the other in the hours following CFC.

An unanswered question is *why* engram neuron populations in the two DG blades respond differently to post-learning sleep vs. SD. One possibility is that overall, granule cell activity levels differ between the blades during SD. Consistent with this, we find that Arc+ and Fos+ neuron numbers in DG inferior blade, but not the superior blade or hilus, consistently decrease after 6-h SD (**Figure 3.2i, Figure 3.3c-d**). Spatial transcriptomic profiling largely corroborates this – with activity-driven transcripts' abundance reduced by SD in the inferior

blade, and simultaneously increased in other hippocampal subregions (e.g., **Figure 3.5b**, **d**, and **f; Figure 3.6b**).

What neurobiological mechanisms underlie the selective SD-driven gating of inferior blade granule cells? Our present findings confirm constitutive differences in cell marker expression (e.g., higher *Npy* and *Penk* expression in superior blade vs. inferior blade; **Figure 3.6b**), which are present between the two blades across conditions. Thus, there are apparent baseline differences in the cellular makeup of the two blades' granule cell populations (32), which may impact the processes of learning and memory storage. The two blades are also known to differ with respect to their cortical inputs (43), with a greater number of lateral entorhinal inputs targeting the superior blade, and more numerous medial entorhinal inputs targeting the inferior blade. Thus, one possibility is that these excitatory presynaptic inputs are differentially active in the context of SD. Another important distinction is that the superior blade also has roughly half the interneuron density of the inferior blade (44). This latter finding suggests that selective inhibitory gating of the inferior blade could serve as a plausible mechanism by which engram neuron reactivation is suppressed during SD (20, 45).

We used spatial transcriptomics in this study as a tool to better understand the broader transcriptomic changes that are spatially and temporally associated with differences in overall activation, and engram neuron reactivation, of the two DG blades during SD. We find that, as was true across all 5 profiled hippocampal subregions (**Figures 3.4** and **3.5; Supplemental Figure S3.5**), the two blades' transcriptomic responses to SD were distinct (**Figure 3.4**; **Supplemental Figures S3.5, 3.7, 3.8**). Moreover, transcript differences between the blades differed substantially between Sleep and SD conditions (**Figure 3.6**). Our analyses identified two key processes – regulation of actin cytoskeleton, and ribosomal biogenesis – which are

significantly downregulated in the inferior blade after SD. Critically, these findings are consistent with available neuroanatomical and biochemical data, which have found disruptions in these pathways after SD, either across the hippocampus as a whole, or specifically within the DG (12, 15, 41, 46). Since both actin cytoskeletal remodeling and ribosomal biogenesis are critically associated with memory storage in the hippocampus (12, 15, 47, 48), disruption of both pathways in inferior blade at the transcriptional level could be sufficient to disrupt consolidation of CFM.

Our spatial profiling of dorsal hippocampus adds to a growing literature emphasizing the heterogeneity of SD effects of gene expression (12, 21) and neural activity (20, 21, 49, 50) in various brain structures. Collectively, these data demonstrate that sleep functions, particularly with regard to synaptic plasticity and cognition, cannot be assumed to be uniform across neuron (or other brain cell) types, or brain circuits (2, 51). It is worth noting that while the transcripts altered by SD varied between hippocampal subregions, with only partial overlap (**Figures 3.4** and 3.**5**), these SD-altered transcripts also only partially overlapped with transcripts altered by SD across whole hippocampus (18), and ribosome-associated transcripts isolated from specific hippocampal cell populations (12, 16) and subcellular fractions (12) after SD (**Supplemental Figures S3.12** and **3.13**). This diversity of SD effects is also present, in our hands, between subregions at the level of protein expression (**Figure 3.8a**). Given this diversity – with SD effects on transcripts and proteins varying with cell compartment, type, and structure, it is plausible that our present findings could by biased due to technical aspects of our spatial profiling strategy. For example, because only the cell body layers are profiled in DG, CA3, and CA1, it is likely that transcripts which are efficiently transported out of the soma (i.e., into dendrites and axons) are undersampled using our technique (12, 35)(52, 53). In addition, we

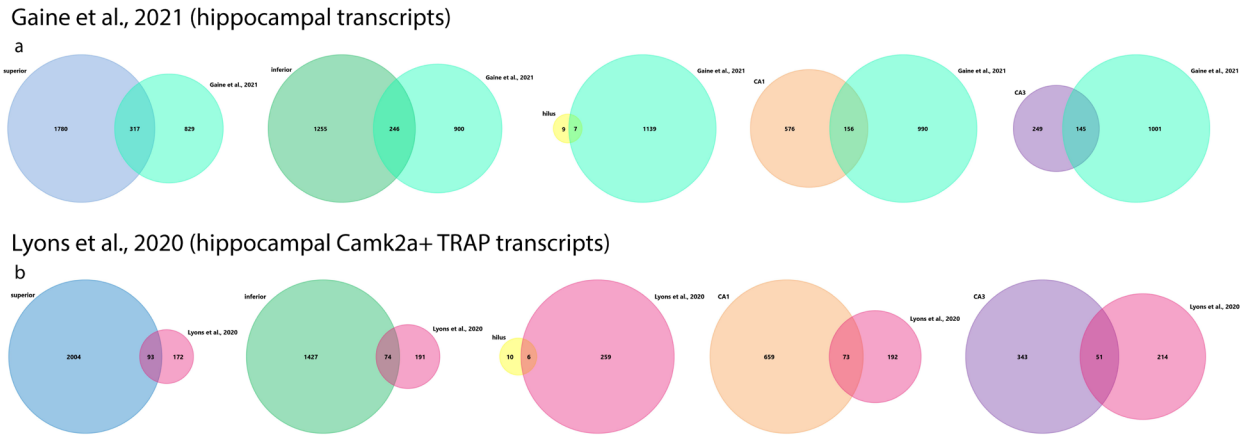

Supplemental Figure S 3.12 Venn diagrams show the overlap for transcripts altered by SD in each hippocampal subregion and those previously reported in **a**, RNAseq of whole hippocampus following SD (Gaine et al., 2021), and **b**, Camk2a+ translating ribosome affinity purification-seq following SD (Lyons et al., 2020).

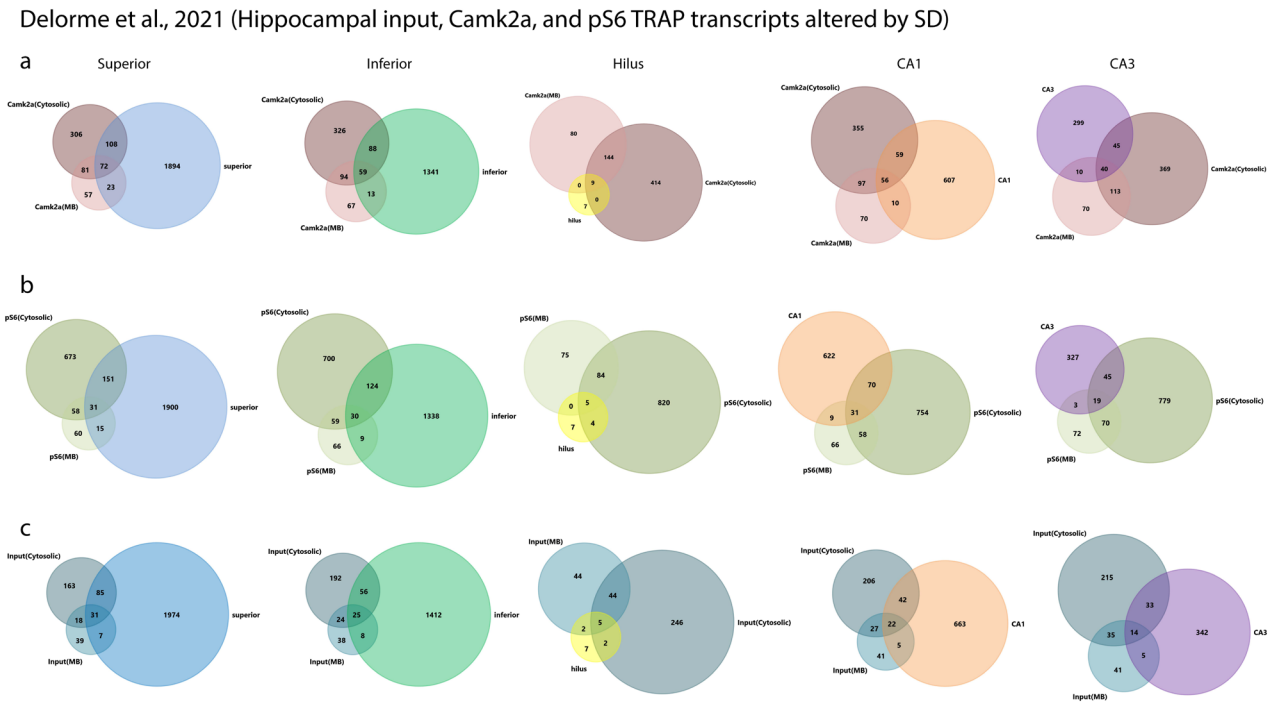

Supplemental Figure S 3.13 Overlap of SD vs Sleep DEGs with previously-characterized SD-altered translating ribosome affinity purification-seq transcripts. Venn diagrams indicate the overlap for transcripts altered by SD in five different hippocampal subregions in the present study, compared with our previous translating ribosome affinity purification-seq study, where DEGs were identified from whole hippocampus, subsampling **a**, Camk2a+ neurons, **b**, highly active, pS6+ neurons, and **c**, input (without subsampling) following SD (Delorme et al., 2021), for both cytosolic and membrane-associated fractions.

cannot discriminate between transcript changes occurring within the principal (i.e., pyramidal or granule) cell bodies, those occurring in presynaptic terminals of other excitatory, inhibitory, or neuromodulatory neurons which terminate in those layers, and those occurring in microglia, astrocytes or oligodendrocytes. For this reason, additional experiments will be needed to precisely identify the cellular sources for some of transcript and protein changes we report here after SD – e.g. differential expression of Olig2 transcript and protein between the two DG blades, which could be driven by changes in mature oligodendrocytes, precursor cells, or neurons. Another example where the cellular source of SD-driven transcript changes is unclear is within the superior blade, where transcripts encoding synaptic release regulatory machinery were downregulated after SD. While this may be due to transcript changes in the granule cells themselves, it is also plausible that this effect of SD is due to altered transcripts in presynaptic terminals located within the superior blade.

We also used spatial profiling as a strategy to identify subregion-specific changes associated with storage of a new memory (CFM) in the hippocampus. One surprising finding from this analysis was the relative paucity of detectable learning-induced transcript changes in the hippocampus at 6 h post-CFC, and that these were present only within the DG blades (**Figure 3.7**). This may be due in part to the fact that measurements occurred several hours after the single-trial learning event; it is plausible that many transcriptional responses to memory encoding are relatively transient, and for that reason are no longer detectable by this 6-h time point. While additional studies will be needed to clarify this point, what is certain is that sustained transcriptomic responses to CFC are restricted to the two DG blades. Critically, we find that transcripts that remain altered several hours after CFC include those critically involved in glutamatergic and GABAergic synaptic functions – which are generally upregulated and

downregulated, respectively, in the superior blade after CFC (**Figure 3.7; Supplemental Figure S3.11**). Identified CFC-driven transcript changes in inferior blade, while fewer, followed a similar overall pattern – i.e., transcripts involved in glutamatergic synapse biogenesis were upregulated, while GABA receptor transcripts were downregulated, after CFC. This strongly supports the hypothesis that excitatory-inhibitory balance changes in specific brain circuits accompanies, and benefits, long-term memory storage (54)(20, 55, 56). The finding that these changes are constrained to DG, among all subregions profiled, is consistent with the prior finding of sustained transcriptomic changes occurring specifically within DG engram neurons 24 h post-CFC (57), and may reflect unique dynamics of the DG network (or the engram neurons within it), which could plausibly outlast changes after learning in other hippocampal structures (11, 58, 59). This interpretation could reconcile the findings that while CFC-associated transcriptomic changes were absent in CA3 and CA1 at the 6-h timepoint, while protein abundance changes due to CFC were still detected (**Figure 3.8**).

Together, our data advance the findings of previous studies (20, 21, 31, 32, 60, 61) highlighting the heterogeneity of hippocampal subregions' function in the context of learning, and response to subsequent sleep or sleep loss. The present findings suggest that the influences of sleep and SD on hippocampally-mediated memory consolidation are linked to subregion-specific changes in both engram neuron reactivation and biosynthetic events related to protein synthesis regulation, synaptic signaling, and remodeling of neuronal cytoskeletal structures.

3.5 Materials and Methods

Animal handling and husbandry

All animal husbandry and experimental procedures were approved by the University of Michigan Institutional Animal Care and Use Committee. Mice from 3 to 6 months old were used for all experiments. With the exception of a 3-day period of constant dark housing following 4-hydroxytomaxifen (4-OHT) administration (see below), mice were maintained on a 12 h: 12 h light/dark cycle (lights on at 9AM) with *ad lib* food and water throughout the study. cfos-CRE^{ER} mice (31) B6.129(Cg)-Fos$^{tm1.1(cre/ERT2)Luo}$/J; Jackson) were crossed to B6.Cg-Gt(ROSA)26Sor$^{tm9(CAG-tdTomato)Hze}$/J (Jackson) mice to induce CRE recombinase-mediated expression of tdTomato (*cfos::tdTomato*). Mice were individually housed with beneficial environmental enrichment in standard caging 4 days prior to genetic tagging of engram cells and/or contextual fear conditioning (CFC), and were habituated to daily handling (2-5 min/day) for 3 days prior to the experiments.

Genetic labeling of hippocampal engram cells

On the day of genetic labeling, starting at lights on (ZT0), mice were individually placed in one of the two novel contexts (Context A or Context B). Context A was a 24 × 24 × 23 cm square arena with metal grid floor, scented with an all-purpose sponge soaked with 5 ml Lysol (lemon breeze scent) attached to the lid of the chamber. Context A was surrounded by 4 LED monitors presenting a 135° flickering oriented grating stimulus (100% contrast, 0.05 cycles/deg, flickering at 1 Hz). Context B was a 23 × 23 × 22 cm cylindrical arena with a pink glossy plastic floor scented with an all-purpose sponge soaked with 1 ml 1% ethyl acetate attached to the lid of the chamber. Context B was surrounded by 4 LED monitors presenting either a vertical oriented grating stimulus or a dark screen. For genetic labeling, immediately following 15 min of free

novel context exploration, mice received an i.p. injection of 4-OHT (50 mg/kg in corn oil). They were then returned to their home cage, which was placed in complete darkness inside a sound-attenuated chamber over the next 3 days to minimize non-specific TRAP-based neuronal labeling (62). 3 days following 4-OHT administration, mice were returned to a normal 12 h: 12 h LD cycle for an additional 3 days prior to behavioral experiments.

Behavioral procedures

For CFC behavioral experiments (**Figure 3.2a-b**), At ZT0, male and female C57BL/6J mice (Jackson) or WT siblings of *cfos::tdTomato* mice underwent single-trial CFC as described previously (11, 58, 59). Briefly, mice were placed in Context A and were allowed 3.5 min of free exploration time prior to delivery of a 2-s, 0.75 mA foot shock through the chamber's grid floor. After 5 min total in the chamber, mice were returned to their home cage, where they were either allowed *ad lib* sleep or were sleep deprived (SD) under normal room light for the first 6 h following training, using the gentle handling procedures (including cage tapping, nest material disturbance, and light touch with a cotton-tipped applicator when necessary). After SD, all mice were allowed *ad lib* sleep. 24 h following CFC, at lights on (ZT0; next day) mice were returned to Context A for 5 min to assess CFM. CFM was measured quantitatively as % time spent freezing during re-exposure to Context A using previously established criteria (63) (crouched, rigid posture with no head or whisker movement). Two scorers blinded to behavioral conditions independently quantified periods of freezing behavior prior to shock during CFC and during CFM testing.

For TRAP labeling and context re-exposure experiments (**Figure 3.1a-f**), at ZT0 on the day of re-exposure, male and female *cfos::tdTomato* mice that underwent TRAP labeling 6 days previously (following Context A exploration) were either returned to Context A, or were placed

in distinct Context B. Following 15 min of free exploration, all mice were returned to their home cage inside of a dark, sound-attenuated chamber to minimize interference and disturbances. 90 min after the second context exposure, mice were sacrificed via an i.p. Injection of Euthasol and were transcardially perfused with ice-cold 1× PBS followed by 4% paraformaldehyde.

For context re-exposure with CFC experiments (**Figure 3.1g-l**), at ZT0 on the day of CFC, male *cfos::tdTomato* mice that underwent TRAP labeling 6 days previously (following either Context A or Context B exploration) underwent single-trial CFC in Context A as described above, after which they were returned to their home cage in a dark, sound-attenuated chamber. 90 min after CFC, mice were sacrificed and perfused as described above.

For context re-exposure with CFC followed by Sleep/SD (**Figure 3.2c-i**), at ZT0 on the day of the experiment, male *cfos::tdTomato* that underwent TRAP labeling 6 days previously (following Context A exploration) underwent single-trial CFC in Context A as described above. All mice were then returned to their home cage, and either were allowed *ad lib* sleep or were sleep deprived (SD) under normal room light for the next 6 h using gentle handling procedures (including cage tapping, nest material disturbance, and light touch with a cotton-tipped applicator when necessary). Immediately following the 6-h post-CFC sleep or SD window, mice were sacrificed and perfused as described above.

For spatial profiling experiments in **Figures 3.3-3.6**, at ZT0 on the day of the experiment, male C57BL/6J mice (Jackson) underwent single-trial CFC in Context A, then were returned to their home cage and either were allowed *ad lib* sleep or were sleep deprived (SD) under normal room light for 6 h as described above. Immediately after SD, all mice were sacrificed and perfused as described above.

Immunohistochemistry

Immediately following perfusions, brains were dissected and post-fixed at 4°C in 4% paraformaldehyde (PFA) for 24 hours. Post-fixed brains were then sectioned coronally at 80-100 μm using a vibratome (Leica VT1200 S). Sections containing dorsal hippocampus were blocked in PBS with 1% TritonX-100 and 5% normal donkey serum overnight, then incubated at 4°C for 3 days in rabbit-anti-cfos 1:1000 (Abcam; ab190289) and either goat-anti-tdTomato 1:600 (SICGEN; AB8181-200) or guinea pig-anti-Arc 1:500 (Synaptic Systems; 156004). Sections were then incubated with secondary antibodies at 4°C for 2 days in CF™ 633 Anti-Rabbit IgG H+L 1:1000 (Sigma-Aldrich; SAB4600132), Alexa Fluor® 488 AffiniPure Donkey Anti-Goat IgG H+L 1:800 (Jackson ImmunoResearch; 705-545-003), DAPI (Sigma-Aldrich D9542) or CF™555 Anti-Guinea Pig IgG H+L 1:1000 (Sigma-Aldrich; SAB4600298). Immunostained sections were coverslipped in ProLong Gold antifade reagent (ThermoFisher; P36930) and were imaged using a Leica SP5 upright laser scanning confocal microscope.

Image quantification

Images of immunostained hippocampi were obtained as 20× z-stacks (step size = 5 μm) spanning the thickness of each brain slice. Settings were fixed for each imaging session. For data reported in **Figure 3.1**, 3-6 dorsal hippocampal DG sections were quantified from each mouse. For data reported in **Figure 3.2**, 7 DG sections were quantified per mouse. For data reported in **Figure 3.3**, 5 sections of DG, and 3 sections of both CA1 and CA3 were quantified per mouse. Fluorescence images were analyzed using Fiji (64). For CA1, pyramidal layer Arc and cFos immunolabeling was quantified as average pyramidal layer fluorescence intensity minus average background intensity. In each image, the entire CA1 pyramidal cell body layer as one region of interest (ROI), and background fluorescence ROIs were outlined in adjacent regions with autofluorescence but without cFos and Arc immunolabeling; mean intensity of each ROI was

obtained using Fiji. For DG and CA3 cFos+ and Arc+ cell quantification, maximum intensity z-projection was applied to each image stack, followed by adjusting the threshold to identify pixels above 1% of the intensity distribution; this yielded a binary image without background autofluorescence. Cell counting was then performed by a scorer blinded to experimental condition using Fiji. The overlap between tdTomato and cFos was quantified using cFos channel-thresholded consecutive single plane images to verify overlap between cFos and tdTomato signals within neuronal cell bodies.

Statistical analysis

Statistical analyses in **Figures 3.1, 3.2**, and **3.3** were performed using GraphPad Prism (version 9). Mann Whitney tests were used for analysis of cFos+, tdTomato+ neurons, or overlap percentages between pairs of treatment groups (**Figure 3.1c-f, Figure 3.1i-l, Figure 3.2e-i, and Figure 3.3**). Wilcoxon matched-pairs signed rank tests were used for analysis of overlap percentages in different subregions within the same animals (**Figure 3.2f** and **h**; superior vs. inferior). A Student's t-test was used for behavioral analysis of CFM (**Figure 3.2b**). For each specific comparison, the statistical tests used are listed in the figure legend. Within figures, *, **, ***, and **** indicate $p < 0.05$, $p \leq 0.01$, $p \leq 0.001$, $p \leq 0.0001$, respectively.

GeoMx Digital Spatial Profiling (DSP) slide preparation

A total of 16 PFA-fixed brains (from $n = 4$ male mice for each condition: HC-Sleep, HC-SD, CFC-Sleep, and CFC-SD) were cryosectioned at 10 μm thickness less than 2 weeks prior to GeoMx Mouse Whole Transcriptome Assay (WTA) and protein panels. Four brain sections containing dorsal hippocampus (1 from each experimental condition) were placed onto each slide (Fisherbrand Superfrost Plus) to reduce technical artifacts introduced on individual slides during the slide preparation process. Slides were stored in -80°C until being prepared for WTA. DSP

was performed as described in detail in Merritt et al. (2020) (65). Briefly, slides with fixed frozen brain sections (1 section per mouse) were baked at 60°C for 1 h, then were post-fixed with 4% PFA in 1× PBS at 4°C for 15 min. Dehydration was performed for 5 min in 50% EtOH, 2 × 5 min in 70% EtOH and 5 min in 100% EtOH, followed by antigen retrieval using boiling 10 mM sodium citrate, pH 6.0 (Sigma Aldrich C9999) for 5 min. Protease III (ACD Cat#322337) was added to brain sections at 40°C for 30 min to expose RNA targets, then *in situ* hybridizations with mouse WTA panel (20175 targets) were performed in Buffer R (NanoString); slides were covered by HybriSlips (Grace Biolabs) and incubated at 37°C overnight. The following day, two 25-min stringent washes were performed using 50% formamide and 2 × SSC, followed by an additional two 2-min washes using 2 × SSC. Brain sections were then blocked with Buffer W (NanoString) for 30 min at room temperature. SYTO 13 (NanoString, 1:100 in Buffer W) was added to each slide for 1 h in a humidified chamber at room temperature; this fluorescent nuclear stain was used to identify borders of hippocampal subregions. Slides were then briefly washed twice using 2 × SSC and were immediately loaded on the GeoMx Digital Spatial Profiler.

For protein panels, slides were baked at 60°C for 1 h followed by dehydration and antigen retrieval. The slides were then blocked using NanoString blocking buffer W for 1 h. A NanoString protein antibody cocktail including Mouse Protein Core + Controls, Mouse PI3K/AKT Module, Mouse MAPK Signaling Module, Mouse Cell Death Module, Mouse Neural Cell Typing Module, Mouse AD Pathology Module, Mouse AD Pathology Extended Module, Mouse PD Pathology Module, Mouse Glial Subtyping Module, and Mouse Autophagy Module (NanoString Technologies) was added to the sections followed by overnight incubation at 4°C. The next day, SYTO 13 was applied to each slide before loading slides on the GeoMx Digital Spatial Profiler. During slide washes for the protein panel experiment, one HC-sleep, one HC-

SD, and one CFC-Sleep brain section were lost, and were excluded from subsequent experiments. Another HC-SD brain section provided only one CA1 subregion that was usable for both WTA and protein experiments.

Each slide was imaged using a 20 × objective, and bilateral ROIs from each hippocampal subregion were selected using SYTO 13 staining using the GeoMx software. After ROI selection, UV light was applied to each ROI to achieve subregion-specific indexing oligonucleotide cleavage. The released oligonucleotides were collected via a microcapillary and dispensed into a 96-well plate; these were dried at room temperature overnight. Sequencing libraries were then prepared per the manufacturer's protocol. Libraries were sequenced on an Illumina NovaSeq 6000 with an average depth of 5.3 million raw reads per ROI.

GeoMx data analysis

Raw FASTQ files were processed using Nanostring's Automated Data Processing Pipeline. This pipeline includes adapter trimming, aligning stitched paired-end reads to barcodes in the reference, and removing PCR duplicates based on the Unique Molecular Identifier (UMI) in each read (GeoMx DSP NGS Readout User Manual, https://university.nanostring.com/geomx-dsp-ngs-readout-user-manual/1193408). All QC and downstream differential expression analyses were performed in R version 4.2.0 (2022-04-22) using the NanoString-developed GeoMxTools package (versions 1.99.4 for WTA and 3.0.1 for protein) (66). Plots were generated using either built-in GeoMxTool functions or the ggplot2 package (version 3.3.6). For the mouse WTA panel (v1.0), each gene target is mapped to a single probe with a total of 20,175 probes, 210 of which are negative probes that target sequences not present in the transcriptome. For each ROI, a Limit of Quantification (LOQ; the geometric mean of negative probes × the geometric standard deviation of negative probes raised to a power of 2) was calculated. All 128 selected ROIs

exceeded a 15% gene detection rate. Gene targets that failed to be detected above the LOQ in at least 10% of the segments were removed as recommended, leaving 11508 gene targets in the final filtered WTA dataset.

For mouse protein panels, 119 out of the initial 121 ROIs passed Nanostring recommended QC thresholds and were used for DE analyses. In total, 93 protein targets were tested, 3 of which are negative controls. Signal to background ratio for each protein target was calculated; 6 protein targets were removed due to low detection levels, leaving 87 protein targets in the final filtered protein data.

Filtered WTA and protein data were normalized using the third quartile normalization method. Linear mixed-effect models (LMMs) were used to perform differential expression analysis. Depending on the comparison, combinations of fixed effects of sleep condition (Sleep/SD), learning condition (CFC/HC), and random effects of slide (taking into account variations during slide processing steps) were adjusted for. Genes, transcripts, and protein targets that have an FDR < 0.1 are considered differentially expressed (DE). Venn diagrams of overlapping DEGs/DE proteins between regions/conditions were made using FunRich (67). Gene ontology (GO), KEGG pathway, and predicted upstream regulator analyses were performed using Advaita Bio's iPathwayGuide (https://advaitabio.com/ipathwayguide), using an FDR < 0.1 multiple comparisons *p* value correction for all analyses. A smallest common denominator pruning method (iPathwayGuide) was used to identify GO terms, due to the high number of DEGs and overlapping GO terms identified. FDR-based p-value correction was used for all other analyses.

Data and code availability: Processed sequencing data and raw data for both RNA and protein are available in the Gene Expression Omnibus (GEO, https://www.ncbi.nlm.nih.gov/geo/) under

accession number GSE229082. Code for all data analyses and input files are available on GitHub for download, at: https://github.com/umich-brcf-bioinf-projects/Aton_saton_CU8-GeoMx.

Acknowledgements: Figures illustrating behavioral paradigms were created with BioRender. We are grateful to the staff of the Advanced Genomics Core at the University of Michigan for assistance with GeoMx slide preparation, library preparation and next-generation sequencing.

3.6 References

1. T. M. Prince, T. Abel, The impact of sleep loss on hippocampal function. *Learn Mem* **20**, 558-569 (2013).

2. C. Puentes-Mestril, S. J. Aton, Linking network activity to synaptic plasticity during sleep: hypotheses and recent data. *Frontiers in Neural Circuits* **11**, doi: 10.3389/fncir.2017.00061 (2017).

3. C. Puentes-Mestril, J. Roach, N. Niethard, M. Zochowski, S. J. Aton, How rhythms of the sleeping brain tune memory and synaptic plasticity. *Sleep* **42**, pii: zsz095 (2019).

4. J. G. Klinzing, N. Niethard, J. Born, Mechanisms of systems memory consolidation during sleep. *Nature Neuroscience* **22**, 1598-1610 (2019).

5. T. Abel, R. Havekes, J. M. Saletin, M. P. Walker, Sleep, plasticity and memory from molecules to whole-brain networks. *Curr Biol* **23**, R774-788 (2013).

6. R. Havekes, P. Meerlo, T. Abel, Animal studies on the role of sleep in memory: from behavioral performance to molecular mechanisms. *Curr Top Behav Neurosci* **25**, 183-206 (2015).

7. S. S. Yoo, P. T. Hu, N. Gujar, F. A. Jolesz, M. P. Walker, A deficit in the ability to form new human memories without sleep. *Nat Neurosci* (2007).

8. M. S. Fanselow, Conditioned and unconditional components of post-shock freezing. *Pavlov J Biol Sci* **15**, 177-182 (1980).

9. L. A. Graves, E. A. Heller, A. I. Pack, T. Abel, Sleep deprivation selectively impairs memory consolidation for contextual fear conditioning. *Learn. Mem.* **10**, 168-176 (2003).

10. C. G. Vecsey *et al.*, Sleep deprivation impairs cAMP signalling in the hippocampus. *Nature* **461**, 1122-1125 (2009).

11. N. Ognjanovski, C. Broussard, M. Zochowski, S. J. Aton, Hippocampal Network Oscillations Rescue Memory Consolidation Deficits Caused by Sleep Loss. *Cereb. Cortex* **28**, 3711-3723 (2018).

12. J. Delorme *et al.*, Hippocampal neurons' cytosolic and membrane-bound ribosomal transcript profiles are differentially regulated by learning and subsequent sleep. *Proc Natl Acad Sci USA* **118** (2021).

13. J. D. Martinez, W. P. Brancaleone, K. G. Peterson, L. G. Wilson, S. J. Aton, Atypical hypnotic compound ML297 restores sleep architecture immediately following emotionally valenced learning, to promote memory consolidation and hippocampal network activation during recall *Sleep* **46**, zsac301 (2023).

14. R. Havekes *et al.*, The tired hippocampus: effects of sleep deprivation on AMPA receptor function and cell proliferation. *Sleep and Biological Rhythms* **5**, A48 (2007).

15. R. Havekes *et al.*, Sleep deprivation causes memory deficits by negatively impacting neuronal connectivity in hippocampal area CA1. *eLife* **5**, pii: e13424 (2016).

16. L. C. Lyons, S. Chatterjee, Y. Vanrobaeys, M. E. Gaine, T. Abel, Translational changes induced by acute sleep deprivation uncovered by TRAP-Seq. *Mol Brain* **13** (2020).

17. J. E. Delorme, V. Kodoth, S. J. Aton, Sleep loss disrupts Arc expression in dentate gyrus neurons. *Neurobiol Learn Mem* **160**, 73-82 (2019).

18. M. E. Gaine *et al.*, Altered hippocampal transcriptome dynamics following sleep deprivation *Mol Brain* **14**, 125 (2021).

19. C. G. Vecsey *et al.*, Genomic analysis of sleep deprivation reveals translational regulation in the hippocampus. *Physiol Genomics* **44**, 981-991 (2012).

20. J. Delorme *et al.*, Sleep loss drives acetylcholine- and somatostatin interneuron-mediated gating of hippocampal activity, to inhibit memory consolidation. *Proc Natl Acad Sci USA* **118** (2021).

21. C. Puentes-Mestril *et al.*, Sleep loss drives brain region- and cell type-specific alterations in ribosome-associated transcripts involved in synaptic plasticity and cellular timekeeping. *J Neurosci* **In Press** (2021).

22. S. A. Josselyn, S. Tonegawa, Memory engrams: Recalling the past and imagining the future. *Science* **367**, eaaw4325 (2020).

23. K. K. Tayler, K. Z. Tanaka, L. G. Reijmers, B. J. Wiltgen, Reactivation of neural ensembles during the retrieval of recent and remote memory. *Cell* **23**, 99-106 (2013).

24. T. Kitamura *et al.*, Engrams and circuits crucial for systems consolidation of a memory *Science* **356**, 73-78 (2017).

25. X. Liu *et al.*, Optogenetic stimulation of a hippocampal engram activates fear memory recall. *Nature* **484**, 381-385 (2012).

26. S. Ramirez *et al.*, Creating a false memory in the hippocampus. *Science* **341**, 387-391 (2013).

27. B. C. Clawson *et al.*, Causal role for sleep-dependent reactivation of learning-activated sensory ensembles for fear memory consolidation. *Nat Communications* **12** (2021).

28. A. F. de Sousa *et al.*, Optogenetic reactivation of memory ensembles in the retrosplenial cortex induces systems consolidation *Proc Natl Acad Sci USA* **116**, 8576-8581 (2019).

29. K. Ghandour *et al.*, Orchestrated ensemble activities constitute a hippocampal memory engram. *Nat Communications* **10**, 2637 (2019).

30. S. Park *et al.*, Neuronal Allocation to a Hippocampal Engram. . *Neuropsychopharmacology* **41**, 2987-2993 (2016).

31. C. Guenthner, K. Miyamichi, H. H. Yang, H. C. Heller, L. Luo, Permanent genetic access to transiently active neurons via TRAP: targeted recombination in active populations. *Neuron* **78**, 773-784 (2013).

32. S. R. Erwin *et al.*, A Sparse, Spatially Biased Subtype of Mature Granule Cell Dominates Recruitment in Hippocampal-Associated Behaviors. *Cell Reports* **31**, 107551 (2020).

33. N. Naidoo, W. Giang, R. J. Galante, A. I. Pack, Sleep deprivation induces the unfolded protein response in mouse cerebral cortex. *J Neurochem* **92**, 1150-1157 (2005).

34. G. Tononi, C. Cirelli, Sleep and the price of plasticity: From synaptic and cellular homeostasis to memory consolidation and integration. *Neuron* **81**, 12-34 (2014).

35. L. Wang, S. J. Aton, Perspective - ultrastructural analyses reflect the effects of sleep and sleep loss on neuronal cell biology. *Sleep* **45**, zac047 (2022).

36. S. J. Aton *et al.*, Mechanisms of sleep-dependent consolidation of cortical plasticity. *Neuron* **61**, 454-466 (2009).

37. A. Saunders *et al.*, Molecular Diversity and Specializations among the Cells of the Adult Mouse Brain. *Cell* **174**, 1015-1030 (2018).

38. M. Bridi *et al.*, Transcriptional corepressor SIN3A regulates hippocampal synaptic plasticity via Homer1/mGluR5 signaling *JCI Insight* **5**, e92385 (2020).

39. S. Yoon *et al.*, Homer1 promotes dendritic spine growth through ankyrin-G and its loss reshapes the synaptic proteome. *Mol Psychiatry* **26**, 1775-1789 (2021).

40. G. Takamatsu *et al.*, Tescalcin is a potential target of class I histone deacetylase inhibitors in neurons *Biochem Biophys Res Commun* **482**, 1327-1333 (2017).

41. F. Raven, P. Meerlo, E. A. Van der Zee, T. Abel, R. Havekes, A brief period of sleep deprivation causes spine loss in the dentate gyrus of mice. *Neurobiology of Learning and Memory* **pii: S1074-7427**, 30072-30078 (2018).

42. B. Rasch, J. Born, About sleep's role in memory. *Physiol Rev* **93**, 681-766 (2013).

43. M. P. Witter, The perforant path: projections from the entrhinal cortex to the dentate gyrus. *Prog Brain Res* **163**, 43-61 (2007).

44. D. G. Amaral, H. E. Scharfman, P. Lavenex, The dentate gyrus: fundamental neuroanatomical organization (dentate gyrus for dummies). *Prog Brain Res* **163**, 3-22 (2007).

45. F. Raven, S. J. Aton, The Engram's Dark Horse: How Interneurons Regulate State-Dependent Memory Processing and Plasticity. . *Front Neural Circuits* **15**, 750541 (2021).

46. J. C. Tudor *et al.*, Sleep deprivation impairs memory by attenuating mTORC1-dependent protein synthesis. *Sci Signal* **9**, ra41 (2016).

47. K. D. Allen *et al.*, Learning-induced ribosomal RNA is required for memory consolidation in mice—Evidence of differentially expressed rRNA variants in learning and memory. *PLoS ONE* **13**, e0203374 (2018).

48. R. Lamprecht, The actin cytoskeleton in memory formation *Prog Neurobiol* **117**, 1-19 (2014).

49. B. C. Clawson *et al.*, Sleep Promotes, and Sleep Loss Inhibits, Selective Changes in Firing Rate, Response Properties and Functional Connectivity of Primary Visual Cortex Neurons. *Frontiers in Systems Neuroscience* **12**, 40 (2018).

50. Q. M. Skilling *et al.*, Acetylcholine-gated current translates wake neuronal firing rate information into a spike timing-based code in Non-REM sleep, stabilizing neural network dynamics during memory consolidation *PLoS Computational Biology* **17**, e1009424 (2021).

51. R. Havekes, S. J. Aton, Impacts of Sleep Loss Versus Waking Experience on Brain Plasticity: Parallel or Orthogonal? *Trends in Neuroscience* **43**, 385-393 (2020).

52. A. Biever *et al.*, Monosomes actively translate synaptic mRNAs in neuronal processes *Science* **367** (2020).

53. P. G. Donlin-Asp, C. Polisseni, R. Klimek, A. Heckel, E. M. Schuman, Differential regulation of local mRNA dynamics and translation following long-term potentiation and depression. *Proc Natl Acad Sci USA* **118** (2021).

54. Q. M. Skilling, N. Ognjanovski, S. J. Aton, M. Zochowski, Critical Dynamics Mediate Learning of New Distributed Memory Representations in Neuronal Networks *Entropy* **21**, 1043 (2019).

55. R. S. Koolschijn *et al.*, Memory recall involves a transient break in excitatory-inhibitory balance. *eLife* **10**, e70071 (2021).

56. X. Sun *et al.*, Functionally Distinct Neuronal Ensembles within the Memory Engram *Cell* **181**, 410-423 (2020).

57. P. Rao-Ruiz *et al.*, Engram-specific Transcriptome Profiling of Contextual Memory Consolidation *Nat Communications* **10** (2019).

58. N. Ognjanovski, D. Maruyama, N. Lashner, M. Zochowski, S. J. Aton, CA1 hippocampal network activity changes during sleep-dependent memory consolidation. *Front Syst Neurosci* **8**, 61 (2014).

59. N. Ognjanovski *et al.*, Parvalbumin-expressing interneurons coordinate hippocampal network dynamics required for memory consolidation. *Nature Communications* **8**, 15039 (2017).

60. J. Delorme, V. Kodoth, S. J. Aton, Sleep loss disrupts Arc expression in dentate gyrus neurons. *Neurobiol Learn Mem* **pii: S1074-7427**, 30091-30091 (2018).

61. R. Yamazaki *et al.*, Granule cells in the infrapyramidal blade of the dentate gyrus are activated during paradoxical (REM) sleep hypersomnia but not during wakefulness: a study using TRAP mice *Sleep* **44**, zsab173 (2021).

62. B. C. Clawson *et al.*, Causal role for sleep-dependent reactivation of learning-activated sensory ensembles for fear memory consolidation. *BioRxiv* 10.1101/2020.04.30.070466 (2020).

63. P. Curzon, N. Rustay, K. Browman, "Cued and Contextual Fear Conditioning for Rodents" in Methods of Behavior Analysis in Neuroscience., J. Buccafusco, Ed. (CRC Press, 2009), pp. 19-37.

64. J. Schindelin *et al.*, Fiji: an open-source platform for biological-image analysis *Nat Methods* **28**, 676-682 (2012).

65. C. R. Merritt *et al.*, Multiplex digital spatial profiling of proteins and RNA in fixed tissue *Nat Biotechnol* **38**, 586-599 (2020).

66. N. Y. Z. Ortogero, R. Vitancol, M. Griswold, D. Henderson, GeomxTools: NanoString GeoMx Tools. (2022).

67. P. Fonseka, M. Pathan, S. V. Chitti, T. Kang, S. Mathivanan, FunRich enables enrichment analysis of OMICs datasets. . *J Mol Biol* **433**, 166747 (2021).

Chapter 4 Conclusion and Future Directions

4.1 Conclusion

Over a century of research suggests that sleep plays an important role in supporting memory consolidation (1). In mice, 5 to 6 hours of sleep deprivation (SD) following contextual fear conditioning (CFC) may disrupt hippocampus-mediated contextual fear memory (CFM) consolidation (2, 3). However, the precise mechanisms responsible for SD-driven disruption of hippocampal memory processing still remain largely unknown. The present work aim to address these questions from the following perspectives: 1) characterize how post-learning SD disrupts the reactivation of memory traces in the hippocampus; 2) determine how SD differentially alters the expression of immediate early genes (IEGs) in hippocampal subregions; and 3) profile transcriptomic and protein expression changes induced by learning and subsequent sleep loss in each hippocampal subregion.

Previous studies have shown that patterns of neural activity present during learning are spontaneously re-activated during subsequent sleep (4). Artificial disturbance of the reactivation was shown to disrupt memory consolidation (5), and artificial enhancement had improved memory task performances (6). Thus, this phenomenon has been proposed to play an important role in memory consolidation. In Chapter 3, we first asked whether memory-encoding neurons in the hippocampal dentate gyrus (DG) reactivate during post-learning sleep. I used a recently developed genetic tool, targeted recombination in active populations (TRAP) (7), to capture and label neurons that are activated by a specific context. Consistent with observations of ensemble

reactivation in the neocortex and hippocampal CA1 (5, 8), we found that the reactivation of these hippocampal DG context-activated neurons was indeed disrupted by SD in the hours following CFC. However, to our surprise, this sleep-dependent reactivation is subregion-specific in the DG, with a significantly higher reactivation rate in the inferior blade of DG compared with the superior blade. The SD-induced disruption also has a strong trend of affecting the inferior blade more than the superior blade.

In addition to the DG subregion specific engram reactivation pattern, we also observed that SD altered IEG expression differently in the hippocampal subregions. We found that 6h of post-learning SD dramatically decreased cFos and Arc protein expression specifically among DG inferior blade granule cells, while in the DG superior blade, hilus, CA1, and CA3, IEG protein expression was significantly increased following the same period of SD. Previous study showed that SD decreased Arc expression in the DG, while increased Arc expression in the cortex (9). Our data indicates that the previously observed total Arc expression decrease following SD is likely a net effect of differential expression within the subregions. Together, these results strongly suggest that SD drives alterations of the activity of DG, especially in the infrapyramidal blade, very differently from elsewhere in the brain.

Based on our previous and current observations of brain region-specific changes of both IEG RNA and protein expression, we speculated that learning and sleep could alter biosynthetic processes in a subregion-specific manner in the hippocampus. I collected RNA and protein expression profiles from 5 different hippocampal subregions, including the superior and inferior blade of DG, the hilus, CA1, and CA3, using NanoString GeoMx Digital Spatial Profiler. Our spatial transcriptomics results first validated our observation that SD differentially altered IEG expression in these subregions. For example, expression of several IEGs, including Arc, Fosl2,

Homer1, Nr4a1, Junb, and Egr4, was upregulated by SD in CA1 while downregulated in DG inferior blade, indicating opposite changes in neuronal activation patterns during SD in these structures. The results also revealed that SD altered other genes' and proteins' expression very differently in each subregion. With hundreds to thousands of genes differentially expressed (DEGs) following SD in each subregion, the number of DEGs overlapping between subregions are relatively small. In turn, largely different Gene Ontology (GO) terms and KEGG pathways are enriched for different subregions following SD. Only one pathway, circadian entrainment, was consistently impacted in CA1, inferior blade, and superior blade. Further, under this pathway, a SD-induced negative perturbation of mitogen-activated protein kinase (MAPK) signal transduction cascade was present across the three subregions, which is consistent with several previous research showing that SD attenuates cAMP signaling and CREB-mediated gene transcription (10, 11). However, although MAPK signaling and CREB were negatively regulated by SD, our data show that the end products (clock genes and immediate early genes) preserved different perturbation patterns across the three subregions. Together, these results indicate functional differences of these hippocampal subregions under Sleep vs. SD conditions.

We then compared the transcriptomic differences between the inferior and superior blade of DG, under either sleep or SD conditions. We found that hundreds of genes were consistently differentially expressed in the two blades regardless of sleep or SD condition. Several of them, such as Penk, Npy, and Col6a1, were previously reported by other studies (12, 13). These DEGs likely reflect constitutive genetic differences between the two blades. We also found that more than 50% of the inferior vs. superior blade DEGs were only altered under either sleep or SD condition, suggesting that sleep and SD have very different effects on the two blades of DG.

Our spatial transcriptomic results also showed that at the time of our tissue collection, learning (CFC)-induced transcriptomic changes are restricted to the hippocampal granule cell layers, especially the superior blade of DG. The GO term GABA receptor complex was found to be significantly enriched in the superior blade. This observation is consistent with previous reports of GABAergic inhibitory interneuron activation in the DG during spatial learning (14). Further, in DG engram cells, GABA receptor signaling pathway was enriched following fear conditioning (15). Together, previous and current data suggest that GABAergic interneurons may play important roles in modulating the network plasticity responsible for contextual fear learning.

In summary, this thesis work demonstrated 1) that hippocampal memory trace reactivation occurs in a sleep-dependent manner, with subregional differences in disruption of reactivation by SD; 2) there is a subregion-specific alteration in hippocampal activity following post-learning sleep loss; and 3) RNA and protein expression changes induced by learning and subsequent sleep/SD loss are distinct within each hippocampal subregion. However, several questions remain unanswered for future research to explore.

4.2 Future directions

One potential direction for further study is blade-specific differences of the DG during memory consolidation. While numerous studies have shown structural and functional differences between the superior and inferior blades of DG, little is known about the two structures' individual roles in memory processing. We and others showed that learning preferentially activates engram cells in the superior blade, and the present data show that sleep selectively reactivates the engram cells in the inferior blade (7, 12). These observations further support the hypothesis that the two DG blades could have different circuit functions during memory

processing. Although we observed the reactivation of engram cells through IEG colocalization with TRAP-based fluorescent labeling, we did not possess the necessary tools or techniques for testing either the necessity or sufficiency of blade-specific engram cell reactivation for memory consolidation.

Another future direction could focus on transcriptomic and epigenomic changes specifically within the engram populations. While several recent studies have characterized transcript changes in engram cells hours to days after the initial learning (16-18), or following memory recall within the reactivated engram cell population (19, 20), none has focused on the effect of sleep loss after learning. Thus, how SD changes the transcriptomic and epigenomic following learning remains completely unexplored. With our present data showing SD-induced hippocampal subregional differences, future research separately analyzing the effect of SD on transcriptome and epigenome of engram cells in each subregion would be highly informative.

Lastly, future studies at brain circuit level are needed to explain our observations in the hippocampus. For instance, we have little knowledge about how sleep and sleep loss affects the entorhinal cortex (EC), a major brain structure that mediates the communication between the cortex and the hippocampus (21). The majority of the EC input to DG comes from layers II and III, which can be further segregated into lateral and medial depending on if the projections arise from the lateral or medial EC. While layer II EC pyramidal cells were shown to branch off and simultaneously project to both the superior and inferior blade of DG, the medial EC was shown to have more projections towards the inferior blade of DG while lateral EC was shown to have greater projections to the superior blade (22). One previous study showed that SD induced robust IEG expression in the entorhinal cortex (23), however, without layer-specific or subregion (medial/lateral) specific signal quantification, no clear conclusions about changes to DG input

after SD can be drawn from the observation. Nonetheless, these questions are extremely interesting and important, and answering them will significantly further our understanding on SD-driven neurobiological changes related to disrupted hippocampal memory functions.

4.3 References

1. S. Diekelmann, J. Born, The memory function of sleep. *Nat Rev Neurosci* **11**, 114-126 (2010).

2. L. A. Graves, E. A. Heller, A. I. Pack, T. Abel, Sleep deprivation selectively impairs memory consolidation for contextual fear conditioning. *Learn Mem* **10**, 168-176 (2003).

3. N. Ognjanovski, C. Broussard, M. Zochowski, S. J. Aton, Hippocampal Network Oscillations Rescue Memory Consolidation Deficits Caused by Sleep Loss. *Cereb Cortex* **28**, 3711-3723 (2018).

4. J. G. Klinzing, N. Niethard, J. Born, Mechanisms of systems memory consolidation during sleep. *Nat Neurosci* **22**, 1598-1610 (2019).

5. B. C. Clawson *et al.*, Causal role for sleep-dependent reactivation of learning-activated sensory ensembles for fear memory consolidation. *Nat Commun* **12**, 1200 (2021).

6. A. F. de Sousa *et al.*, Optogenetic reactivation of memory ensembles in the retrosplenial cortex induces systems consolidation. *Proc Natl Acad Sci U S A* **116**, 8576-8581 (2019).

7. C. J. Guenthner, K. Miyamichi, H. H. Yang, H. C. Heller, L. Luo, Permanent genetic access to transiently active neurons via TRAP: targeted recombination in active populations. *Neuron* **78**, 773-784 (2013).

8. K. Ghandour *et al.*, Orchestrated ensemble activities constitute a hippocampal memory engram. *Nat Commun* **10**, 2637 (2019).

9. J. E. Delorme, V. Kodoth, S. J. Aton, Sleep loss disrupts Arc expression in dentate gyrus neurons. *Neurobiol Learn Mem* **160**, 73-82 (2019).

10. C. G. Vecsey *et al.*, Sleep deprivation impairs cAMP signalling in the hippocampus. *Nature* **461**, 1122-1125 (2009).

11. J. Delorme *et al.*, Hippocampal neurons' cytosolic and membrane-bound ribosomal transcript profiles are differentially regulated by learning and subsequent sleep. *Proc Natl Acad Sci U S A* **118** (2021).

12. S. R. Erwin *et al.*, A Sparse, Spatially Biased Subtype of Mature Granule Cell Dominates Recruitment in Hippocampal-Associated Behaviors. *Cell Rep* **31**, 107551 (2020).

13. H. E. Scharfman, A. L. Sollas, K. L. Smith, M. B. Jackson, J. H. Goodman, Structural and functional asymmetry in the normal and epileptic rat dentate gyrus. *J Comp Neurol* **454**, 424-439 (2002).

14. T. Stefanelli, C. Bertollini, C. Luscher, D. Muller, P. Mendez, Hippocampal Somatostatin Interneurons Control the Size of Neuronal Memory Ensembles. *Neuron* **89**, 1074-1085 (2016).

15. P. Rao-Ruiz *et al.*, Engram-specific Transcriptome Profiling of Contextual Memory Consolidation *Nat Communications* **10** (2019).

16. B. Lacar *et al.*, Nuclear RNA-seq of single neurons reveals molecular signatures of activation. *Nat Commun* **7**, 11022 (2016).

17. P. Rao-Ruiz *et al.*, Engram-specific transcriptome profiling of contextual memory consolidation. *Nat Commun* **10**, 2232 (2019).

18. J. Fernandez-Albert *et al.*, Immediate and deferred epigenomic signatures of in vivo neuronal activation in mouse hippocampus. *Nat Neurosci* **22**, 1718-1730 (2019).

19. B. N. Jaeger *et al.*, A novel environment-evoked transcriptional signature predicts reactivity in single dentate granule neurons. *Nat Commun* **9**, 3084 (2018).

20. A. Marco *et al.*, Mapping the epigenomic and transcriptomic interplay during memory formation and recall in the hippocampal engram ensemble. *Nat Neurosci* **23**, 1606-1617 (2020).

21. M. P. Witter, T. P. Doan, B. Jacobsen, E. S. Nilssen, S. Ohara, Architecture of the Entorhinal Cortex A Review of Entorhinal Anatomy in Rodents with Some Comparative Notes. *Front Syst Neurosci* **11**, 46 (2017).

22. B. Schmidt, D. F. Marrone, E. J. Markus, Disambiguating the similar: the dentate gyrus and pattern separation. *Behav Brain Res* **226**, 56-65 (2012).

23. C. L. Thompson *et al.*, Molecular and anatomical signatures of sleep deprivation in the mouse brain. *Front Neurosci* **4**, 165 (2010).